Formability and Strength of Sheet Metals Subjected to Complex Strain Paths

By

Trevor Davis

A Thesis Submitted for
the Degree of Doctor of Philosophy

To

The University of Aston in Birmingham

August 1985

The University of Aston in Birmingham

Title: Formability and Strength of Sheet Metals Subjected to Complex Strain Paths

Author: Trevor Davis

A Thesis Submitted for the Degree of Doctor of Philosophy, August 1985

SUMMARY

The effects of changes in strain path on the plastic flow behaviour of steel sheet have been investigated for plain carbon, re-phosphorised and dual-phase steels. Prestraining has been carried out in simple tension, plane-strain tension and equi-biaxial stretching . A wide range of prestrain levels has been used in each case. Final testing is done in simple tension with continuous monitoring of flow stress, work-hardening behaviour and plastic anisotropy throughout the test. The tensile tests have been carried out in several directions relative to the prestrain direction.

The results show that the work-hardening characteristics and instability conditions can be greatly modified by the changes in strain path investigated. The major conclusions are:-

A). All of the steels behaved similarly.
B). At low prestrains, a Bauschinger Effect is observed (a 'Bauschinger Hump').
C). Increasing prestrain leads to 'latent hardening' and a drastic loss of ductility at a critical prestrain. This is due to changes in the dislocation substructure restricting the number of active slip-systems.
D). A near constant strain to instability is observed at high prestrains. This is attributed to activation of previously unfavourable dislocation sources.
E). There is a transient increase in r-value after uniaxial and plane-strain prestraining. This is most likely due to exhaustion of mobile dislocations left over from the prestraining operation.
F). The dual-phase steel does not show any increase in necking strains after biaxial stretching. This is attributed to failure of the martensite/ferrite interfaces.

Key Words: Strain Path Change, Steel, Plasticity, Ductility, Formability

Contents

List of Tables

List of Figures

List of Symbols

σ = True Stress

ε = True Strain

s = Nominal Stress

e = Nominal Strain

$\bar{\sigma}$ = True Effective Stress

$\bar{\varepsilon}$ = True Effective Strain

$\bar{s}$ = Nominal Effective Stress

$\bar{e}$ = Nominal Effective Strain

$\bar{\varepsilon}_p$ = True Effective Prestrain

$\bar{e}_p$ = Nominal Effective Prestrain (Also $\bar{e}_{prestrain}$)

r = Plastic Strain Ratio (Ratio of True Width to Thickness Strain in Tension Testing)

$\bar{r}$ = Average Plastic Strain Ratio

Δr = Planar Anisotropy Parameter

r_i = Incremental r (for a Given Increment of True Strain)

n = Strain-Hardening Exponent

$\dot{\varepsilon}$ = True Strain-Rate

m = Strain-Rate Sensitivity Index

e_u = Nominal Uniform Elongation (or Strain to Maximum Load)

ε_u = True Uniform Elongation

e_t = Total Nominal Strain (Elongation to Fracture)

Y = Uniaxial Yield Stress

σ_n = A Principal Stress (Where n = 1,2,3)

ε_n = A Principal Strain (Where n = 1,2,3)

ρ = Strain-Ratio ($\varepsilon_2/\varepsilon_1$)

INTRODUCTION

In November of 1973 the Secretary General of the OPEC cartel made the following remarks at a conference on North Sea oil:-

"I am of the opinion that we must commence to give oil a real value ie: consider it as a precious wealth, expensive by definition and subject to protection from wasteful useage."

(taken from Petroleum Times, 16th Nov. 1973)

This statement, and the so-called "oil-crisis" that followed, indicated to the worlds' automobile manufacturers that future generations of motor vehicles would have to consume less petroleum if private car ownership was not to become too expensive for the majority of their customers. It also brought a new awareness of the true value of consumeable energy sources and the need for conservation on a global scale.

Driven by the desire to design more economical motor vehicles (and in some countries forced by legislation) the major manufacturers have made great

strides in many areas of automotive design (for example aerodynamics, lean-burn engines etc). However, fundamental to these reseach programmes is the necessity to reduce the overall weight of vehicles without impairing their structural integrity.

The trend away from cast-iron cylinder blocks to aluminium and the incorporation of many low density non-metallic materials within the passenger compartment has gone a long way towards reducing vehicle weight. However, nearly half of the weight of a modern, unitary construction vehicle is still comprised of low-carbon sheet steels. This choice of material has not changed for mass produced vehicles for a variety of technical and financial considerations: the ease with which they can be formed into the many shapes required in large quantities and at low cost, familiarity with the design techniques needed and the massive capital investment necessary to change to either aluminium or non-metallic body shells (new forming, joining and surface finishing would be required). Current signs are that this situation will not change significantly until past the end of this decade, although the search for lower density alternatives to steel will inevitably lead to the utilisation of other materials.

Since the density of formable steels is

essentially a constant, it is only by using thinner panels that weight reduction can be achieved. In order to still have a vehicle which will pass the various mandatory crash regulations, stronger steels are needed as well as improved structural designs. To satisfy the emerging demand for high strength formable grades of steel, new alloys have been developed by the steel producers which purport to meet the requirements of this new generation of body-shell design philosophy (eg: HSLA, Dual-Phase, Re-Phosphorised etc).

Initially, these new grades have been employed in small quantities for brackets, wheels, bumpers, small structural members and the like. Even so the weight savings have been impressive: for example, a typical American compact car will contain about 80 Kg of high-strength steels. Assuming this represents a 15% reduction in gauge, 15 Kg per vehicle has been saved. This translates into a saving of (very roughly) 250 litres of petrol over the design life of the vehicle. Although this doesn't look very impressive by itself, when one considers that there are about 300 million motor vehicles (cars, trucks, buses etc) in the world this represents a worthwhile saving. However, there is still a great potential for weight savings by replacing as many as possible of the remaining conventional sheet-steel members and panels with thinner

alternatives: on a typical 1000 Kg automobile, total savings by this route could amount to 75 Kg.

In order to increase the application of these new grades of steel a new level of sophistication in the design process is required. The widespread adoption of computer based design tools such as CAD and CIM (Computer Aided Design and Computer Integrated Manufacture), both by the automotive manufacturers and their suppliers, has placed a new emphasis upon understanding the basic deformation processes in sheet-metal forming so that accurate predictive models can be devised and optimium structural-strength to weight designs achieved.

One of the major problems facing anyone attempting to model the plastic behaviour of commercial alloys is the lack of data concerning their behaviour during the complex changes in strain-path that occur in the forming of even simple automotive components. Traditionally, the approach has been to consider the overall effect to be the sum of its component stages, but there is a growing body of experimental and theoretical evidence which suggests that this may not be valid in many forming operations. This problem is compounded when one considers the new grades of steel, where the years of practical experience accumulated

using conventional steels is not available.

This thesis explores the influence of strain-path changes similar to those found in actual forming operations on the parameters considered significant in the modelling of sheet formability. As well as a conventional low-carbon, deep-drawing quality steel, a Dual-Phase and a Re-Phosphorised steel are investigated since these are two of the more likely candidates for replacing the former in large body panels and structural members etc. Emphasis is placed on findings that cannot be accounted for by treating each stage of deformation as independent from those that precede it.

CHAPTER 1

General Concepts and Literature Review

1.1 General Considerations

Sheet formability is really a complex mixture of many parameters describing the mechanical behaviour of materials under certain loading conditions. Before dealing specifically with the known effects of strain-path changes on formability, it is useful to review the traditional measures of formability as obtained from the tensile test and from forming limit data. These tests feature most frequently in the literature due to their relative simplicity and ease of interpretation.

1.1.1 Tensile Testing

The uniaxial tensile test is widely used for evaluating formability. By recording the response of a material during the test, the following properties can be obtained:-

a) Yield strength or offset proof stress

b) Uniform elongation (ie: that upto the formation of a neck-usually maximum load)

c) Total elongation to failure

d) Maximum stress or Ultimate tensile strength

e) Plastic strain ratio (or r-value)

f) Strain hardening capacity

g) Strain rate sensitivity

h) Flow curve

The form of the stress-strain curve gives valuable information concerning the type of initial yielding and associated ageing effects (ie: continuous or discontinuous yielding), as well as describing the plastic work-hardening behaviour of the material.

Since this test is so well known it is only necessary to clarify certain of the above list and to put them into the current context.

1.1.1.1 Plastic Strain Ratio

The plastic anisotropy present in most commercially available sheet materials has a marked effect on their mechanical behaviour. Where the properties vary in the plane of the sheet and through

the thickness, it is referred to as normal anisotropy. Lankford et al (1) proposed the plastic strain ratio or r-value as a measure of this form of anisotropy:-

$$r = \frac{\varepsilon_w}{\varepsilon_t}$$, where ε_w=true width strain

ε_t=true thickness strain

This parameter is easily calculated from a tensile test by measuring length and width strains during the test and applying constancy of volume to obtain the thickness strain. Care must be taken when taking measurements since small errors lead to a large variation in r-value (2). In physical terms this value can be thought of as the resistance to thinning, and so high values are required for deep-drawing applications (see below).

The r-value often varies relative to the sheet rolling direction (RD). Hence, an average r-value or $\bar{r}$ is required when assessing pressing performance:-

$$\bar{r} = \frac{r_0 + 2r_{45} + r_{90}}{4}$$, where r_0, etc = r-value measured at the stated angle to the RD of the sheet

$\overline{r}$= 1 indicates equal flow strengths in the plane and through the thickness directions of the sheet

$\overline{r}$< 1 indicates that the average stength in the plane of the sheet is higher than through the thickness

$\overline{r}$ > 1 indicates the converse of $\overline{r}$<1

Hence, to resist thining an $\overline{r}$-value greater than unity is desirable.

Since the flow properties in the plane of the sheet often vary relative to the rolling direction, another parameter is required to express this planar anisotropy:-

$$\Delta r = \frac{r_0 - 2r_{45} + r_{90}}{2}$$, where r_0 etc = as above

It is planar anisotropy which leads to the 'earing' phenomenom observed in deep-drawing.

For a fully isotropic sheet:-

$\overline{r}=1$

$\Delta r=0$

It is important to realise that the r-value is not a fundamental property : instead, it is a function of the underlying crystallographic texture (or preferred orientations) present in the material. To study these directly it is necessary to resort to pole figures and orientation distribution functions (ODFs) obtained from x-ray diffraction data.

1.1.1.2 Strain-Hardening Capacity

Beyond the yield point, plastic deformation results in hardening processes which resist further deformation and so the load required for continued deformation increase with strain up to the start of the localised necking. The simplest indicators of strain-hardening capacity are the uniform elongation and yield strength/tensile strength ratio taken from the tensile test. Whilst useful as rule-of-thumb measures, it is necessary to study the flow curve of a material to discover more meaningful parameters.

There have been many fundamental and empirical studies to model the flow behaviour of a wide variety of metallic and non-metallic materials. Below are listed the four most commonly employed relationships:-

Eqn. 1. $\sigma = A + B\varepsilon^{n}$ after Ludwik (3)

Eqn. 2. $\sigma = K\varepsilon^{n}$ after Holloman (4)

Eqn. 3. $\sigma = A(B + \varepsilon)^{C}$ after Swift (5)

Eqn. 4. $\sigma = A - (A - B)e^{(-\varepsilon/C)}$ after Voce (6)

where A, B, C, K, n are material constants

None of these constitutive equations model the entire stress-strain curve for all metals, but they are sufficiently accurate to be used as a basis for describing work-hardening behaviour for simple cases.

Due to the simplicity of calculation and general applicability of the two parabolic or power-hardening laws (equations 1 and 2 above) they have gained wide acceptance. The simpler form suggested by Holloman will be used for this study:-

$\sigma = K\varepsilon^n$, where K = strength coefficient determined by the true stress at $\varepsilon = 1.0$

n = strain-hardening exponent

n = 0 , perfectly plastic solid

n = 1 , ideally elastic solid

n = 0.1 - 0.5 , real metals

A logarithmic plot of true stress and true strain will be a straight line of slope n and intercept log K if this law is followed.

The strain-hardening exponent can be shown to have the following important relationships:-

Eqn. 5. $n = \varepsilon_u$, where ε_u = true uniform strain in the tensile test

Eqn. 6. $n = \frac{\varepsilon \, d\sigma}{\sigma \, d\varepsilon}$, where ε = true strain, σ = true stress

$\frac{d\sigma}{d\varepsilon}$ = true strain-hardening rate

At instability, leading to localised deformation, the increase in stress caused by decreasing cross-section exceeds the increase in load-bearing capacity due to strain-hardening as given by:-

Eqn. 7. $\sigma = \frac{d\sigma}{d\varepsilon}$ at instability

In physical terms a high value of n is desired for press-forming operations since it implies a high period of stable flow before strain-localisation.

1.1.1.3 Strain-Rate Sensitivity

As with the power-hardening laws of the previous section, the stress-strain rate relationship for most metals can be approximated by:-

Eqn. 8. $\sigma = C\dot{\varepsilon}^m$, where $\dot{\varepsilon}$ = true strain-rate
m = strain-rate sensitivity index

Typically, m is calculated from differential strain-rate tensile tests. A typical low carbon forming steel would have an m-value of about 0.015.

In certain metals (particularly low C steels) there is still considerable ductility remaining after maximum load is reached in the tensile test. As a neck forms, material within the necked region may exhibit higher flow stresses than that outside due to strain-hardening (ie: it has been worked more). Since the strain-rate in the neck is higher than outside (7), strain-rate hardening may also occur (dependent upon the m-value). The combined effect is to stabilise plastic flow by transferring the deformation away from the neck.

1.1.2 Yield Criteria for More General Stress States

Prediction of yield stresses (ie: those at the onset of plastic flow) during deformations other than the simple uniaxial case requires criteria which take into account the yielding behaviour of both isotropic and anisotropic materials. Such criteria must be consistent with experimental observations, particularly

that pure hydrostatic pressure does not cause yielding.

By considering all of the stress states resulting in yielding produces the so-called yield locus, the formal, mathematical description of which is the yield criterion. For isotropic materials two such criteria have dominated the literature : that of Tresca (maximum shear stress criterion) and von Mises. Since the von Mises criterion has been shown to be more relevant to real materials it is to be preferred:-

$$\text{Eqn. 9. } (\sigma_1 - \sigma_2)^2 + (\sigma_2 - \sigma_3)^2 + (\sigma_3 - \sigma_1)^2 = 2Y^2,$$

where σ_1, σ_2, σ_3 = principal stresses

Y = uniaxial yield stress

The von Mises criterion implies that yielding in a complex strain-state will be a function of all three principal stresses ie: when this function exceeds some function of the uniaxial yield stress then yielding will occur.

It should be noted that von Mises chose his criterion on empirical observations and for its mathematical simplicity. Subsequent workers (notably

Hencky in 1924) have provided a physical basis - often referred to as the distortion-energy crirerion.

Most commercial sheet metals exhibit a significant preferred orientation or texture which results in different properties through the thickness to those in the plane of the sheet (see the earlier discussion of r-values), which in turn affects the yield locus and yield criterion. Hill (8) and others, using von Mises's criterion as a starting point have extended it to cover anisotopic materials of orthotropic symmetry:-

Eqn. 10. $F(\sigma_2 - \sigma_3)^2 + G(\sigma_3 - \sigma_1)^2 + H(\sigma_1 - \sigma_2)^2 = 1$

where $\sigma_1, \sigma_2, \sigma_3$ = principal stresses

F, G, H = anisotropy coeffs.

$$G + H = \frac{1}{X^2}, \quad H + F = \frac{1}{Y^2}, \quad F + G = \frac{1}{Z^2}$$

where X, Y, Z = yield stresses in 1, 2, 3 directions respectively

For those cases where the through thickness

stress can be ignored, the equation for an anisotropic yield locus can be expressed as follows (assuming yield stresses in the plane of the sheet are equal (9)):-

Eqn. 11. $$\sigma_1^2 + \sigma_2^2 - \left|\frac{2r}{1+r}\right| \sigma_1 \sigma_2 = Y^2 \text{ , where } r = \frac{\varepsilon_w}{\varepsilon_t}$$

This implies a texture strengthening effect ie: a material with an r-value greater than 1 will yield at higher stresses than an isotropic material under biaxial straining. The resulting distortion of the yield locus can be seen in Figure 1.

1.1.3. The Concept of Effective Stress and Strain

It is frequently necessary to compare the flow stresses of strain-hardened materials in stress states other than uniaxial tension, with the uniaxial values. This can be accomplished for isotropic materials by using effective stresses and strains derived from the von Mises criterion:-

Eqn. 12. $$\bar{\sigma} = \frac{\sqrt{2}}{2}\sqrt{((\sigma_1 - \sigma_2)^2 + (\sigma_2 - \sigma_3)^2 + (\sigma_3 - \sigma_1)^2)}$$

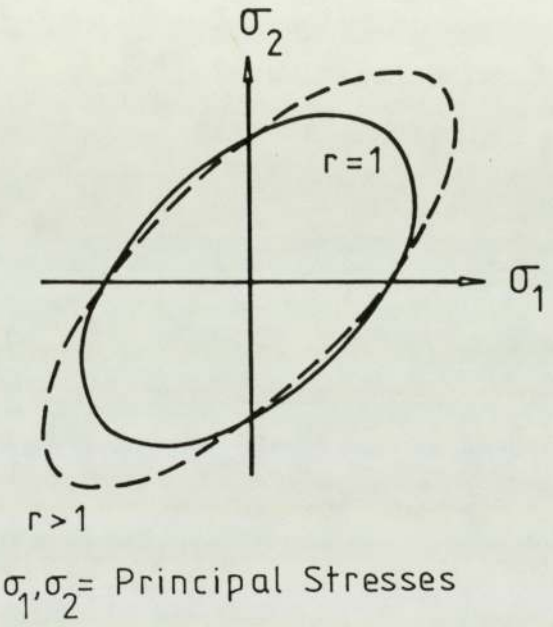

Fig. 1. Effect of an Increase in r-Value upon a von Mises Yield Locus (r = 1).

Eqn. 13 $$\bar{\varepsilon} = \frac{\sqrt{2}}{3}\sqrt{((\varepsilon_1 - \varepsilon_2)^2 + (\varepsilon_2 - \varepsilon_3)^2 + (\varepsilon_3 - \varepsilon_1)^2)}$$

Eqn. 14. $\bar{\sigma} = K\bar{\varepsilon}^n$, where $\bar{\sigma}, \bar{\varepsilon}$ = Effective Stress and Strain

It should be noted that Eqn. 13. only holds when the imposed strain ratio is constant during deformation. The definitions above form the basis of the isotropic work-hardening model.

As with the yield locus it is possible to expand these concepts to incorporate anisotropy (8).

1.1.4 Instability and Strain Localisation

In a typical tensile test on thin, sheet metal, uniform extension occurs until the true axial strain reaches the n-value. At this point the deformation begins to concentrate in one region of the specimen: this form of instability is known as a diffuse neck and occurs at the maximum load reached during the test. As the deformation progresses, local thinning occurs

within the diffuse neck producing a groove or local neck. It can be shown that for isotropic metals in pure tension this groove will be inclined at 55 degrees to the axial stress. It is the local neck which is of most interest in sheet metal forming since this often determines the forming limit-strain (10).

For diffuse necking the instability criterion has already been defined as :-

$$\frac{d\sigma}{d\varepsilon} = \sigma$$

It can be shown (11) that for a local neck the criterion becomes:-

Eqn. 15. $$\frac{d\sigma}{d\varepsilon} = -\frac{\sigma}{2} \quad \text{or} \quad \varepsilon = 2n \text{ ('double n')}$$

For this to occur the strain in the neck must rise until some element has reached twice the uniform elongation before localised thinning will occur. Marciniak and Kuczynski (12) proposed that the partitioning of strains between different areas can be explained by considering defects or inhomogeneities

(present before necking begins) which have a high stress compared to surrounding material, leading to strain concentration. These defects can be surface scratches or microstructural damage, usually in the form of voids. Under an applied stress nucleation of voids is associated with the presence of impurities or second-phases (11): in bands of highly localised shear there is decohesion at the particle/matrix interfaces or fragmentation of the particle itself. Coalescence of these voids with continued straining leads to crack growth and eventual failure. In the tensile testing of ductile metals this is the source of the familiar cup and cone fractures.

The necking strains have been shown to be strain-state dependent (13). Figure 2 illustrates the theoretical relationship between these necking strains and the ratio of major and minor principal strains. As can be seen, for tensile deformations both diffuse and local necks are possible. In plane-strain the strains for diffuse and local necks coincide.

It is against this theoretical background that the forming limit curves discussed in the next section have arisen.

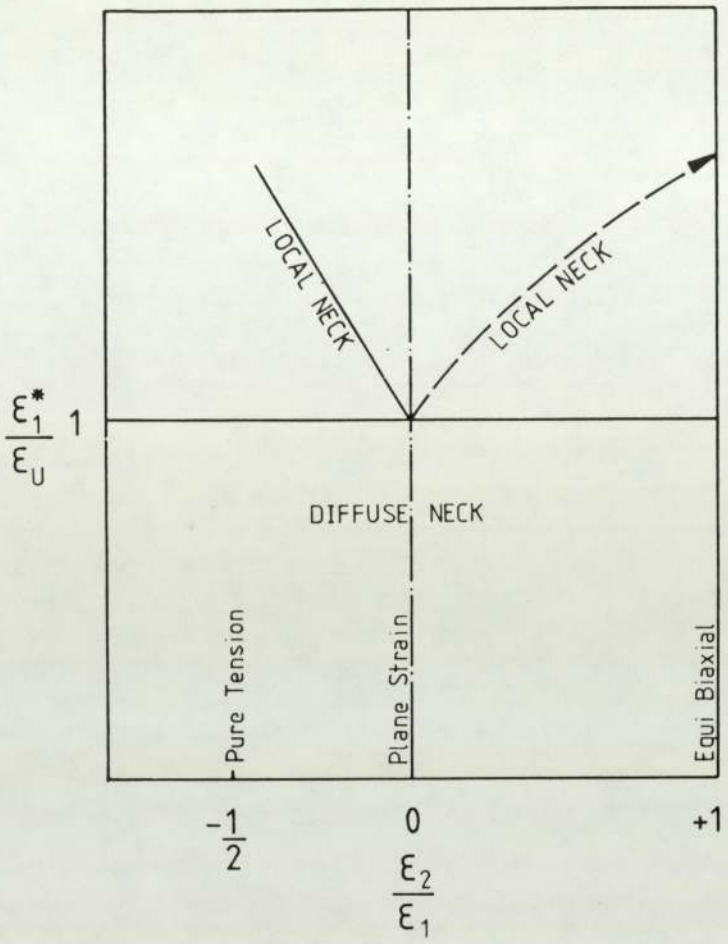

$\varepsilon_1, \varepsilon_2$ = Major and minor principal strains
ε_1^* = Local necking strain in ε_1 direction
ε_U = Diffuse necking strain in tension

Fig. 2. Theoretical Variation of Necking Limits with Imposed Strain-Ratio.

1.1.5 Forming Limit Curves

Amongst the commonest graphical representations of formability is the forming limit diagram or FLD (see Fig.3). On these diagrams, first proposed ky Keeler and Goodwin in the early 1960's, values of major and minor limit strain are plotted against each other. Usually, a single stage forming operation is used to fracture the specimens employed and, although not necessarily, the strain path involved is assumed to be linear.

In the strain-space of the FLD a strain-path is represented by a vector (see Fig. 4). For a linear path, a strain-ratio (ρ) can be used to describe it:-

$$\rho = \frac{\varepsilon_2}{\varepsilon_1}$$

, = 1 for equi-biaxial tension

= 0 for plane strain

=-.5 for uniaxial tension

Curved strain-paths are usually represented by a tangent to the vector at a given point, while a multi-stage forming operation may be illustrated by a series of contiguous strain vectors, one per stage. For non-linear or multiple strain-paths (the latter are also known as indirect strain-paths), the strain at any point can be calculated by integrating the effective

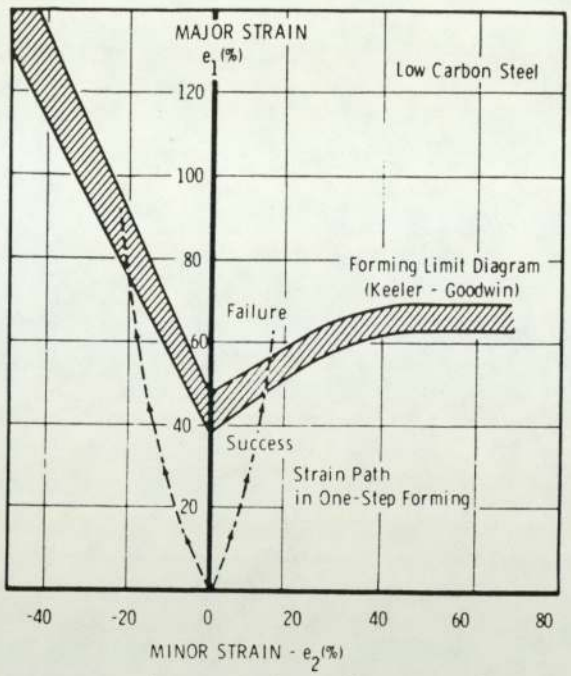

Fig. 3. A Typical Forming Limit Diagram for a Low C Steel.

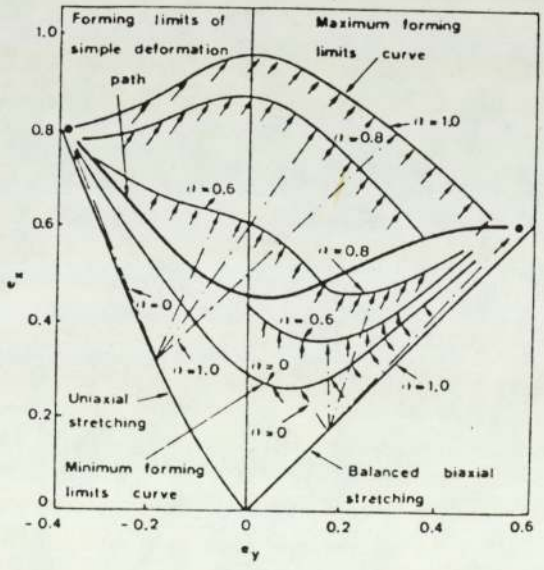

Fig. 4. Some Examples of Strain-Paths on a FLD (Direct and Indirect).

strain along each path as far as required, or until some failure criterion is met (in the case of limit strains).

1.2 Effect of Strain Path Changes on the Yield Locus

Amongst the earlier published work concerned directly with the influence of strain-path changes on plastic flow behaviour is that of Tozawa, Nakamura and Shinkai (15). These authors determined the work-hardening behaviour of prestrained Al-Killed, low C steel sheets under conditions of combined stress, by biaxial compression of multi-layer, glued test pieces. Yield loci were plotted from the results of a series of tests and compared to theoretical loci calculated from Hill's theory using uniaxial stress values and r-values. The calculated curves differ substantially from the experimental observations, indicating that the work-hardening behaviour under combined stresses cannot be predicted from uniaxial tensile data.

Prestraining the sheet in uniaxial tension by varying amounts before biaxial compression results in increasing amounts of distortion of the yield locus, although the shape remains similar. However, varying the mode of prestraining causes the shape of the locus

to alter accordingly (Fig.5). This is similar to the effect of a change in r-value, which in turn suggests some change in the anisotropic nature of the prestrained sheet. Unfortunately, the use of a composite specimen, made up of initially anisotropic layers, complicates the issue.

It is found that the extent of work-hardening subsequent to the prestrain is not always a maximum under the same stress conditions as the prestraining. For the steel tested, maximum hardening occurs when the subsequent stress vector differs by 90 and 270 degrees from the initial loading, independent of direction and magnitude.

1.3 Effect of Prestrain on Subsequent Flow Behaviour

One of the pioneer papers in this area is that of Garofalo and Low in 1955 (28). This paper defined the general experimental approach used by most subsequent researchers: typically, uniaxial or biaxial prestraining followed by (usually) uniaxial tensile testing. Later authors developed the technique to cover other strain-paths in the pre- and post-straining stages. The end result is some measure or indication of a change in flow behaviour caused by the indirect

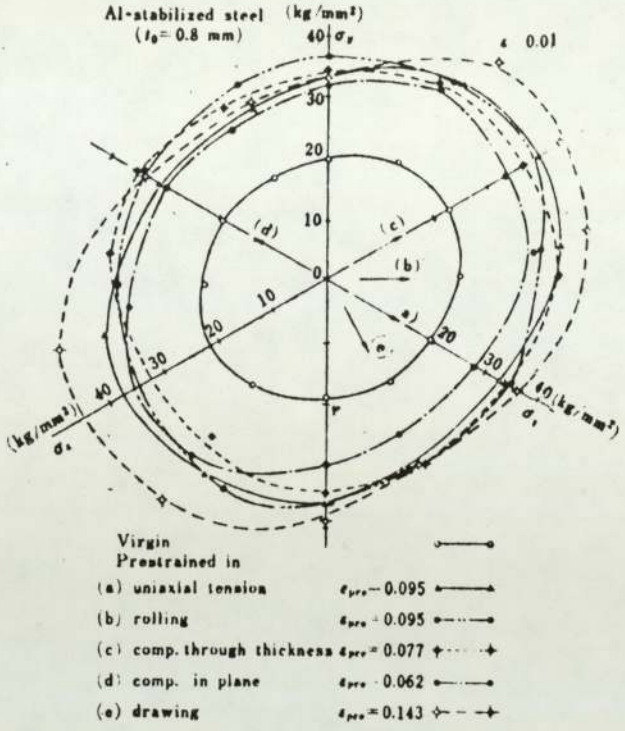

Fig. 5. Effect of Various Prestrains upon the Shape of the Yield Locus for an Al-Killed Steel.

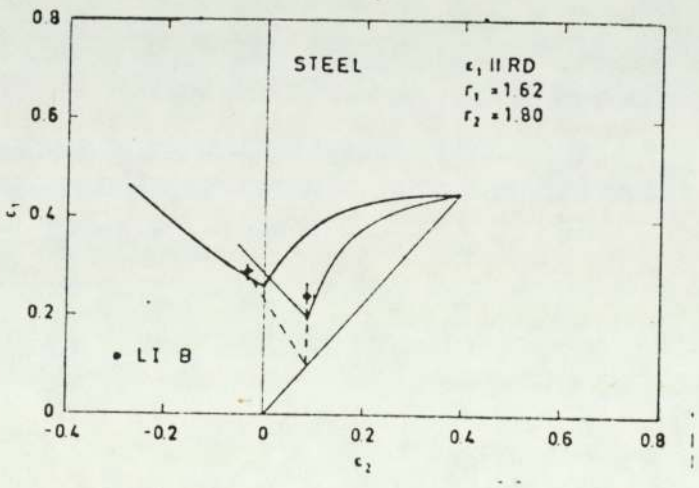

Fig. 6. Effect of Biaxial Prestrain upon the Limit Strains of an Al-Killed Steel in Subsequent Uniaxial Deformation.

strain-path. What Garofalo and Low discovered was that for low C steels, a prestrain in either biaxial or uniaxial tension followed by a strain-path change to uniaxial tension (at a different angle to the prestrain in the case of a prior uniaxial path) resulted in:-

a). Higher flow stresses (greater than predicted by the effective stress-strain concept.
b). Decreased strain-hardening.
c). After a certain prestrain level the extension to maximum load becomes constant at a low level.

Ghosh and Backofen (16) examined the effect of various proportional preloading paths on the subsequent uniaxial tensile behaviour and limit strains for a drawing quality, Al-Killed steel, 70/30 brass and 1100-1 aluminium (99% Al and 0.12% Cu). Using a variety of imposed strain-ratios ($\varepsilon_2/\varepsilon_1$) the following observations were made: for steel, the overall hardening rate increases as the imposed strain-ratio changes from -0.5 (pure uniaxial tension) through 0 (plane-strain) to 1 (equi-biaxial tension). The brass exhibited directly opposite behaviour, while the aluminim alloy was hardly affected. The reduction in the uniaxial ductility of the steel after a biaxial prestrain is consistent with the observations of Tozawa

et al with regard to yield loci, and has been widely reported since. Romano, Rault and Entringer (17), Kleemola and Pelkkikangas (18), Laukonis and Ghosh (19) and Ranta-Eskola (20) have all made similar observations for low C, Al-Killed sheet steels after biaxial prestraining. Figure 6 shows the effect of biaxial prestrain upon the limit strains of an Al-Killed steel (taken from ref.18); the allowable surface limit strains after prestraining are reduced. A similar lowering of limit strains can be seen in figure 7 (taken from ref.19).

Laukonis and Ghosh (19) also investigated the changes in tensile elongation and flow curves caused by prestraining. Figures 8 and 9 contrast the behaviour of a steel and 2036-T4 (an aluminium alloy containing 2.6% Cu, 0.45% Mg and 0.25% Mn, the T4 referring to the temper). As can be seen, the biaxial hardening curve of the steel shows increased hardening over purely uniaxial deformation. Also, biaxial 'n' appears greater than the equivalent uniaxial value. Hence, with a strain-path change from biaxial tension to uniaxiality, the steel undergoes strain-softening resulting in a drastic loss in the ability to undergo uniform deformation (reflected in an abrupt drop in uniform strain beyond a certain effective prestrain). However, the aluminium alloy does not exhibit this

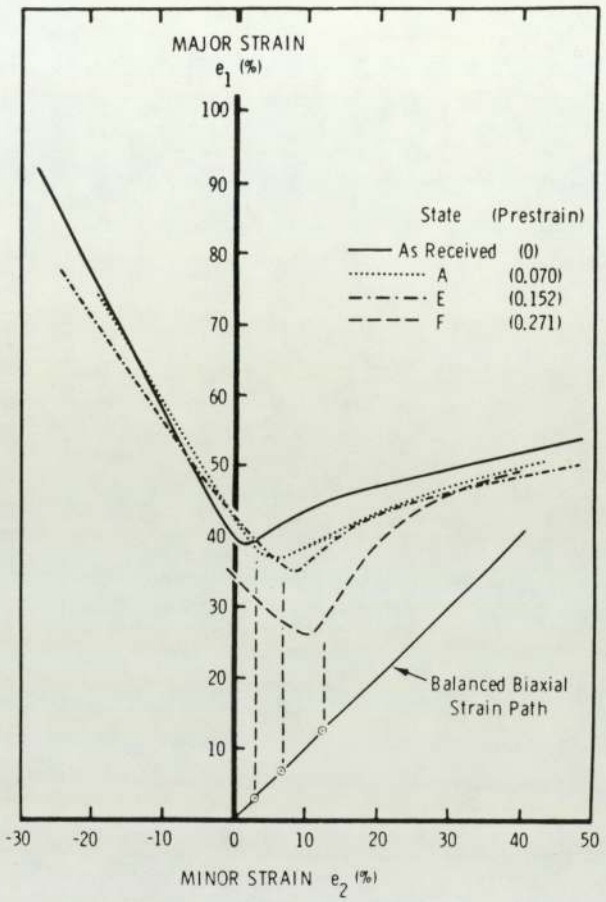

Fig. 7. Effect of Various Biaxial Prestrains upon the Subsequent Uniaxial Limit Strains for an Al-Killed Steel.

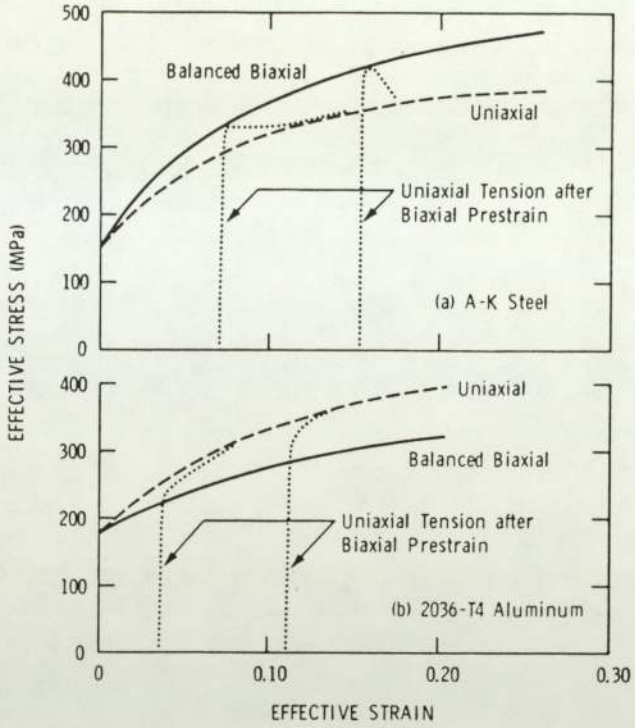

Fig. 8. Effect of Biaxial Prestrain upon Subsequent Uniaxial Flow Curves for:-
a). An Al-Killed Steel and
b). 2036-T4 Aluminium Alloy.

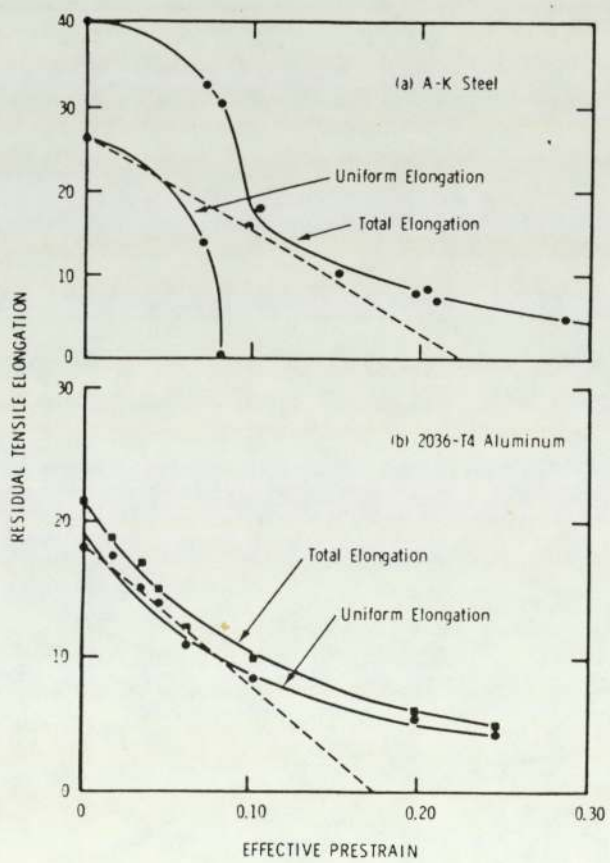

Fig. 9. Effect of Biaxial Prestrain upon Subsequent Residual Tensile Elongations for:-
a). An Al-Killed Steel and
b). 2036-T4 Aluminium Alloy.

premature instability as a result of prestraining, instead biaxial prestraining results in a greater residual uniform flow capability. It should be borne in mind, however, that the residual formability of both materials is reduced in direct proportion to the amount of biaxial prestrain.

By far the easiest indirect strain-path combination to study is uniaxial tension-uniaxial tension, where the second stage takes place at some angle to the first (often 90 degrees). The initial straining usually uses an outsize tensile test specimen from which smaller tensile test pieces are cut for the second stage. It has already been implied that the rate of work-hardening to be achieved by this combination of strain-paths is lower than from a biaxial tension-uniaxial tension combination (16). Also, there is evidence to suggest that premature instability often occurs when the second stage of an interrupted tensile test is carried out at some angle to the first (compared with monotonic loading). Hutchinson,Arthey and Malmstroem (21) investigated the stress-strain behaviour of five different materials (an Al-Killed deep-drawing quality steel, a rimming steel, manganese containing aluminium alloy, copper and 70/30 brass) by subjecting them to an interrupted tensile test where the second stage was orthogonal to

the first. The rate of strain-hardening was indeed observed to be lower than would be expected for momotonic loading. For both the steels and the aluminium alloy a consequence of the loss in work-hardening rate is the onset of premature instability and necking after small prestrains (7-9% depending on the materials-see Fig.10). This type of behaviour was also noted by Lloyd and Sang (22) for aluminium alloys 1100-0, 3003-0 and SW30 (3003 and SW30 are manganese containing alloys), although other alloys exhibited either the opposite effect or no change at all (2036-T4 belonging to the latter class). Hence, the situation for aluminium is complicated by the presence of various strengthening mechanisms and associated dislocation microstructures.

In the case of Al-killed steel, further evidence for premature loss of stability after a certain critical prestrain is given by Laukonis (23) who, in a series of experiments based on the work of Hutchinson et al, considered the residual mechanical properties in tension at 0, 45 and 90 degrees to the original tensile axis. Those specimens at an angle to the original axis exhibit anomalously large flow stresses and, as with the earlier study, there is a rapid loss of residual uniform strain at about 7.5% prestrain (in the rolling direction). However, it can now be seen (Fig.11) that

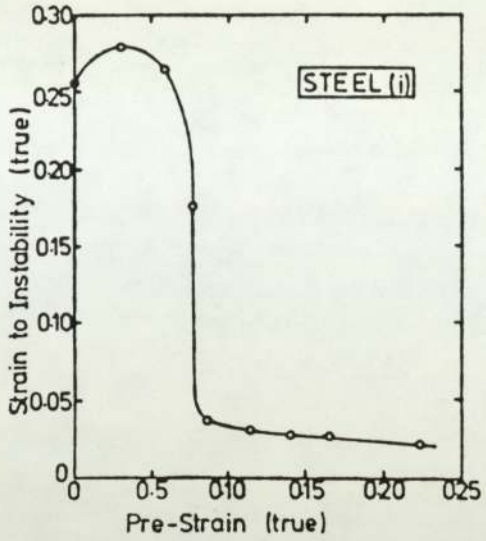

Fig. 10. Example of Premature Instability at a Critical Prestrain for a Steel Subjected to a Tensile-Tensile Strain-Path Change (the Second Stage being Orthogonnal to the First).

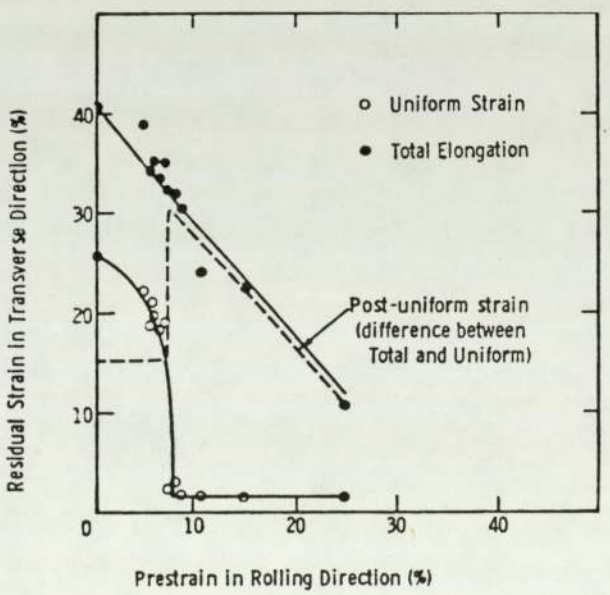

Fig. 11. Residual Elongations as a Function of Uniaxial Tensile Prestrain (Tested at 90 Degrees to Prestrain). Note the Increase in Post-Uniform Straining.

there is an associated increase in post-uniform strain. At this prestrain it was found that in a conventional tensile test the onset of visible localised necking occured at a higher strain than that corresponding to maximum load. By examining the strain distribution behaviour during the 45 and 90 degree tensile sequences it was found that strain localisation commences at strains considerably beyond maximum load. Hence, the apparently rapid increase in post-uniform strain really contains a signifcant percentage of uniform extension (contiuing after maximum load). To account for the continued uniformity of straining, a rapid increase in n-value (from $\sigma = K\varepsilon^{n}$) after maximum load is proposed for those prestrained by the critical amount. Extracting two sets of n-values from his results (tensile data extrapolated beyond maximum load on the basis of extended uniform straining), Laukonis indicates the possibilty of 'double-n' behaviour beyond a certain strain (see Fig.12). The diagram presented is based on several assumptions: firstly, the n-values near to maximum load are in fact true strain values at the point chosen and, due to inadequancies of the Ludwik equation etc., the true value of 'n' may differ from the strain value. Secondly, the n-values near to the onset of visible necking rely on accurate identification of the exact start of strain localisation. Also, the validity of uniform extension

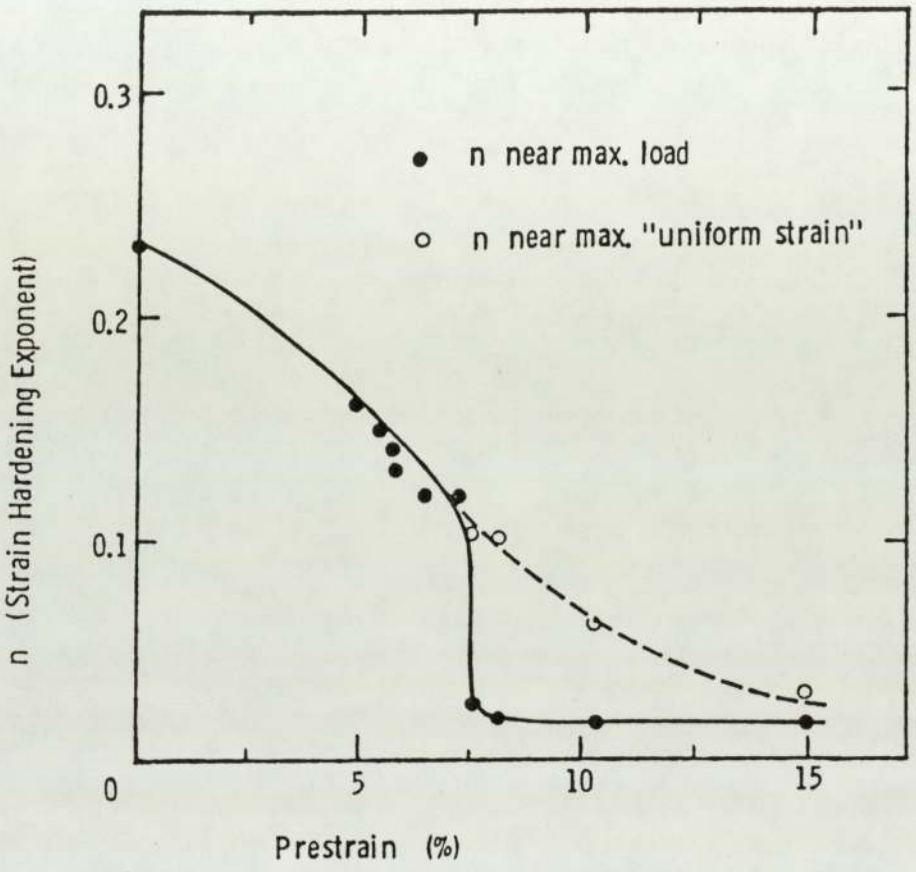

Fig. 12. Example of 'Double n' Behaviour in an Al-Killed Steel Subjected to Interrupted Tensile Testing (Second Stage Orthogonal to First).

after maximum load is implicit in extrapolating the tensile data. Bearing these reservations in mind, the 'double-n' behaviour illustrated is a plausible explanation of the observed behaviour.

Another possible combination of strain-path changes is uniaxial tension followed by biaxial stretching (eg: hydraulic bulging of prestrained tensile specimens). Several researchers have found that this particular combination increases the permissible surface limit strains, specifically for steels (17), (18). However, Ranta-Eskola (20) could not find any evidence to support this, although, as will be shown later, there is theoretical and microscopial support for such behaviour. Romano et al (17) found that an ε_1 strain gain of up to 100% was possible via this strain-path change (Fig.13). Likewise, Kleemola et al (18) found an increase in tensile limit strains (ie: for tensile minor strains).

Although other strain-path combinations are possible, there have been few published results. This is probably due to the difficulties in preparing usable specimens under these imposed strain-path combinations.

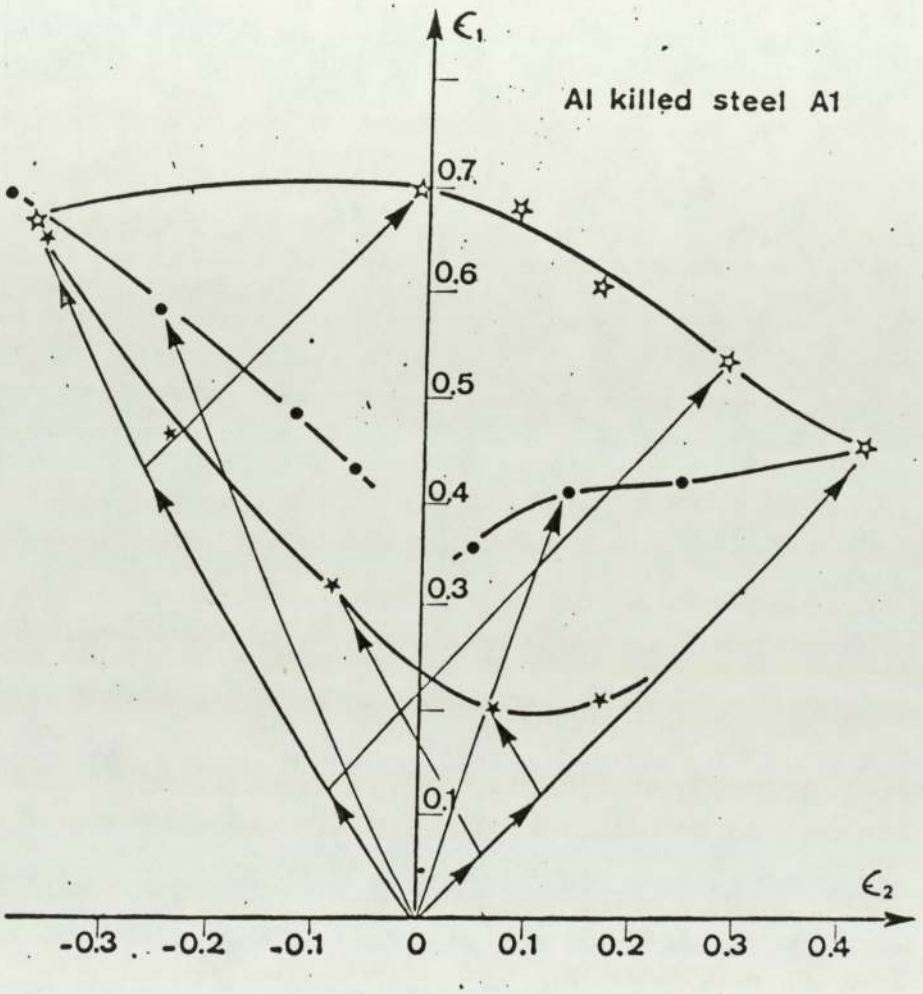

Fig. 13. FLD for an Al-Killed Steel Showing the Increase in Limit Strains Resulting from a Strain-Path Change from Tension to Biaxial Stretching.

1.4 Microstructual Changes and the Role of Anisotropy

In order to gain a fundemental understanding of the metallurgical factors influencing, or being influenced by, strain-path changes one must consider the roles of dislocation microstructure and preferred orientation.

Perhaps the simplest approach is to assume that the changes in work-hardening are a function of the number of active slip-systems during each stage of straining (21). Where the rate of work-hardening is low and premature instability occurs after prestraining, the number of active slip-systems during the second stage of deformation is restricted.

Several authors have attempted to correlate strain-path changes with changes in dislocation cell structures (17), (22), (24), (25), (26). While these studies yield valuable information with regard to understanding the processes at work, it is unwise to make generalisations on the basis of electron microscopial studies of this nature, due to the small areas of sample being observed: metallurgically interesting micrographs are not always representative. Despite this, some common threads are starting to emerge. If one considers tensile prestraining, the

initial cell structure is regular and prismatic (17) with poorly developed, thick cell walls. Ronde-Oustau and Baudelet (24) found that after about 10% strain the cell walls became better defined (thinner and denser), but less regular. After 30% deformation the dislocation density within the walls of the cell is higher, coupled with misalignment between neighbouring cells. However, for specimens prestrained in equi-biaxial tension, a 5% strain leads to a few poorly defined , equi-axed cells in a loose, disordered dislocation tangle. With increasing strain, misorientation between cells is low since the cell walls remain thick.

The dislocation structure produced by equi-biaxial deformation leads to short mean free paths of mobile dislocations preventing high strains in subsequent tensile deformation (since this needs long mean free paths). In contrast, the cell structure produced by uniaxial tension gives a mean free path at least equal to that required for a strain-path change to biaxial stretching, so high strains can be obtained in subsequent equi-biaxial deformation.

The onset of premature instability at low equi-biaxial prestrain appears to coincide with the formation of stable dislocation cells in the

prestraining, which subsequent tensile deformation cannot rearrange to allow high stresses or strains to be attained (24).

Little attention has been paid so far to the role of preferred orientation under conditions of changing prestrain-path. There is some mention in the literature of how a change in strain-path influences planar anisotropy (Δr-value) and normal anisotropy ($\bar{r}$-value). Hutchinson et al observed a significant increase in r-value with uniaxial prestrain in tension. Similarly, an increase in the degree of planar anisotropy has also been reported (20). However, there is one reported instance where biaxial prestrain produced a decrease in r-value with increasing prestrain (19). An increase in r-value is in agreement with the distortion of the yield locus discussed earlier.

The only work specifically attempting to relate the influence of various stress and strain-ratios upon preferred orientation is that by Grzesik and Vlad (27). The authors investigated the effect of a variety of strain-ratios (between equi-biaxial and pure uniaxial tension) on texture in a low C, deep-drawing quality steel and a micro-alloyed steel. Their most significant observation in the present context is that the highest degree of texture hardening results from

equi-biaxial prestrains due to the presence of {111} orientations in the sheet plane. Such a prestrain will lower the forming limit strains for subsequent strain-path changes. Once more, this is in agreement with earlier observations.

1.5 Summary

a). Prestraining distorts the yield locus.

b). The following general observations can be made about the effect of indirect strain-path combinations:-

BIAXIAL + UNIAXIAL TENSION

STEEL: LOWER FORMING LIMITS, HIGHER FLOW STRESSES, PREMATURE NECKING

BRASS: NO EFFECT OR AS FOR STEEL

Al : VARIES BY ALLOY AND TEMPER ETC.

UNIAXIAL + UNIAXIAL (45/90) TENSION

STEEL: AS ABOVE

Cu/BRASS: NO EFFECT OR HIGHER FORMING LIMITS, LOWER FLOW STRESSES, FLOW STABILISATION

Al : AS ABOVE

UNIAXIAL + BIAXIAL TENSION

STEEL: INCREASED SURFACE LIMIT STRAINS ON TENSILE SIDE OF FLD ETC.

Cu/BRASS: HIGHER FORMING LIMITS ETC.

Al : AS ABOVE

c). The uniform uniaxial strain of steel decreasees with all forms of prestrain.

d). Following equi-biaxial prestraining of steel (and some Al alloys there is an abrupt drop in the capacity for uniform strain in subsequent deformation after a critical prestrain.

e). Prestraining of steels leads to an increase in anisotropy.

The picture presented is one of a progressively changing dislocation microstrucure as the strain-path changes, with the amount of slip on each active slip-system also varying gradually. The variation in subsequent flow behaviour and formability would appear to be a function of the ability of successive modes to modify the dislocation microstructure left by the previous stage. This determines the residual mechanical properties.

1.6 Areas for Investigation Arising from Literature Review

The preceeding sections have shown how published research has concentrated on Al-killed, low-C steels, various brasses and a selection of formable aluminium alloys ie: the traditional choices for metal-forming operations. However, as stated in the introduction, there is currently much interest in formable, high strength steels (HSS), which have only become available on a commercial scale in the last few years. Automobile manufacturers are the driving force behind much of the research into HSS, since they are the volume consumers of sheet metals.

Davies and Easterlow (43) have reviewed the trends in material selection for automobile bodies and have concluded that mild steels will continue to dominate body manufacture until tool design and manufacturing processes are developed sufficiently to take advantage of alternative materials such as HSS, aluminium and composites. The high cost of aluminium alloys and composites will prevent their widespread useage for the foreseeable future and so HSS are regarded as the only immediate choice for weight reduction in sheet-metal structures. Hence, the practical content of this thesis will concentrate on HSS, using a conventional body steel for comparison.

The principal classes of high strength steel are:-

a). High Strength Low-Alloy (HSLA).

b). Dual-Phase.

c). Re-Phosphorised.

A full discussion of the physical metallurgy of these steels can be found in reference 32.

High strength, low-alloy steels (often referred to as micro-alloyed steels) possess relatively poor formability, but high strength. This strength is

obtained by a combination of precipitation hardening and grain-size control, by additions of V or Nb. Since these steels are not usually used in applications where extensive formability is the primary requisite, an example will not be included in this study.

Dual-phase steels offer high strength combined with better formability than the HSLA family of steels. These properties are a function of a microstructure composed of martensite islands dispersed in a matrix of ferrite. Such a structure is produced by an intercritical quench, but expensive alloying elements may be needed to lower the critical cooling velocity sufficiently for martensite to be formed (this is determined by the processing plant available). Despite a cost penalty, these steels are very much favoured by the worlds' automotive manufacturers for large body-pressings, such as floor-pans etc. An example of this class of steels will be included in the practical content of this thesis.

Re-phosphorised grades are a cheap alternative to the other grades discussed and are already used in large quantities by some manufacturers. Relatively high P levels, in a mild steel base, lead to a large increase in the plastic strain-ratio, as measured in the tensile test. This, coupled with strength levels

similar to dual-phase steels, means that these steels are suitable for those applications where a large drawing-ratio is necessary, and where a high yield strength in the final component is an important design factor. A re-phosphorised steel will be used in this study.

A more detailed discussion of the individual grades chosen is given in the following chapter.

Until recently, the majority of authors researching the effect of strain-path changes on formability have concentrated on experimentally obtained forming limit diagrams. However, in order to more clearly understand the physical processes at work, it is better to use the many parameters available from a uniaxial tension test, after a prestrain has been applied to the sample. In particular, data concerning the effect of prestraining on the work-hardening rates in subsequent testing has not been fully explored, even for mild steels. Likewise, the effect of a strain-path change on the plastic strain-ratio or r-value should be examined in greater detail. This approach also has the advantage that the strength and formabiltity data obtained can be incorporated into the constitutive models used as the basis of computer-aided tool design and for the theoretical derivation of forming limit

diagrams. This in turn will aid in the adaptation of knowledge obtained from studies of Al-killed steels into the context of the HSS.

Uniaxial tensile and biaxial prestrains have been used for Al-killed, low-C steels, but not for the HSS listed above. Little has been published on the effect of plane-strain prestrain on subsequent properties in conventional steels, let alone dual-phase or re-phosphorised steels. Since these three strain-path changes represent many of those found in actual sheet-forming operations, they will form the basis of the practical work performed in this study.

There is much to be gained from electron microscopial studies of dislocation microstructures, before and after a strain-path change. However, the amount of work, and the difficulties often experienced in interpretation of Transmission Electron Micrographs, would not allow the completion of the mechanical testing requirements of this project. Similar arguments apply to the generation of pole figures or orientation distribution functions for the study of texture changes: approximation by the plastic strain-ratio does not reveal as much about the processes at work, but does allow a wide range of prestrain combinations to be examined.

To summarise, it is proposed to compare and contrast the effect of a wide range of strain-path changes on three steels: an Al-killed, deep-drawing quality steel and two HSS. The strength and formability data produced will be of use to those researchers involved in the evaluation of HSS for large scale pressings and in the modelling of sheet-forming processes. Observed behaviour will be explained from a dislocation theory viewpoint.

CHAPTER 2

Experimental Procedure

2.1 Materials

The bulk of the literature so far has related to the low C steels used for most press-forming applications. In this study it is intended to extend the range to cover two additional classes of formable steel, which are of current interest, namely dual-phase and re-phosphorised grades. A conventional low-C steel has been included as a control.

British Leyland Technology supplied a quantity of each of the following grades of steel:-

ORIGIN	GRADE	GAUGE	CLASS
British Steel Corp.	CR1	0.80mm	Conventional
---------"---------	REPHOS	0.71mm	Re-phosphorised
Kawasaki Steel Corp.	CHLY40	0.71mm	Dual-Phase

Table 1. contains the chemical analyses obtained from samples of each steel. Below is a brief description of the major attributes of each of these

Steel	Major Alloying Elements (Wt. %)							
	C	Mn	Ni	Cr	S	P	Si	Al
CR1	0.06	0.25	0.03	0.02	0.016	0.012	0.02	0.030
REPHOS	0.08	0.33	0.01	0.02	0.018	0.087	0.01	-
CHLY40	0.05	1.21	0.04	0.57	0.007	0.017	0.05	0.055

Notes: a). A blank entry means no analysis available.
b). All of the quoted results are averages of spectrographic and 'wet' results.
c). Mo, V, Ti all less than 0.01%

Table 1. Chemical Analyses for the Three Steels Used.

Steel	Average in Rolling Direction (um)	Average in Through Thickness Direction (um)	c/a Ratio
CR1	11.0	16.7	0.66
REPHOS	9.4	37.5	0.25
CHLY40	5.4	6.4	0.83

Notes: a). The values quoted are the average of 5 line counts.
b). A low c/a ratio indicates a large degree of cold-work.

Table 2. Measured Grain-sizes for the Steels used.

materials:-

CR1

This is a fairly typical cold-rolled, low C, Al-killed deep-drawing quality steel. The microstructure (see fig.14) is a matrix of ferrite with finely dispersed carbide (lamellar pearlite cannot exist at these low C levels). Common applications for this steel include automobile door skins where the drawing ratio required is quite severe.

REPHOS

Normally, P is not associated with favourable effects on ferrous properties. However, in these steels the P is added as a solution strengthening agent at about five times the level normally found in formable grades of steel. This results in higher strength levels than the conventional steels and also results in enhanced r-values (frequently greater than 2.5). Once more, the microstructure is ferrite and dispersed carbide (fig.15).

CHLY40

This steel is the lowest strength variant in a family of dual-phase steels offered by Kawasaki. All of these steels are the product of an intercritical anneal after, usually, continuous annealing (gas or water jets are commonly used). The high Mn/Cr chemistry of this steel reduces the critical cooling velocity needed for 'dual-phasing'. The folowing features characterise dual-phase steels:-

a). A microstructure of martensite islands in a ferrite matrix. The percentage martensite determines strength level by a dispersion hardening type mechanism. CHLY40 has about 5% second phase (see fig.16).
b). Continuous yielding curves.
c). Low yield to tensile ratios (about 50%).
d). High ductility coupled with high strength levels.
e). r-values approximately 1.0
f). High n-values, particularly at low strains (good strain distributing ability).

The re-phosphorised steel and the dual-phase steel have similar strength levels, although the

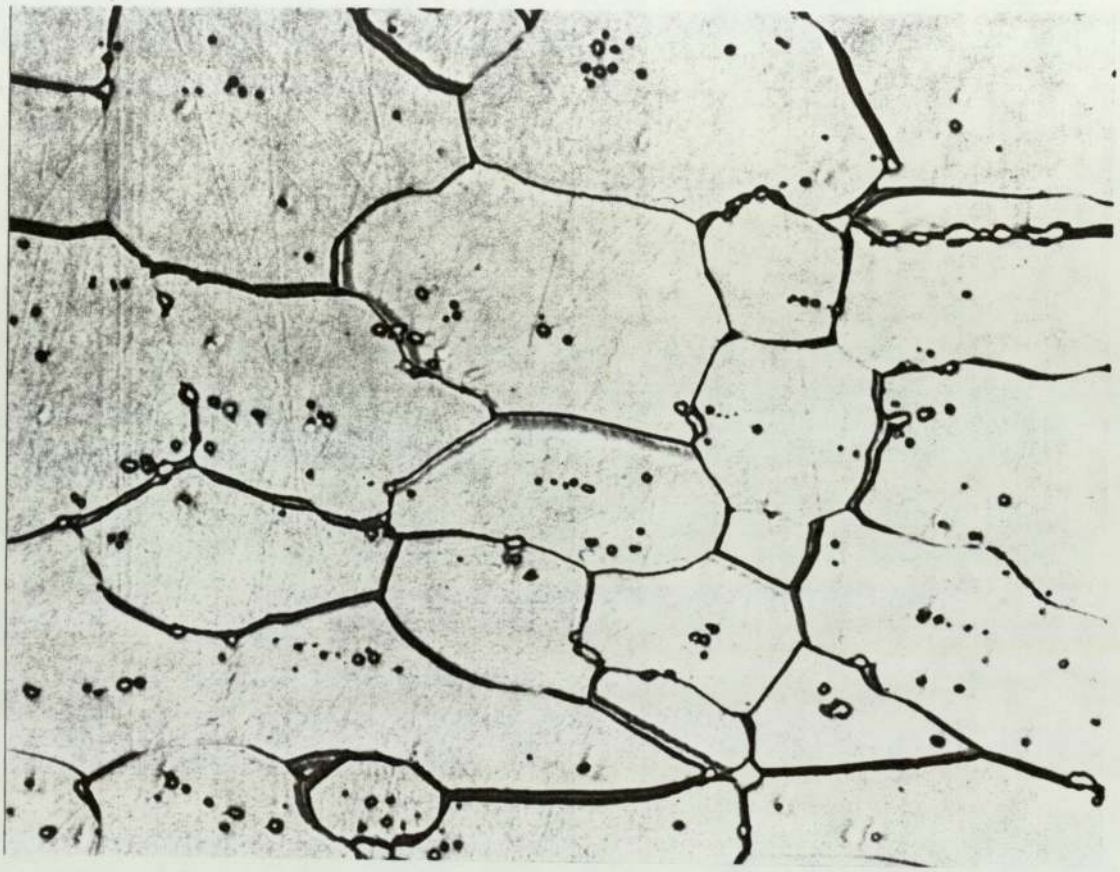

Fig. 14. Optical Micrograph of CR1 (Al-Killed, Low-C Steel). Etched in Nital, X2000.

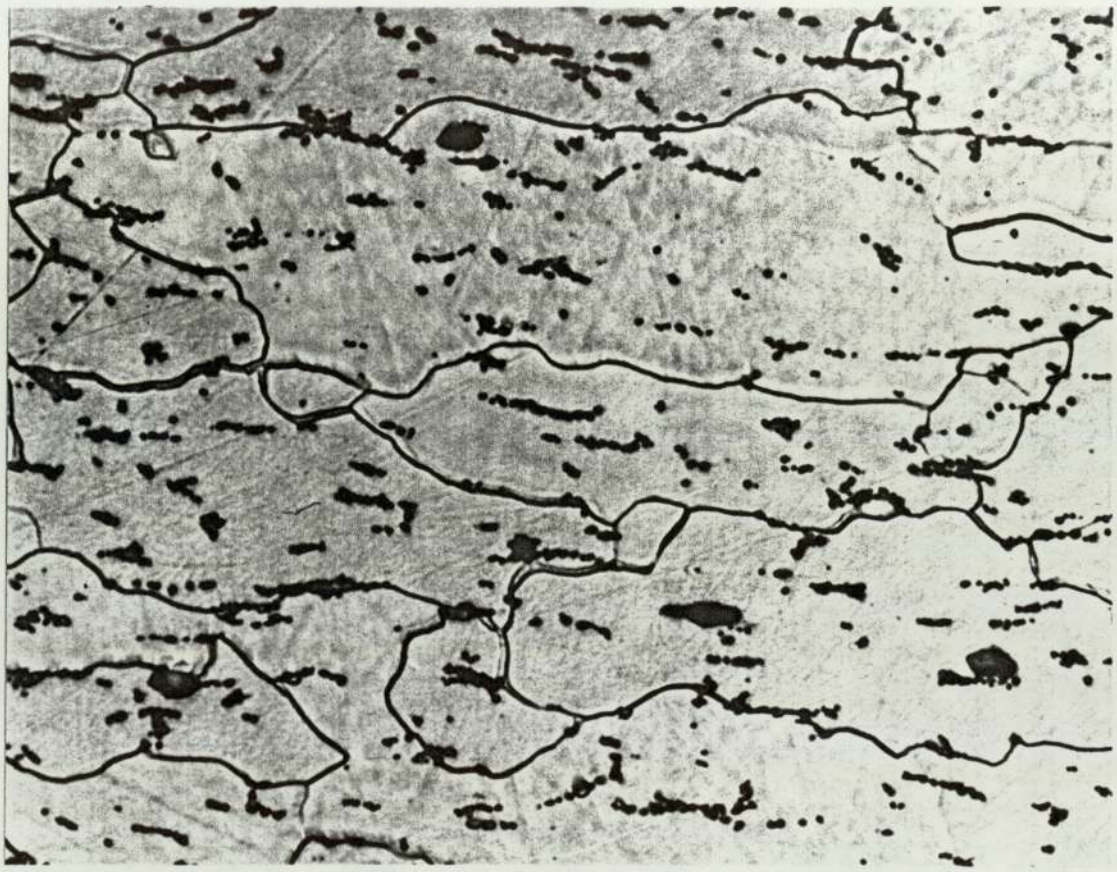

Fig. 15. Optical Micrograph of BSC Rephos' (a Rephosphorised Steel). Etched in Nital, X2000.

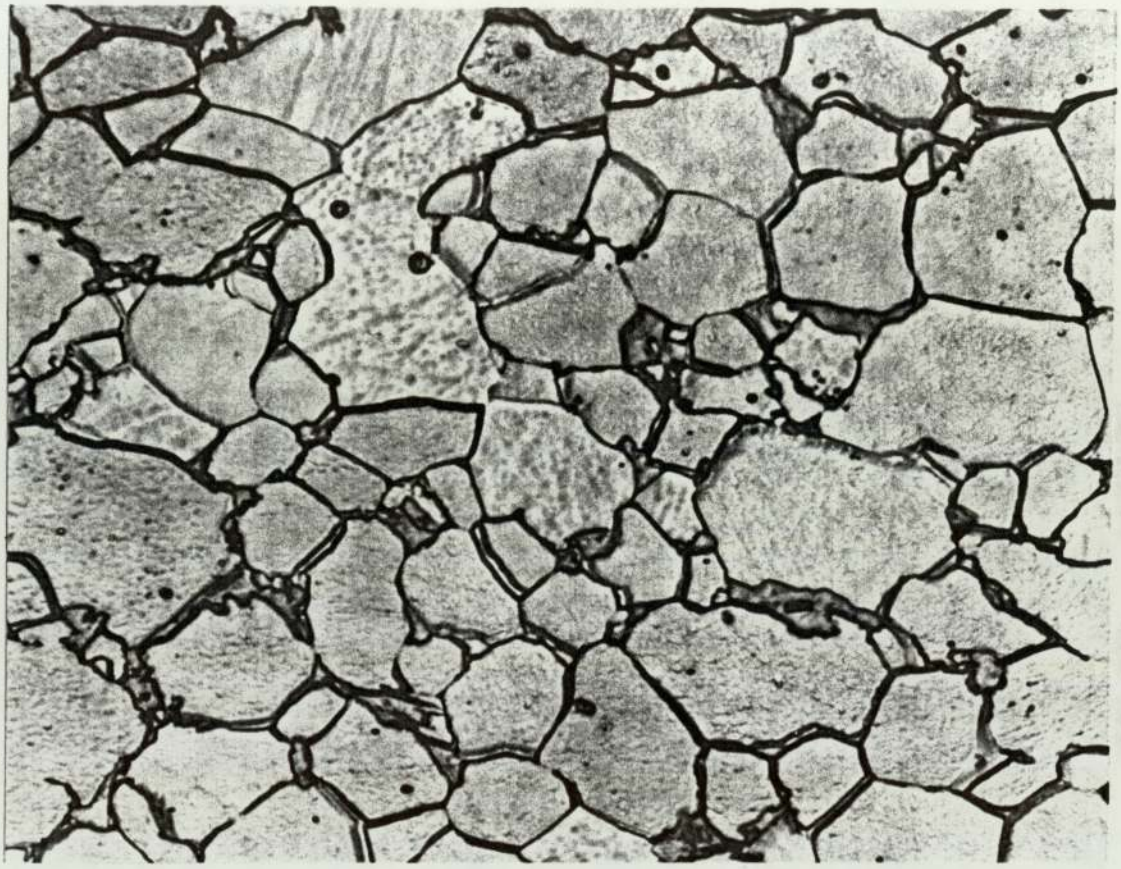

Fig. 16. Optical Micrograph of CHLY40 (a Dual-Phase Steel). Note the Small Volume Fraction of Martensite Islands. Etched in Nital, X2000.

hardening mechanisms are different.

Table 2. gives grain-size data for the three grades. CR1 and REPHOS are similar, with 'pancake' shaped ferrite grains (more so in the case of REPHOS). On the other hand, the dual-phase steel is much finer grained, with the grains being equi-axed.

For the remainder of this text the above steels will be referred to by the following abreviations:-

CR1	AK
REPHOS	RP
CHLY40	DP

2.2 Prestraining Operations

The following prestrain paths were chosen on the basis of the available load-frames:-

i). Uniaxial

ii). Biaxial

iii). Plane Strain

2.2.1 Uniaxial Tension

Simple tensile prestraining was carried out on a 50 tonne Instron load frame (screw-driven). The specimen used is shown in Figure 17. and is essentially an oversized, parallel-sided tensile specimen (515mm long by 150mm wide) with a useable 315mm gauge length available. After straining, further test specimens could be machined at various angles to the prestrain.

Each blank was coated with Engineers' Blue and lightly scribed with 25mm squares to be used for prestrain determination: the percentage extension was based on a 150mm gauge length located midway between the grips. This gauge length and extension was measured with dividers to an accuracy of within 1.0mm while prestraining. The quoted prestrain is an average of four results across the width measured on a travelling microscope to within 0.5mm (ie: a reported elongation of 10% is actually plus or minus 0.3% at worst). As an additional check on the prestrain accuracy the prestrain load was recorded and used for a cross-check via the Holloman/Ludwick power law.

Testing took place at a constant cross-head displacement rate of 10mm/min (equivalent to strain rate of approx. 0.0005 per second).

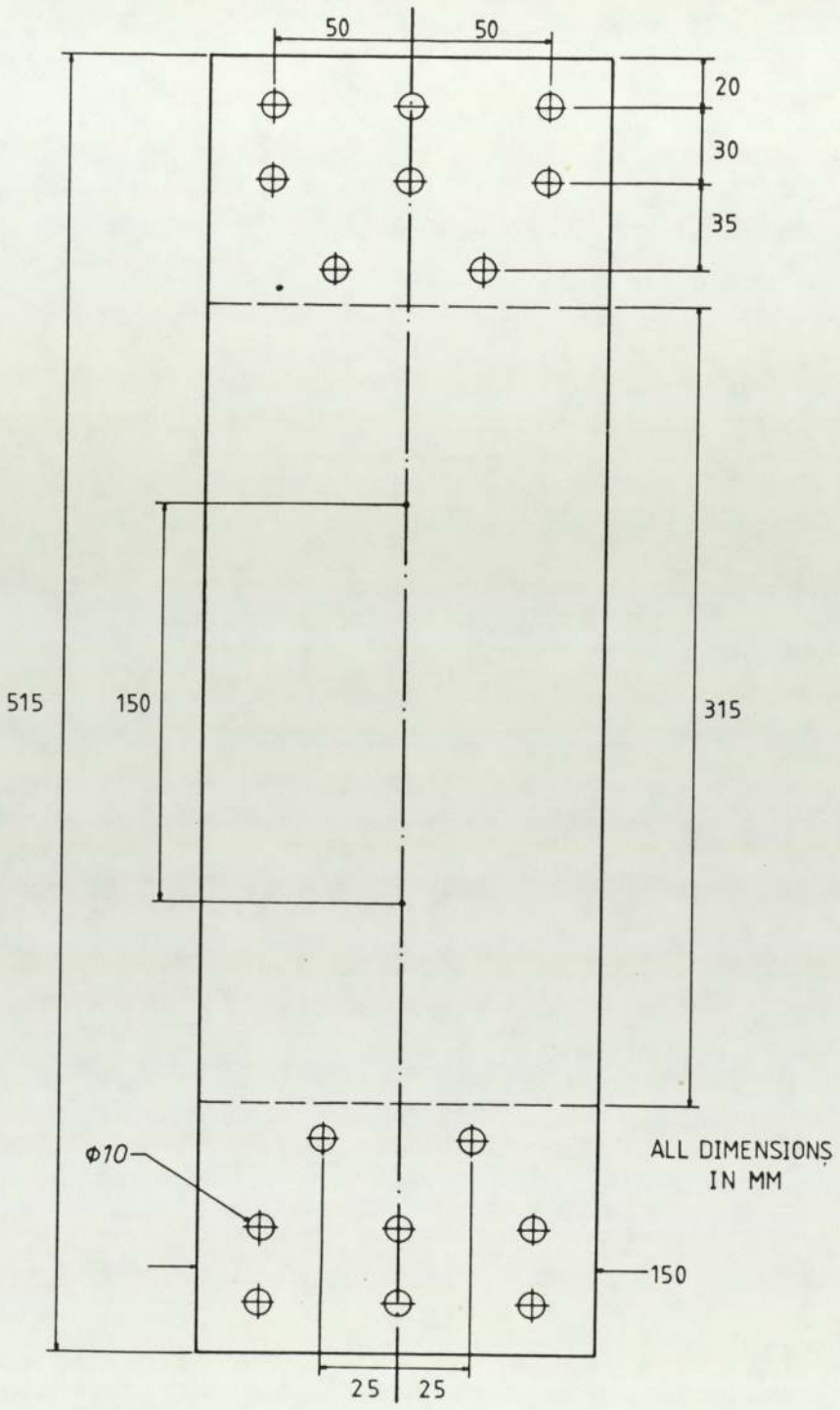

Fig. 17. Oversized Tensile Blank used for Uniaxial Prestraining. Clamping is Achieved by Bolting the Grips onto the Blank.

Initially, two blanks were prestrained transverse to the rolling direction at each of the following levels (for all three steels):-

2.5, 5.0, 7.5, 10.0, 15.0, over 15.0%

After studying the results, or where extra material was required, fresh samples were prepared. The choice of prestrains was taken from the literature.

2.2.2 Equi-biaxial Stretching

Equi-biaxial stretching of clamped specimens was performed on a 100 tonne Mayes hydraulic load-frame. A hollow, flat-nosed punch of circular cross-section (225mm diameter) was used to generate a blank large enough for subsequent tensile specimens to be cut from it (a 150mm diameter was useable after the prestrain). Figure 18. shows the Mayes machine, while Figure 19. gives a more detailed view of the clamping arrangement and the punch profile. Polythene and grease was used for lubrication, and in all cases the sheet surfaces were free from contact with the tooling.

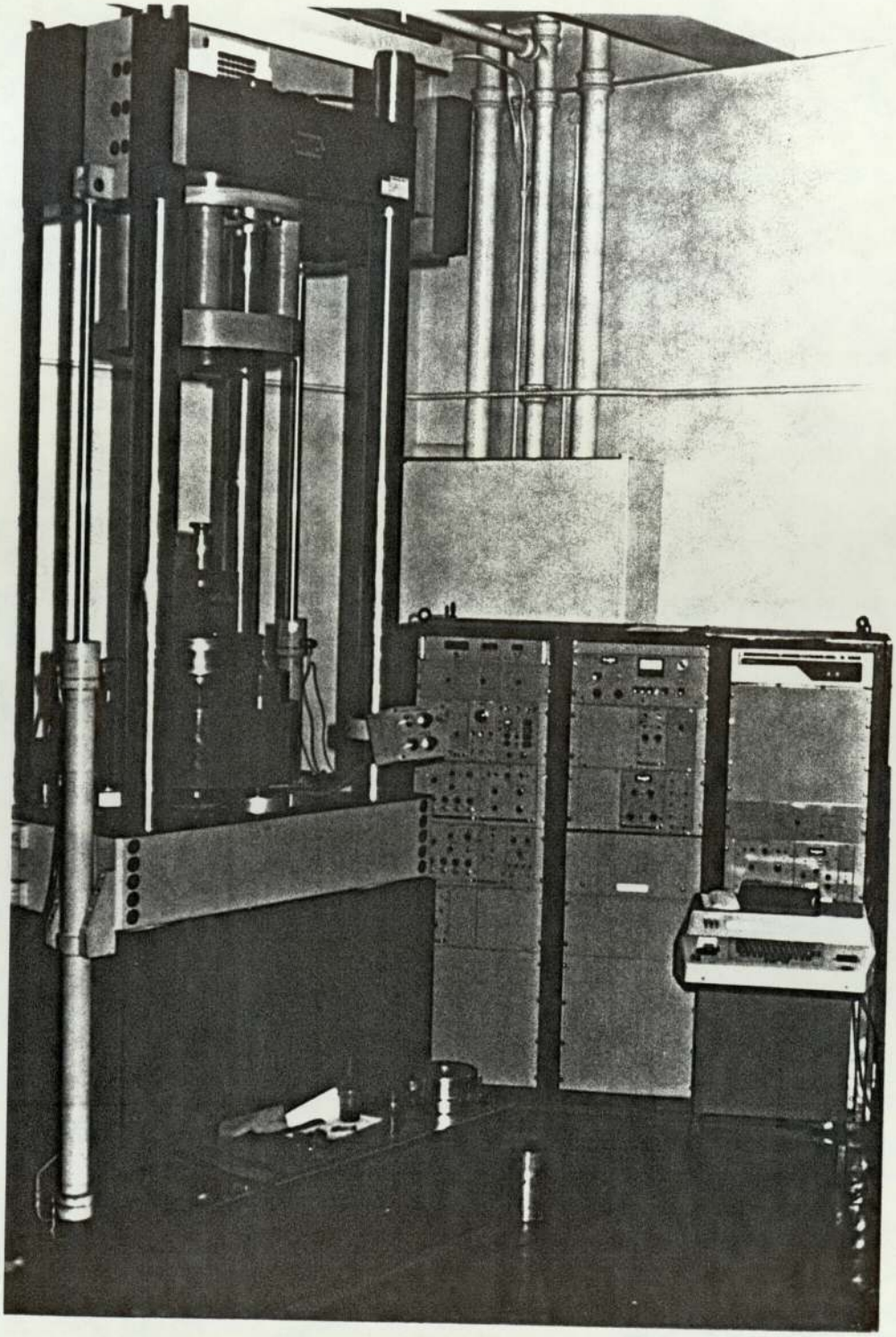

Fig. 18. The Mayes 100 Tonne Hydraulic Press. This is a Four-Post Machine. Note the DEC PDP-11 Computer used for Control Purposes.

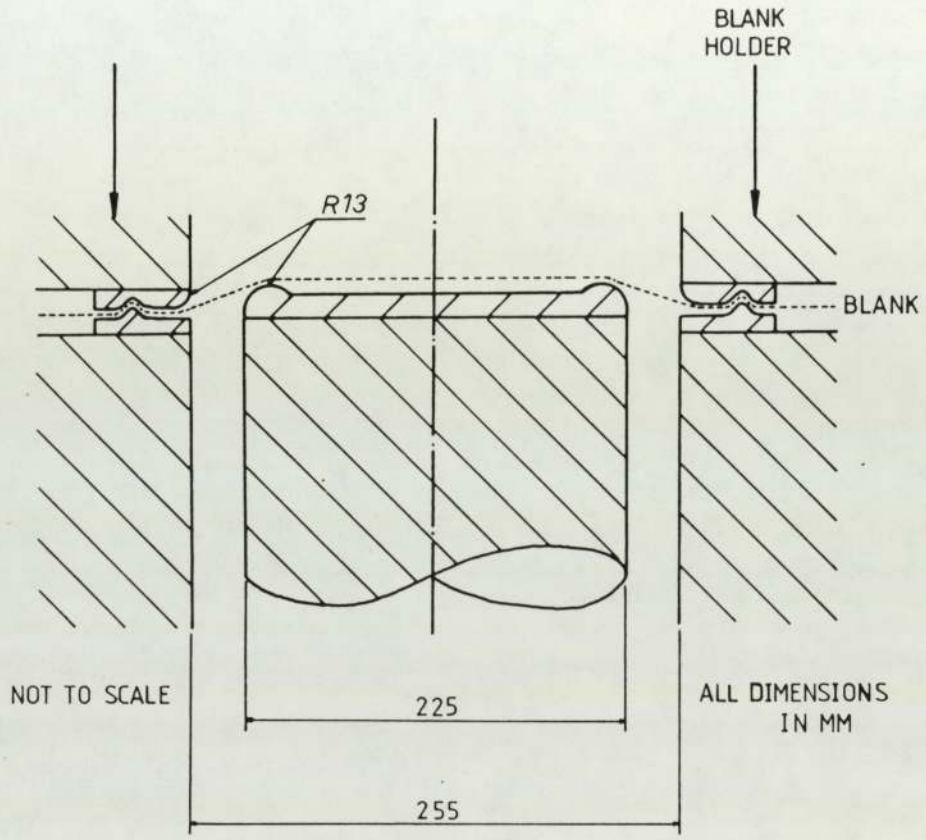

Fig. 19. Close-Up of Biaxial-Stretching Tooling (this Type of Tooling is Often Referred to as 'Marciniak Tooling').

As with the simple tension specimens each blank was pre-gridded with 25mm squares for strain determination and the same accuracy criteria apply. Again, a 150mm gauge length was used, the quoted strains being averages of four measurements (two in the rolling direction and two transverse). The clamping load was constant at 20kN throughout the tests since this allowed high prestrains to be reached while still producing a satisfactory blank.

A punch displacement rate of between 5 and 10mm/min was used for each blank.

In order for comparisons to be drawn between the different prestrains, it is necessary to employ the concept of effective strain, as defined earlier according to von Mises, for non-uniaxial states. Hence, the true effective prestrain in equi-biaxial tension is twice the linear strain measured across the blank. Bearing this in mind, the selection of effective prestrains was chosen based on the uniaxial results for each material.

Once more, duplicate specimens were prepared where possible.

2.2.3 Plane Strain

The specimens used for this prestrain mode were box-sections constructed from two of the simple tension specimens welded along each edge. An internal former (see Fig. 20) prevented lateral contraction. Once more, the 50 tonne Instron was used for prestraining. Unfortunately, difficulties in alignment betwen the two sides of the box meant that only one of the two was suitable for further straining. Care was taken when welding not to heat-up the gauge lengths and introduce ageing effects or distortion.

The same gridding procedure was employed for these samples and the true effective prestrain calculated from the linear strain using von Mises (ie: true effective strain is 15.5% above the linear strain). Again, prestrain determination was based upon repeat measurements.

As for the simple tension blanks, a prestrain transverse to the rolling direction of the sheet was used. The prestrain levels were chosen to coincide with the previous prestrain modes.

Where needed, duplicate blanks were prepared as before.

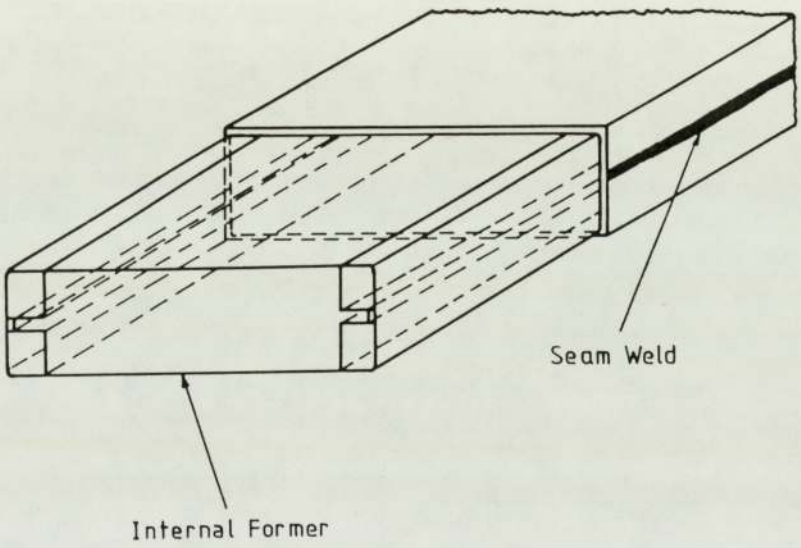

Fig. 20. Exploded View of Plane-Strain Arrangement. Two Oversized Tensile Blanks are MIG Welded Together and an Internal Former Inserted to Prevent Lateral Contraction.

2.3 Handling after Prestraining

It is well known that prestraining can result in a return of the yield point after room temperature ageing, even in Al-killed steels. This is a particular worry in the case of the plane-strain blanks where there may have been localised heating during welding. To minimise ageing effects all blanks were kept at -30 degrees C between each stage in specimen production and testing.

2.4 Subsequent Tensile Testing

Standard ASTM E-8 tensile specimens with a gauge length of 50mm and width of 12.7mm (see Fig.21) were machined from the as-received sheets and from the prestrained blanks at various angles to the prestrain according to the cutting patterns shown in Figure 22. and the table below:-

Steel	Prestrain	Angle of Subsequent Tensile Tests
AK, RP	UNIAXIAL	0, 15, 30, 45, 60, 75, 90
DP	----"---	0, 45, 90
AK, RP, DP	BIAXIAL	ROLLING DIRECTION
AK, RP, DP	PLANE STRAIN	0, 45, 90

Please note that the angles given above are relative to a transverse (TD) prestrain in the uniaxial and plane-strain cases (ie: a subsequent angle of 90 degrees is in the rolling direction of the sheet, orthogonal to the prestrain).

These second-stage tensile tests were carried out on a 20 tonne Zwick load-frame (screw-driven) located at British Leyland Technology, Cowley. A cross-head speed of 10mm/min was used once again (a strain-rate of approx. 0.003 per second).

The Zwick offers many special facilities for the testing of sheet metal specimens. Premier among these is the provision of both length and width extensometry, allowing direct r-value measurement. The length extensometer measures over a nominal 50mm gauge length and the width extensometer operates over a 35mm contact

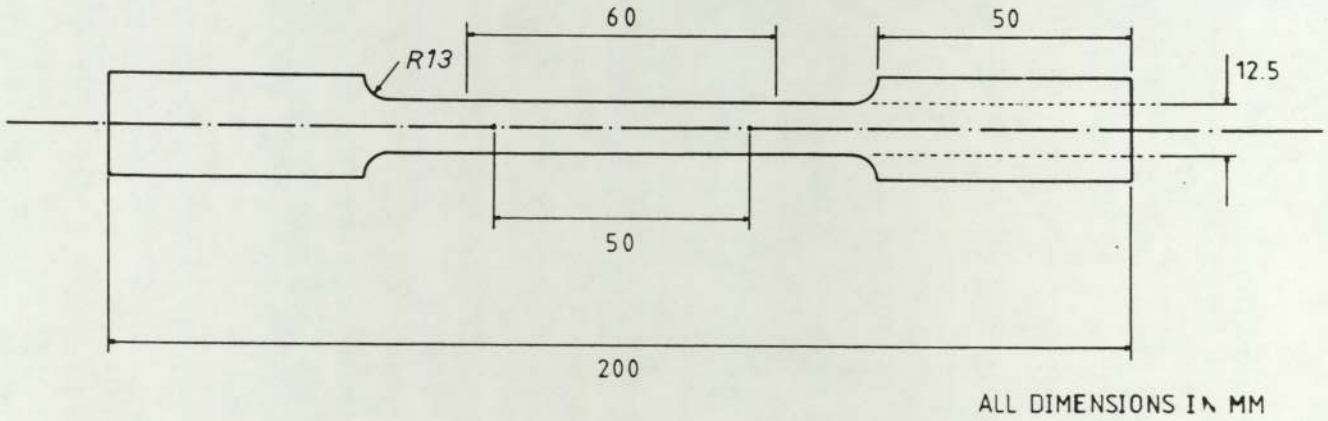

Fig. 21. ASTM-E8 Tension Specimen for Sheet Metals (50mm Longitudinal Gauge Length).

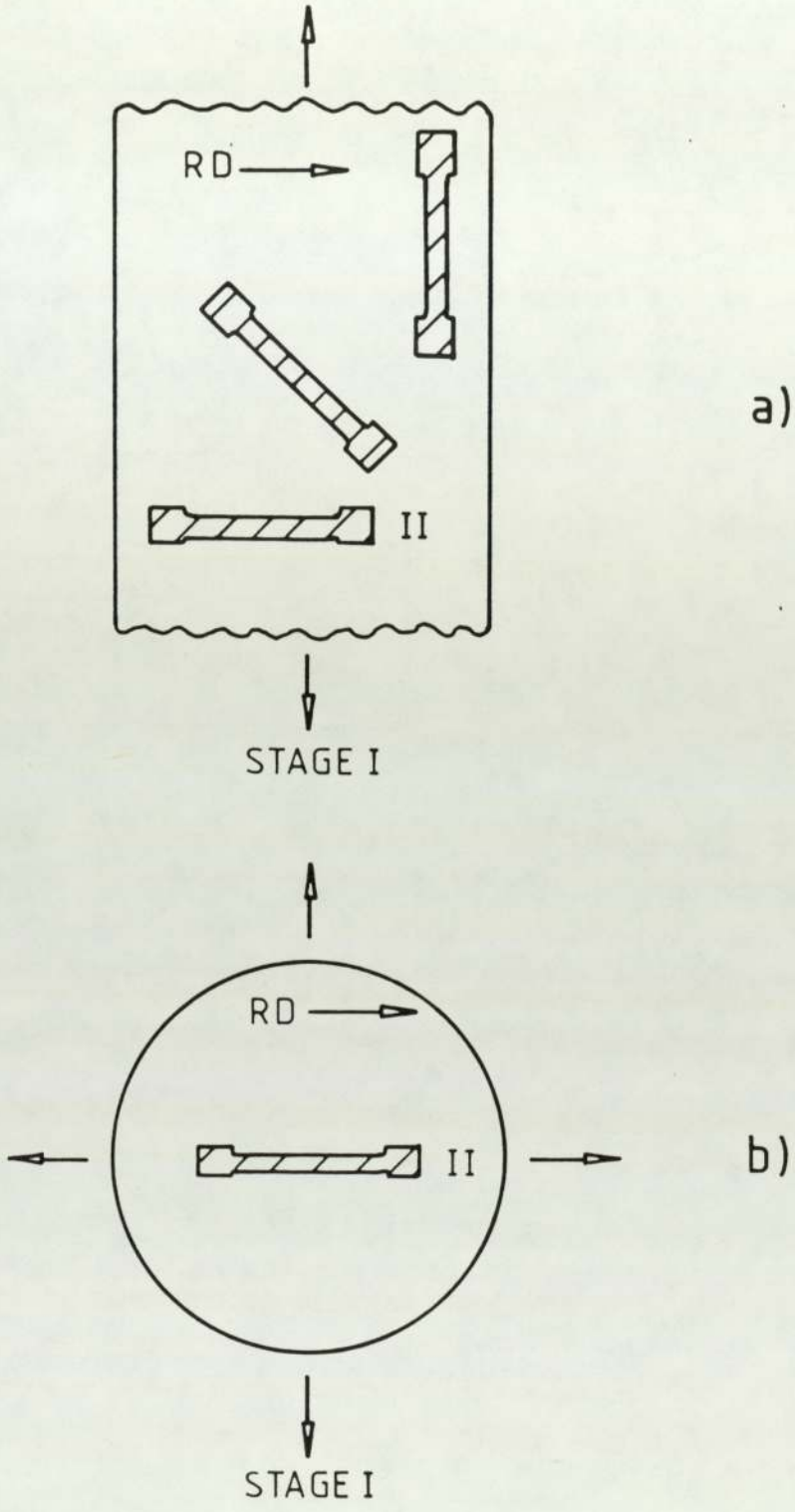

Fig. 22. Schematic Indicating the Prestrain Direction (Stage I) and the Direction of Subsequent Tensile Tests (Stage II) for:-
a). Uniaxial and Plane-Strain Prestrain
b). Equi-Biaxial Prestrain.

length within the main gauge length. Microprocessor control gives direct readout of the following parameters:-

a). 0.2% Proof Stress

b). 0.5% Proof Stress

c). Maximum Stress or UTS

d). Extension to maximum load

e). Total elongation

f). r-values at up to 8 strains during test

g). n-values at the same strains as above

A permanent, printed record is produced for each test as well as load-extension and width extension-length extension curves on a Hewlett-Packard digital X-Y plotter. The machine calculates the r and n-values according to the following relationships:-

$$r = \frac{\ln \frac{b}{(b - \Delta b)}}{\ln \frac{(L + \Delta L)(b - \Delta b)}{L \cdot b}}$$

, where b = initial width

L = gauge length

b = width

Δb = change in width

ΔL = change in length

$$n = \frac{\ln \frac{(1+e_2)}{(1+e_1)} + \ln \frac{p_2}{p_1}}{\ln \frac{\ln (1+e_2)}{\ln (1+e_1)}}$$

, where e_1 , = preset strains e_2

p_1 , = loads at p_2 e_1 , e_2

At least two replicate tensile tests were performed for each of the steel-prestrain-tensile combinations given above.

2.4.1 Processing of Load-Extension Data

Usually, the conversion of a large number of load-extension curves to flow curves and calculation of various parameters is very time consuming. To alleviate this problem the author has written a suite of programs for use on a Tektronix 4052A graphics workstation in conjuction with a digitising tablet and a graph plotter which improve productivity and enhance the quality of the information extracted.

Schematically, the interpretation process becomes:-

a). Perform the tensile test

b). Lay load-extension graph on digitising tablet and digitise the curve(s) using a program called 'DIGICURVE'. Output from this program

is a file of load-extension points with identifying information and a printout of the following:-

i). Identity

ii). Nominal stress-strain

iii). True stress-strain

iv). n and K from the power hardening law (from a log-log regression)

v). The degree of fit to the power law

c). Plot the stress-strain curve.

Since the data is available as a tape or disk file it is a simple matter to enter the results into other programs for further processing. A typical example of this is the production of work-hardening curves from the true stress-strain data. For the purposes of this study two such programs were used for extracting the work-hardening data and instantaneous-n values:-

1). A simple program which differentiates the flow curve data after a five point parabolic smoothing. This program was written for the Tektronix by the author.

2). A more complex program on the Aston Univ. Harris H800 super-minicomputer which uses cubic splines to achieve smoothing before differentiating. This program was based on

an original written by Dr. P. Bate,
presently at Birmingham University.

Both of these programs give work-hardening rate and instantaneous-n as a function of strain during the tensile test. This replaces the manual technique of drawing tangents to the flow-curve, which usually gives a very 'lumpy' work-hardening curve due the failings of the human eye. Most of the curves produced for this thesis came out of the first program (source code listed in Appendix 2). However, certain shapes of flow curve (particularly those after severe prestrains) gave more consistent results when processed by the second program. To facilitate the use of this program, the author has written a file transfer utility from the Tek' to the H800 and vice versa to save re-typing of the data.

The main advantage of this approach to stress-strain curve analysis is the accuracy and repeatability of the measurements made, combined with speed: on the charts produced from the Zwick the limiting factor is the thickness of the pens used on the chart recorder (ie: typically, stresses to within 1MPa and strains to plus or minus 0.05% at worst). Obviously, if high scale magnifications are used the manual technique can equal this, but still requires considerably more time for a similar analysis.

2.5 Miscellaneous Tests

As well as the tests mentioned above, some extra data was generated from the as-received sheets for background information.

2.5.1 Forming Limit Diagrams

For steels RP and DP simple FLDs were constructed by the method of Nakazima (29). This involves fracturing accurately photogridded, parallel-sided strips of varying width over a solid punch giving the variation in strain-state needed to plot the FLD.

Nine strips varying from 25mm to 127mm wide were prepared for each steel across the rolling direction and gridded with 1.93mm diameter circles. Each strip was then tested to failure on a Hill-Wallis hydraulic press. A 50mm die-set was used, and the blank-holder pressure controlled to moderate the tendency to draw-in. No lubrication was used.

Three circles close to the point of failure (but not containning localised necking) were measured in major and minor directions to estimate the limit strains. Measurements were accurate to within 0.01mm.

These measurements provide the basis for the FLD.

In the case of steel AK, a standard FLD used by Pressed Steel at Cowley for many years (and based on a very large number of results) was used.

2.5.2 Pole Figures

Pole figures are one of the commonest methods for graphically depicting the distribution of crystallographic directions in polycrystalline aggregates. A full description of these simple stereographic projections is outside the context of this text, but most metallurgical text-books have sections devoted to X-ray crystallographic methods (the monograph by Hatherly and Hutchinson (30) carries a particularly complete treatment of the subject).

For present purposes incomplete pole figues by the Scultz Reflection Technique are considered adequate (31). This requires a specimen approximately 25mm square and no less than 0.2mm thick. The coupon for each steel was ground down on one face to within about 0.2mm of the centreline. The remaining material was then removed chemically (a 5% sulphuric acid saturated with oxalic acid-peroxide etchant) to give a

scratch free surface to prevent interference with the diffracting beam.

A Siemens X-ray diffraction set was used to produce an intensity profile for a (200) reflection for each steel. From the chart-recorder output the pole figure is plotted. Before running the actual samples, a (200) steel random sample (without texture) was run to provide for defocussing correction and to act as a reference level (ie: a 1 random level region on the pole figure is depleted in poles).

Plotting of the pole figures was performed manually according to the technique described in reference 30.

CHAPTER 3

Results and Observations

3.1 Comparison of As-Received Properties

3.1.1 Tensile

Tables 3-5. contain the various parameters obtained from the tensile tests on all three steels. As can be seen, steels RP and DP have similar tensile strengths about 30-40% higher than CR1. However, the dual-phase steel has a much lower proof stress than the re-phosphorised grade, reflected in the typical yield strength/tensile strength ratios:-

AK	56%
RP	63%
DP	52%

A low value is usually desireable for forming operations.

Steel AK has the highest uniform and total

Dirn. to RD	0.2% Proof Stress (MPa)	UTS (MPa)	Uniform Elongn. (%)	Total Elongn. (%)	n	K (MPa)	r
0	177	309	24.9	42.6	0.242	560.8	1.72
15	175	310	23.1	40.8	0.242	564.3	1.54
30	176	313	22.9	40.1	0.241	568.0	1.42
45	178	319	22.6	39.8	0.239	576.0	1.38
60	183	322	21.2	39.9	0.238	573.8	1.22
75	169	312	23.0	40.6	0.236	563.4	1.70
90	170	308	23.0	41.4	0.238	556.5	2.10

Notes: a). Above results are averages of at least two specimens.
b). Elongations measured over 50mm gauge length.
c). r-values are quoted at 15% nominal strain.
d). From the above data:-

$$\bar{r} = 1.64$$
$$\Delta r = 0.53$$

Table 3. Tensile Properties for Steel AK As-Received.

Dirn. to RD	0.2% Proof Stress (MPa)	UTS (MPa)	Uniform Elongn. (%)	Total Elongn. (%)	n	K (MPa)	r
0	256	410	19.9	32.6	0.192	682.7	1.94
15	261	412	19.0	31.5	0.189	685.0	1.78
30	266	419	18.6	31.0	0.186	691.7	1.62
45	276	429	17.3	29.9	0.184	705.0	1.42
60	279	428	17.3	29.4	0.184	693.2	1.42
75	265	415	17.9	31.6	0.189	675.6	1.89
90	254	410	18.4	33.2	0.179	665.0	2.18

Notes: a). Above results are averages of at least two specimens.
b). Elongations measured over 50mm gauge length.
c). r-values are quoted at 15% nominal strain.
d). From the above data:-

$$\bar{r} = 1.74$$
$$\Delta r = 0.64$$

Table 4. Tensile Properties for Steel RP As-Received.

Dirn. to RD	0.2% Proof Stress (MPa)	UTS (MPa)	Uniform Elongn. (%)	Total Elongn. (%)	n	K (MPa)	r
0	236	445	19.8	33.9	0.263	848.4	1.23
45	239	454	19.8	33.4	0.261	863.1	1.03
90	225	443	21.7	36.3	0.259	840.4	1.43

Notes: a). Above results are averages of at least two specimens.
b). Elongations measured over 50mm gauge length.
c). r-values are quoted at 15% nominal strain.
d). From the above data:-

$$\bar{r} = 1.18$$
$$\Delta r = 0.30$$

Table 5. Tensile Properties for Steel DP As-Received.

elongations as would be expected from its lower proof and ultimate values. Of the two higher strength steels, DP is slightly superior, particularly with respect to uniform extension. This is reflected by the n-values obtained which rank RP the worst and DP the best. It should be noted that there is good agreement between the true uniform extension and n-value except in the case of steel DP which infers that the Holloman/Ludwick relationship may not be a good model for dual-phase steels over the limited strain-range employed in the tensile test.

As expected steel RP has the highest r-values of the steels tested, although other re-phosphorised grades tested by the author have exhibited even higher values (eg: Kawasaki grade CHR40 has comparable strength levels to the steel used here, but gives r-values as high as 2.7 !). Steel AK comes a close second, with DP possessing an r of close to unity. Much work is underway to control the inherent anisotropy of dual-phase steels to improve their deep-drawing performance.

The nominal Stress-Strain curves for all of the steels are given in figure 23. All three exhibit continuous yielding, although there is a tendency to form a 'shoulder' in the stress-strain curves at the

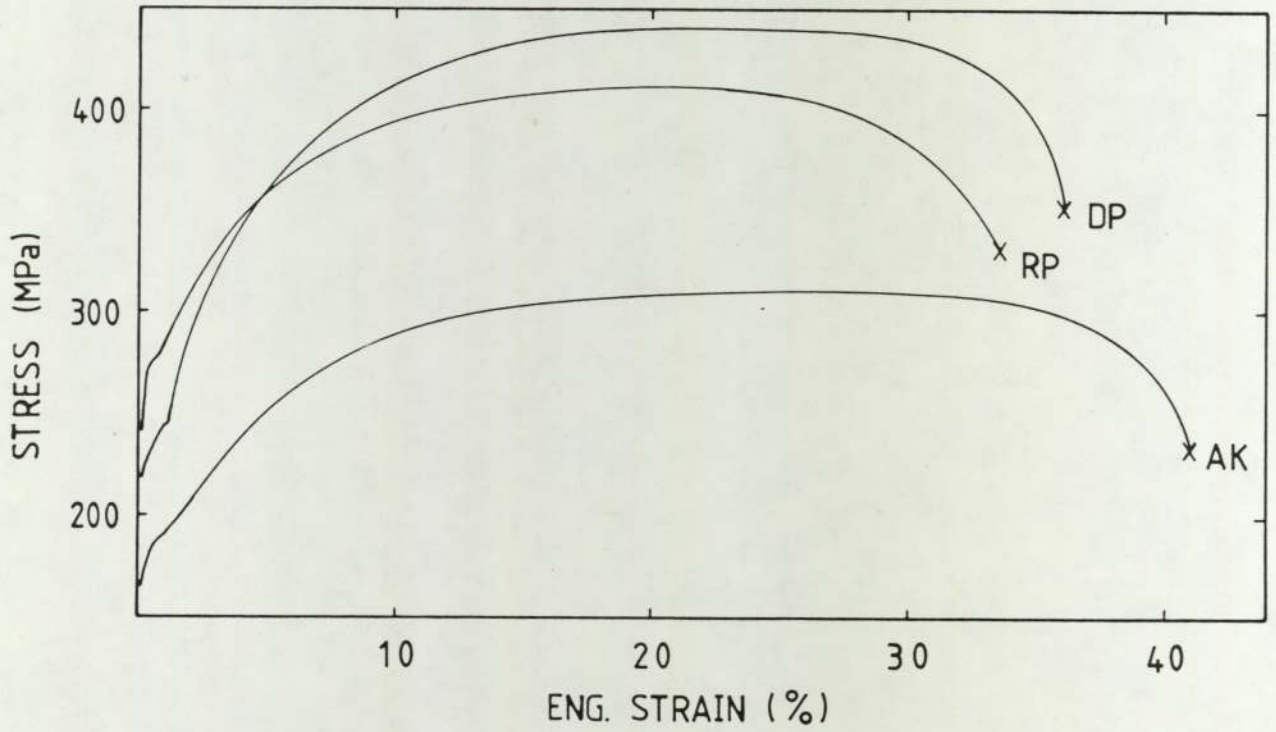

Fig. 23. Nominal Stress-Strain Curves for Steels AK (CR1), RP (BSC Rephos') and DP (CHLY40).

onset of plasticity which is more noticeable in the transverse direction than any other. This may indicate some ageing is present.

Strain-hardening data derived from the stress-strain curves is presented in Figures 24a-24c. Particularly at low strains (less than 10%) steel DP offers much higher work-hardening rates than the other two. At higher strains the various curves tend to converge. It is interesting that steel RP exhibits similar instantaneous-n values above 10% strain to DP, even though the power-law derived n-value (for the entire stress-strain curve) is much lower.

3.1.2 Forming Limit Diagrams

Figure 25. gives the simple FLDs obtained from Nakazima strip data. As can be seen, the two high-strength steels tend towards the lower limit of the AK steel envelope, with RP having one point well below the limit on the equi-biaxial side. It would be unwise to deduce too much from such an incomplete diagram, but there is little to differentiate between the steels on the basis of these FLDs.

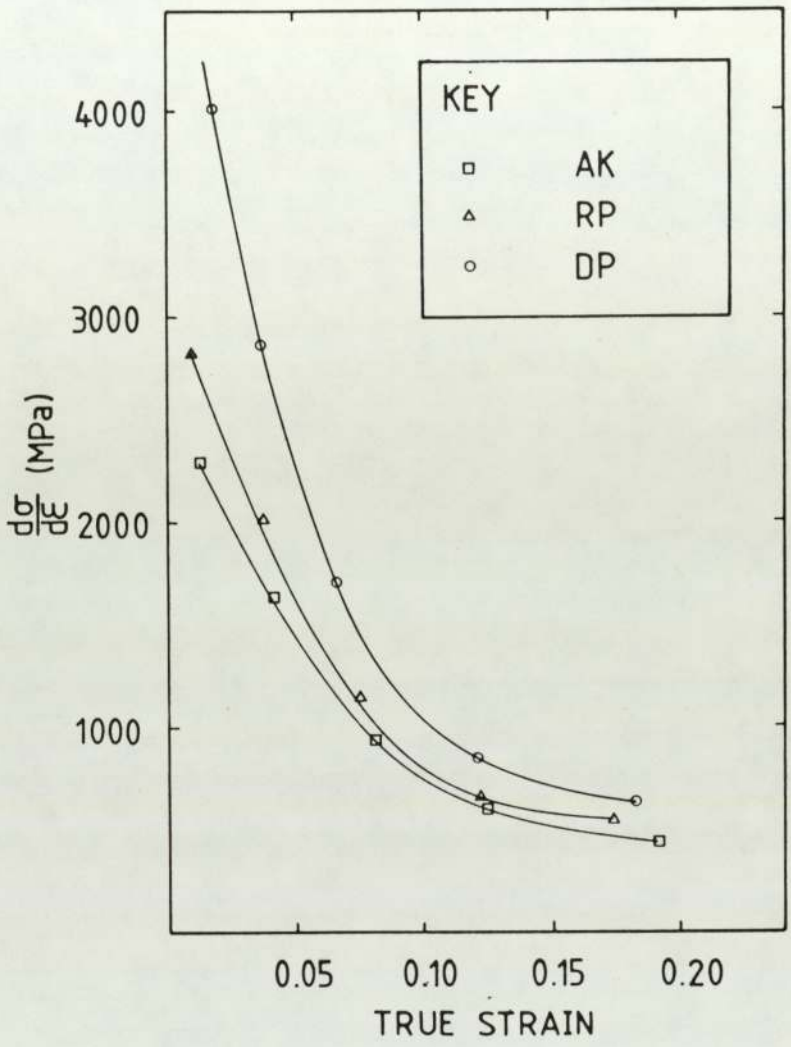

Fig. 24a). Work-Hardening Rate as a Function of True Strain for Steels AK, RP and DP (Tension Tested in the Rolling Direction of the Sheet).

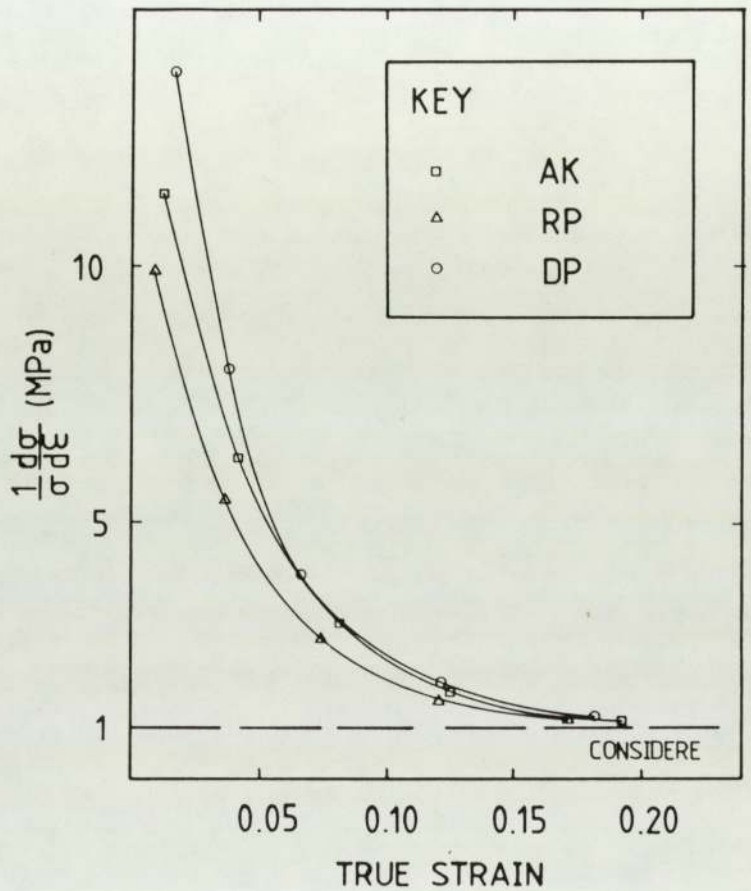

Fig. 24b). Normalised Work-Hardening Rate as a Function of True Strain (Same Data as Fig. 24a).

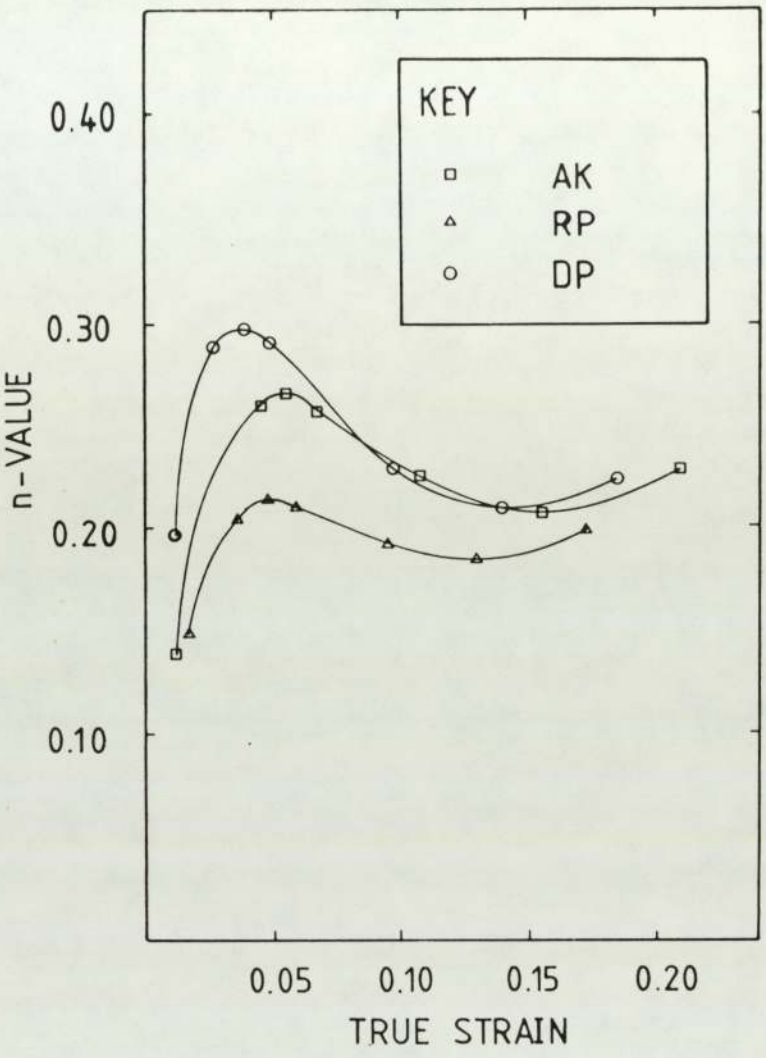

Fig. 24c). Instantaneous n-Values Derived from the Work-Hardening Curves Presented in Fig. 24a).

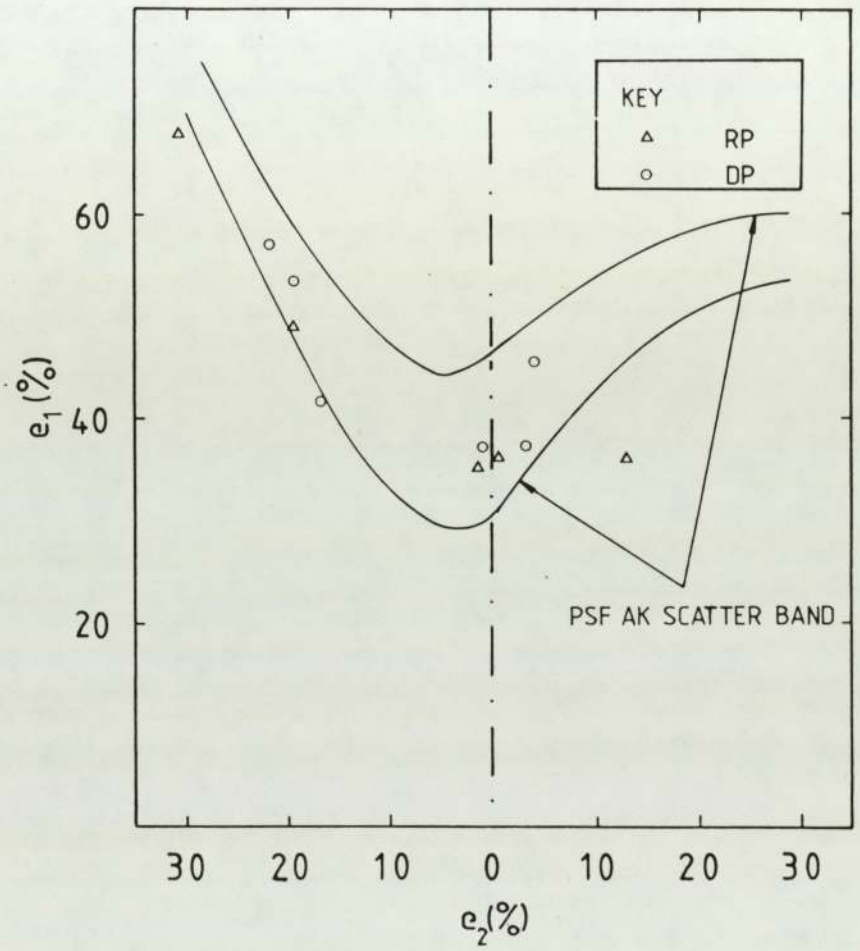

Fig. 25. Experimental FLD's for Steels RP and DP.
The AK FLD has been Supplied by B.L. Technology.

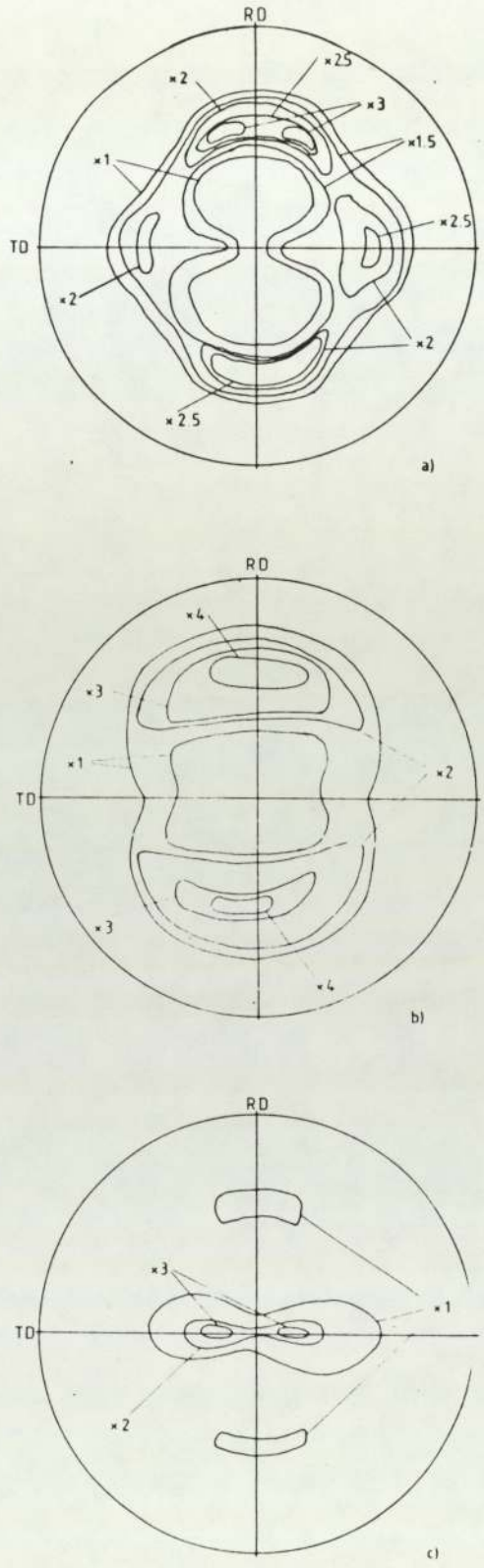

Fig. 26. (200) Incomplete Pole Figures for:-
a). Steel AK
b). Steel RP
c). Steel DP
The Numerals Indicate Multiples of the Random Level.

3.1.3 Pole Figures

Incomplete pole figures for all three steels are presented in Figures 26a-26c.

As would be expected from the r-values already quoted for these steels, AK and RP are both highly textured, with DP depleted in poles.

3.3 Effect of Uniaxial Prestrain on Subsequent Properties

The actual prestrains achieved for each steel, by angle to the TD prestrain, are given below. It should be noted that it was often possible to machine more than one direction's tensile test specimens from the same blank:-

AK

0 : 3.0, 4.2, 7.3, 10.1, 15.0, 18.9

15 : as 0 above

30 : as 0 above

45 : 2.6, 4.5, 7.4, 9.5, 16.0, 19.0

60 : as 45 above

75 : as 45 above (but NOT 16.0)

90 : as 45 above

RP

0 : 3.0, 5.0, 7.4, 8.1, 9.7

15 : as 0 above

30 : as 0 above

45 : 2.6, 5.0, 7.5, 8.8, 10.0

60 : as 45 above

75 : 2.6, 5.0, 7.5, 8.1, 10.0

90 : 2.6, 5.0, 7.5, 8.1, 8.8, 10.0

DP

0 : 3.0, 4.5, 7.5, 10.0, 14.5, 17.1

45 : 2.9, 5.0, 7.4, 9.8, 12.4, 15.1

90 : as 45 above

KEY:-

Angle in Degrees : List of Prestrains

All of the above are nominal strains (%).

Please note that from now on the prestrain will

be referred to as stage I of deformation and the subsequent tensile tests as stage II.

There are no flow curves for steels AK and RP at 15, 30, 60 and 75 degrees to the prestrain direction.

Since the true strain-hardening rate is available from the stress-strain data the n-values produced by the Zwick tensile machine will not be presented here. Appendix 2 includes a comparison of Zwick n-values to those obtained from the flow curves.

Tables 6-14 contain the proof stress and elongation data for the three steels, expressed as a function of the angle of the second-stage tension tests relative to the transverse prestrain. These results are presented graphically in Figures 27 to 47 along with the flow curves and strain-hardening curves obtained (although strain-hardening curves are not available for all prestrains). Tables 15-23 and Figures 48a-c to 50a-c contain the Zwick r-values as a function of prestrain for the three steels. Please note that r-values are not available for every prestrain due to measurement difficulties.

In the case of the elongation figures the individual results obtained are quoted, while averages

of two or more tests are presented for the other parameters.

3.3.1 Steel AK

Considering the stage II proof stresses shown in Fig.27, it can be seen that as the direction of the second stage tests deviates from coincidence with the prestrain the stresses rise. A maximum is reached at an angle of 60 degrees relative to the prestrain, after which there is a rapid drop in the measured proof stresses. This increase in flow stresses can be described as a latent hardening effect resulting from the first stage of deformation.

When the two stages of testing are aligned, the behaviour is much as would be expected in an interrupted tensile test. The strain to instability (usually referred to as the uniform extension in the tension test) and the total elongation curves fall in concert, with the sum of stage I and stage II strains remaining constant at roughly the virgin material levels (Fig.28). The flow curves in stage II coincide with the non-prestrained curve after 1-2% strain ie: the stage II proof stresses are lower than the virgin curve. As would be expected, the work-hardening curves

all fall within a narrow band about the curve obtained from the as-received material (within experimental scatter).

As the second stage is progressively angled away from the prestrain direction there are quite noticeable disturbances in all of the tensile test parameters. At an angle of 15 degrees (Fig.29) the uniform extension curve drops more rapidly than before and appears as two straight line portions. The total curve stays linear but drops more rapidly. When the angle between the two stages is 30 degrees (Fig.30) both elongation curves are deviating significantly from a linear dependence on prestrain: both curves have become sigmoidal in appearence. The initial uniform values deviate upward from the interrupted tensile test line before descending much more rapidly than before. By 15% prestrain the uniform extension has become constant at a residual level of 2.5% strain (compared to 5% for the coincident case).

At 45 degrees from the prestrain direction, the sigmoidal behaviour at 30 degrees has become accentuated (Fig.31). Again, the elongations at low strains are above the levels observed at 0 degrees, but now there is a precipitous drop in the strain to instability after a prestrain of between 7.5-9.5%.

There is a similar drop in the total elongation, but this occurs at a few percent higher prestrain ie: there is a transient rise in the straining actually taking place after maximum load (necking strain) which is illustrated in Figure 35. From 9.5% prestrain onward the residual uniform extension in stage II has become constant at 0.5-1.0%. Similarly, the total elongation remains almost constant at 5-11% above 15% prestrain.

The deviations in elongation values are reflected in the flow and strain-hardening behaviour. As the prestrain increases, the flow stresses rise above the as-received level (latent hardening) and there is a slight downward trend in the work-hardening curves until the critical prestrain is reached. At this prestrain there is a rapid loss of work-hardening capacity resulting in a minimum at a combined strain of 0.10. Continued straining sees a return of stable flow and an increase in hardening-rate and by a combined strain of 0.18 the prestrained curve has returned to a similar level of work-hardening rate as that found in the interrupted tensile tests.

Above the critical prestrain level, the flow curves (and hence hardening-rates) become difficult to measure due to the very low plastic strains involved. However, there is pronounced latent hardening and low work-hardening rates (after initially very high rates

in stage II).

At 60 degrees from the prestrain direction the behaviour is similar to that at 45 degrees. Destabilisation of stage II flow occurs at prestrains greater than 7.5% and a post-instablity plateau is again reached after 9.5% prestrain. The total elongation similarly becomes constant at approximately 5% residual strain at the highest prestrains. This stage II angle produces the lowest residual strains to instablity (see Fig.32).

Figure 33 shows that at 75 degrees to the prestrain direction the uniform curve obtained is similar to that at 60 degrees. However, at the higher prestrains the residual total elongation has risen to about 12.5% compared to 5% at 15% prestrain ie: there is a rise in necking strains.

When the second stage test is orthogonal to the first (Fig.34) the behaviour at 30-75 degrees is repeated: low prestrains result in enhanced elongations followed by a rapid loss of ductility at a critical prestrain (7.5-9.5%). Again, the total elongation undergoes the precipitous drop with prestrain at a higher strain than the uniform curve (2% later). The elongation levels achieved in the post-instability region are higher than those observed at 45-75 degrees from the prestrain. As with the 15 to

45 degree cases there is no plateau in the total elongation curve after the critical prestrain. As can be seen from Figure 35 this orientation exhibits the greatest transient rise in necking strain, peaking at about 10% prestrain, returning to a lower level than the coincident tests (but still 5 times that at 45 degrees).

The flow stresses are significantly lowered at the lower prestrains compared to the virgin curve. This is similar to the classical Bauschinger effect. By 0.071 true prestrain the stage II flow curve coincides with the as-received curve, and higher prestrains result in the latent hardening already observed. As with the 45 degree case the prestrain nearest to the precipitous loss in ductility has a work-hardening rate curve which drops much more rapidly than at low prestrains and in fact develops a minimum. Again, continued straining in the second stage results in a return of work-hardening capacity to a similar level to the virgin material at combined strains above 0.16. Above the critical level the curves again become very steep and drop to very low levels after less than 1% stage II strain: for example, the virgin material has a strain-hardening rate of approximately 750 MPa at 0.11 strain - after a true prestrain of 0.091 a rate of 125 MPa is measured when a strain of 0.019 is reached in an orthogonal strain II test.

When considering the observed behaviour of the r-values measured during stage II it is important to appreciate that there is considerable statistical scatter in these measurements (see discussion of errors later). This can best be seen in the case of the interrupted tensile tests where one might expect the curves to lie on top of each other. In fact, they form a band 1.0 r-value wide about the as-received curve. The 3.1% prestrain curve does not fit in well with the rest of the data at low strains (see Fig.48a)) and should be considered suspect. There is an apparent dependence of r-value on strain, with a rapid drop in the first few percent becoming a linear reduction with strain at higher strains. Typically, a reduction of 1.0 - 1.5 in r-value is observed over the range 2-15% strain.

As the direction of the second stage deformation moves away from coincidence with the first, the r-value curves begin to separate, a higher prestrain giving higher r-values for a given stage II strain. At 90 degrees away from the prestrain direction the displacement is greatest. The first few percent strain of stage II produces very high r-values (5.0 in some cases), but these drop rapidly with increasing strain. It is interesting to note that r-value appears to be independent of strain in tension for 45 and 90 degree

tests when there is no prestrain involved.

3.3.2 Steel RP

In general terms this steel performs much as AK and so the comments above will apply with the specific exceptions noted below.

Firstly, at 45 and 90 degrees to the prestrain the stage II residual elongations are seen to rise by as much as 2.5% above the non-prestrained level (Fig.40 and Fig.43). This is associated with an observed drop in flow stresses in the orthogonal case, and an increase in the work-hardening rates calculated. In the orthogonal case the effect is so pronounced that it is only at the highest prestrains that the virgin curve is achieved (no latent hardening).

Again, a critical prestrain level is reached at angles greater than 15 degrees from the prestrain at which a precipitous drop in uniform extension is observed. This critical level would appear to be lower than for steel AK at 5-7.5% prestrain, but the subsequent extensions obtained with continued prestraining are roughly twice those of AK.

Steel RP exhibits greater stability of the total elongation than AK and only at 75 degrees to the prestrain direction is there a tendency to follow the uniform line through a premature onset of instability.

At 45 degrees to the prestrain direction there is pronounced latent hardening above the critical range. The work-hardening curves again show a tendency to form minima near to, or during the critical range. Both at 45 and 90 degrees work-hardening curves can be seen with significant horizontal portions before the more usual behaviour resumes (see Fig.40 and 43). These curves are associated with straight line portions in the stress-strain curves and occur at lower prestrains than the curves with minima.

The r-value curves (Fig.49) indicate behaviour similar to AK.

The dependence of stage II proof stress on prestrain is similar to AK, although at angles greater than 75 degrees there is a concave curvature to the flow curve.

3.3.3 Steel DP

Once more, elongation behaviour is very similar to AK in most of the important respects, with the critical drop occuring at 7.5-10.0% prestrain. At low prestrain levels the 45 and 90 degree uniform elongation values are considerably higher than those in the non-prestrained condition (see Figs.46 and 47). In fact, at 45 degrees the uniform extensions recorded for 2.9% prestrain exceed the as-received values! In the orthogonal tests the reduced flow stresses noted before are present. Above the critical range there is pronounced latent hardening.

The 45 degree work-hardening curves follow the pattern set by RP in particular, although the final work-hardening rates observed for this mis-orientation are the lowest of all the steels.

At 90 degrees the situation is more interesting, with a noticeable increase in work-hardening rates at low prestrains associated with the reduced flow stresses and higher elongations. As previously observed, continued prestraining leads to reduced hardening rates and the development of curves with constant sections and minima.

The stage II proof stresses are similar to those observed for RP, with the 90 degree curve exhibiting upward curvature.

The r-values produced by prestraining exceed unity by a comfortable margin and are affected by prestrain and angle in the same way as in the other two steels (see Fig.50).

3.4 Effect of Equi-Biaxial Prestrain on Subsequent Properties

As stated in earlier sections there is a fundamental difficulty in assigning the prestrain level when the strain state differs from uniaxiality. This problem becomes even more serious when materials posessing large degrees of anisotropy are involved. Hosford and Kim (41) have demonstrated with crystal-slip calculations that Hill's theory of plasticity for anisotropic metals usually over-estimates the effective strain in the types of steel used for these experiments. Hence, it was decided to use the von Mises relationships, as already outlined, for effective strain. Since this ignores anisotropy and changes therein, the actual numerical values cannot be strictly valid. However, the errors

involved are sufficiently small to not invalidate the overall arguments.

The effective prestrains (hereafter referred to as prestrains) achieved are given below. Where possible three tensile specimens were machined from each blank in the rolling direction of the sheet:-

AK

2.4, 5.0, 6.7, 7.5, 10.0, 14.9

RP

5.1, 11.3, 16.0

DP

2.6, 5.1, 7.6, 9.1, 12.5, 15.1

All of the above are nominal strains (%)

Tables 24-29 contain the proof stress and elongation data for the three steels. These results are presented graphically in Figures 51-53 along with flow curves and work-hardening rate curves for the corresponding tests. The r-values (where available)

are stated in Tables 30-32 and illustrated by Figures 55a-c.

3.4.1 Steel AK

The behaviour shown in Figure 51 is very similar to that after uniaxial prestraining when the second stage is orthogonal to the first. There is an abrupt loss of ductility after 7-7.5% prestrain and residual elongations of less than 1% are observed at higher prestrains (post-drop plateau). There is no increase in the elongation values at low prestrains as was observed for uniaxial elongation. The total elongation curve drops at the zero prestrain rate up to about 6.5% prestrain, above which a more rapid decline is seen (but not precipitous): at 15% prestrain the residual total elongation is about 5%.

Even at small prestrains there is pronounced latent hardening which accounts for the poorer ductility values.

The critical prestrain is preceded by a fall in work-hardening rate to a minimum of less than half the as-received level. As stage II straining continues, there is partial restoration of the strain-hardening

capacity before failure.

The r-value behaviour is significantly different from the uniaxial case (see Fig.55): up to 10% prestrain the r-value appears to be independent of stage II strain, although increasing prestrain reduces the observed r-values (from about 1.75 as-received to 1.15 at 6.7% prestrain). There is no enhancement of r-value at low second stage strains as indicated before. Above 10%, however, the previous behaviour returns (ie: post critical event). It is important to note that r-values measured at strains of less than 1.0% are prone to significant measurement errors.

3.4.2 Steel RP

The lack of data for this strain-path change makes detailed observations difficult. However, the indications are that the behaviour of steel AK is likely to be followed.

3.4.3 Steel DP

As can be seen in Figure 53 the uniform and total elongation curves fall linearly with prestrain up to

about 7.5%. The slope thus far is steeper than the uniaxial tests and again there is no enhancement of elongation values for low prestrains.

Between 7.5-9.0% prestrain both elongation curves undergo an abrupt decline. Unlike the typical uniaxial results, the drop occurs simultaneously. This is contrasted with the other steels in Figure 54 and the lack of a transient rise in necking strains at about 7.5% prestrain appears peculiar to steel DP.

The r-values follow the pattern set by steel AK.

3.5 Effect of Plane-Strain Prestrain on Subsequent Properties

The arguments used for the biaxial case, about calculation of effective prestrain, apply here with the same solution.

Below are listed the actual effective prestrains reached for each steel according to the angle in degrees relative to a TD prestrain:-

AK

0 : 2.4, 5.0, 7.4, 9.6, 11.0

45 : 2.5, 5.2, 7.4, 8.1, 10.0

90 : as 45 above

RP

0 : 3.0, 5.0, 7.4, 8.2, 9.7

45 : 2.6, 4.1, 5.0, 7.5, 8.8, 10.0

90 : as 45 above

DP

0 : 3.0, 5.1, 6.1, 7.5, 9.8

45 : 2.8, 5.0, 6.3, 7.5, 9.6

90 : as 45 above

KEY:-

Angle in Degrees : List of Prestrains

All of the above strains are nominal (%).

Tables 33-41 contain the proof stress and elongation data obtained for the three steels as a function of the direction of the second-stage tension tests to the transverse prestrain. All of the results

are the average of two tests unless stated otherwise. These results are presented graphically in Figures 56-67 along with the flow curves and work-hardening curves. Tables 42-50 and Figures 68-70 detail and illustrate the r-values as a function of strain.

3.5.1 Steel AK

Even when the second stage is coincident with the first, there is evidence of the behaviour previously observed with uniaxial prestraining away from the prestrain direction and with biaxial prestrains (see Fig.57). The uniform extension curve exhibits a mild downward swing at about 4% prestrain. By 10% prestrain both the elongation curves are about 8% below the interrupted tensile test levels.

There is latent hardening even at low prestrains, which results in a nearly constant offset from the virgin curve as prestraining is continued. The rate curves are not markedly affected by prestraining, until the highest prestrains are reached.

At 45 degrees to the prestrain direction (Fig.58) the uniform and total elongations are enhanced above the as-received level, for prestrains up to 2.5%.

Beyond this there is a rapid fall off in ductility (greater than for uniaxial prestraining), and a critical range of 5-7% prestrain is observed. Typical residual elongations after the precipitous drop are 0.5-0.7% in the case of the strain to instability. Although the total elongation curve falls rapidly with increasing prestrain there is no abrupt drop in ductility. At 10% prestrain the residual total elongation has fallen to 5% (the uniaxial case was closer to 25%).

Increasing prestrain results in lower work-hardening rates. As the critical prestrain is approached the rate curves develop significant regions of constant work-hardening rate, and then drop to a very low level (although there is still evidence of a recovery in hardening capacity with continued stage II straining). After the critical drop the curves become very steep again. At all prestrains there is considerable latent hardening.

Figure 59 illustrates the behaviour observed when the second stage is orthogonal to the first. At low prestrains (less than 2.5%) there is little to choose between this and the uniaxial behaviour (similarly enhanced elongations and lowered flow stresses). However, when 5.2% prestrain is reached the loss of stability in stage II is well under way, leading to a constant 1.0% uniform extension from 7.4% prestrain

onward. As before, the total curve doesn't undergo an abrupt drop at a critical prestrain, but instead falls much more rapidly than before: at 10% prestrain the total elongation is three times the elongation at 45 degrees from the prestrain but this is still less than half the comparable uniaxial value.

After the initially low flow stresses and associated increased strain-hardening rates, increasing prestrain results in latent hardening and a loss of work-hardening rate. Although very low values of strain-hardening rate are observed, there is no tendency towards the formation of horizontal, linear sections or minima in the curves obtained.

The r-values recorded at all angles from the prestrain direction (Fig.68) behave like the uniaxial prestrain when the latter is followed by orthogonal straining ie: the values after prestraining are displaced upward from the virgin material line and there is considerable enhancement of the values taken during the first few percent strain of stage II. The deviation from as-received behaviour is greatest for the orthogonal second stage tests.

The stage II proof stresses measured at 45 and 90 degrees from the prestrain direction are offset from the coincident curve, but do run parallel (Fig.56).

3.5.2 Steel RP

Figures 61 to 63 indicate elongation behaviour consistent with steel AK, except that at low prestrains the 45 and 90 degree tests begin to exhibit a pronounced 'hump' in the elongation curves. As would be expected this is reflected in the flow curves (particularly at 90 degrees) by a large reduction in observed stresses and a rise in work-hardening rate (90 degree tests only).

As the prestrain rises, there is a reduction in hardening rate and the development of latent hardening. As the strain to instability undergoes the typically abrupt reduction noted before, the work-hardening curves develop a plateau or even a minimum. As stage II straining continues in these tests, there is a recovery of strain-hardening rate when a minimum is observed, or a return to conventional behaviour after the constant rate regimes. The premature drop in measured uniform extension is associated with less dramatically reduced work-hardening rates than for the other prestrain modes.

The r-value and proof stress behaviour follows that of steel AK.

3.5.3 Steel DP

As with RP the residual elongations after low prestrains are significantly enhanced above even the as-received levels, particularly when the second stage is orthogonal (Fig.67). There is an associated increase in strain-hardening rate and reduction in stage II flow stresses.

Increasing the prestrain to the level required for the critical event, causes latent hardening to appear. Concurrently, the strain-hardening rates fall as before. Higher prestrains still, cause even higher flow stresses and lower hardening rates than observed in the orthogonal case (there is also the evolution of the peculiar work-hardening rate curves observed for most of the previous prestrain modes). The behaviour at 0 and 45 degrees does not fit the pattern established so far, and so interpretation is difficult.

Once more, the pattern set by AK and RP for r-value and proof stress dependence on orientation is followed by this steel.

3.6 Summary

At the beginning of the test programme it was anticipated that the re-phosphorised and dual-phase steels would respond quite differently from the conventional, deep-drawing steel because of the different strengthening mechanisms involved. However, these results suggest that all three steels behave in an essentially similar manner. Further, the prestrain mode does not appear to significantly affect the form of the subsequent behaviour in tensile testing, instead it is the extent of prestrain that defines stage II behaviour, although there are certain parameters (strain to critical event, r-values etc) which are prestrain mode dependent. Obviously, there are detail differences between the steels and their response to the various prestrains, but these are not of the magnitude anticipated at the beginning of the test series.

Hence, to summarise the more significant observations:-

1. Interrupted tensile testing results in a return to as-received behaviour after a few

percent strain in stage II. This indicates that the precautions to eliminate strain-ageing were succesful.

2. As the degree of mismatch between stage I and stage II straining directions increases for uniaxial and plane-strain prestraining the following phenomena are observed:-

   a). At low prestrains there is a rise in elongation values, sometimes to above the as-received values. This is associated with low flow stresses and a rise in work-hardening rate.

   b). Continuing prestraining leads to a more rapid drop in elongation values than expected, associated with an increase in flow stresses above the virgin line. Increasing prestrain often increases this effect, for which the tag 'latent hardening' has been chosen. In this regime there is usually a reduction in the observed work-hardening rates.

   c). As the work-hardening rate is further reduced by higher prestrains an abrupt and catastrophic loss of ductility is observed (at a critical prestrain).

The total elongation curves are less likely to follow this type of behaviour than the uniform extension curves. Large increases in flow stress are observed, and the strain-hardening rate curves develop significant regions of constant rate as a function of stage II strain or even minima.

d). With the attainment of the critical prestrain, there is a rapid increase in the amount of straining taking place after maximum load in stage II (necking strains).

e). After the critical prestrain the residual strain to instability is frequently reduced to less than 1%. This remains constant for higher prestrains (a plateau).

f). Plane-strain prestrain disrupts subsequent flow behaviour more than uniaxial prestrain (or biaxial for that matter). See Figure 71.

g). An overall increase in r-value is found when stage I and stage II directions do not coincide. The virgin materials exhibit only mild strain dependence of the r-value, but even at

low prestrains the r-value becomes highly strain dependent (particularly at low stage II strains).

3). Biaxial prestraining results in many of the same phenomena with the following important differences:-

a). There is no enhancement of elongation for low prestrains.

b). There is considerable latent hardening at all prestrain levels.

c). Increased prestraining gives lower r-values in stage II, and there is no strain dependence of the r-value until the critical prestrain is reached.

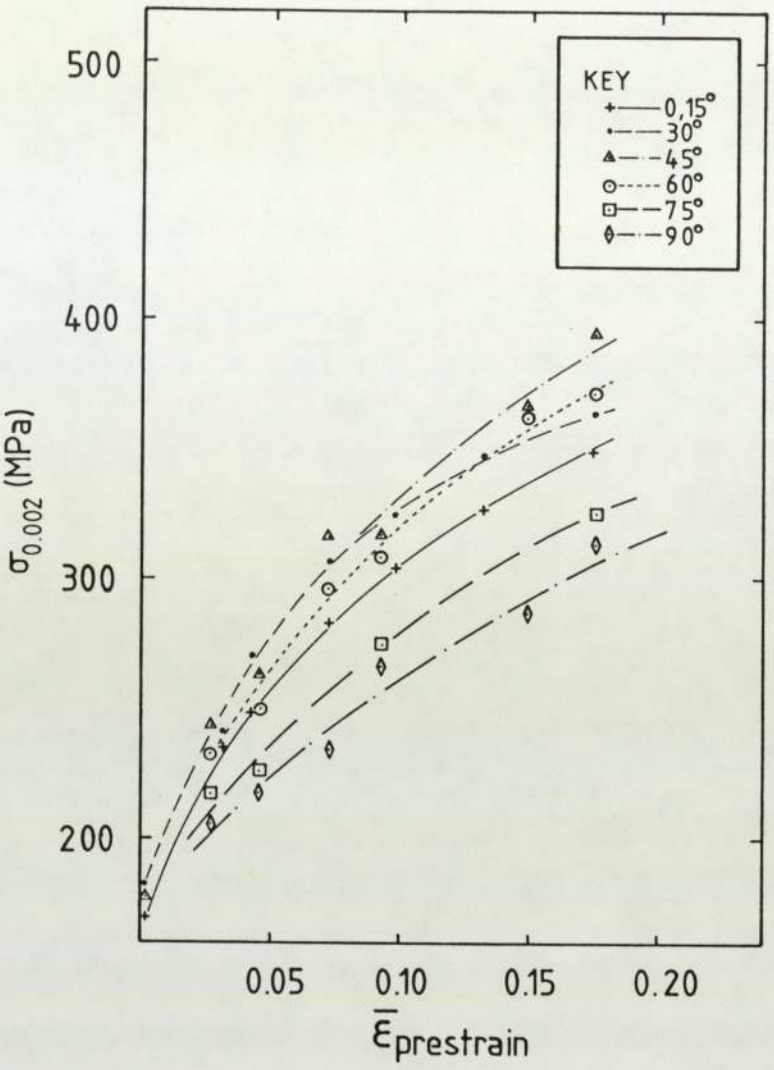

Fig. 27. Steel AK, Uniaxial Prestrain: Variation of True 0.2% Proof Stress with Prestrain Level and Angle of Separation Between Stage I and II Straining.

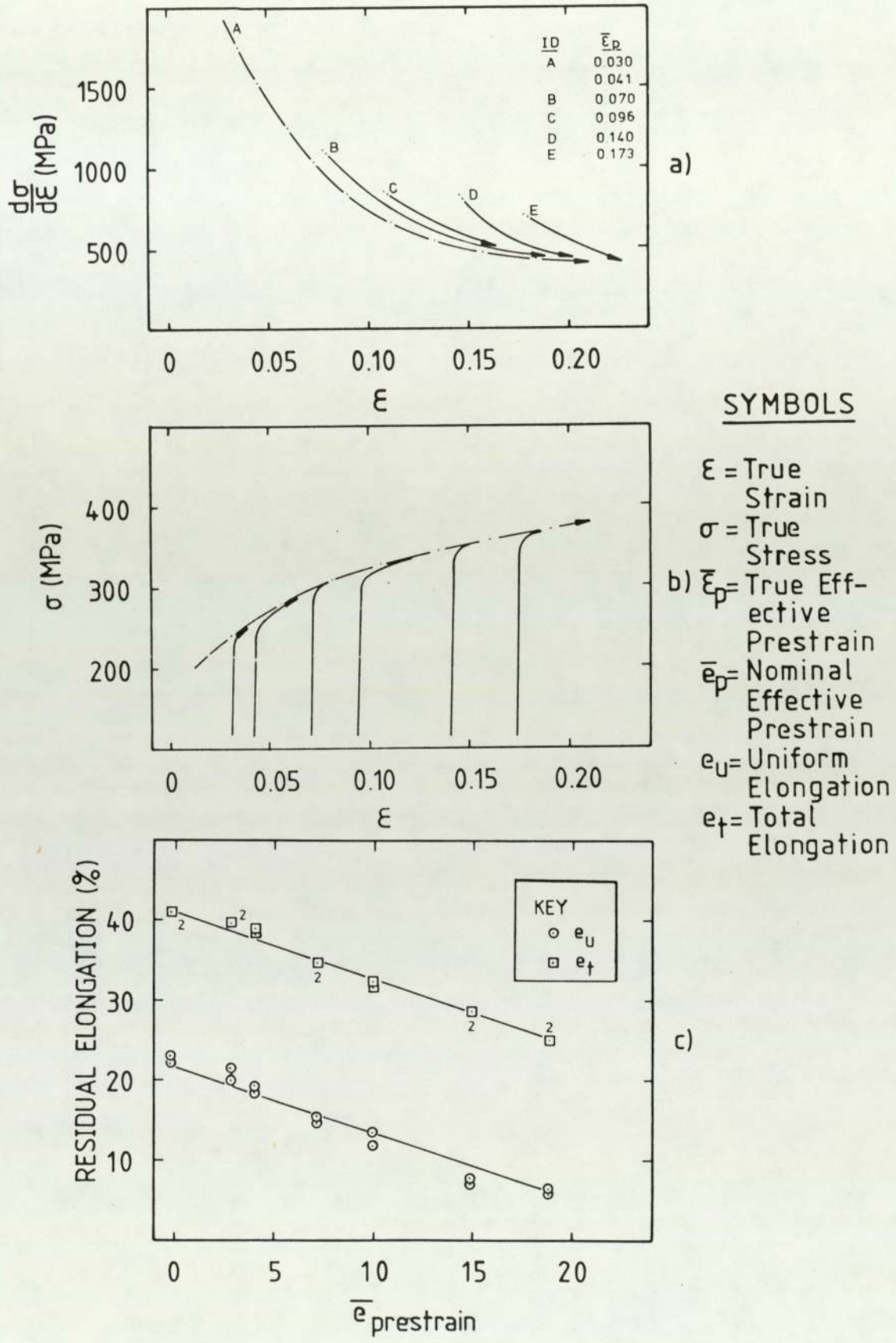

Fig. 28. Steel AK, Uniaxial Prestrain: Tensile Test Results, Stage II Rotated 0 Degrees from the Prestrain Direction. (a) Work-Hardening Curves, (b) True Stress-Strain Curves (Each Offset by the Prestrain), (c) Residual Tensile Elongations. Chain Dotted Lines Represent As-Received Properties.

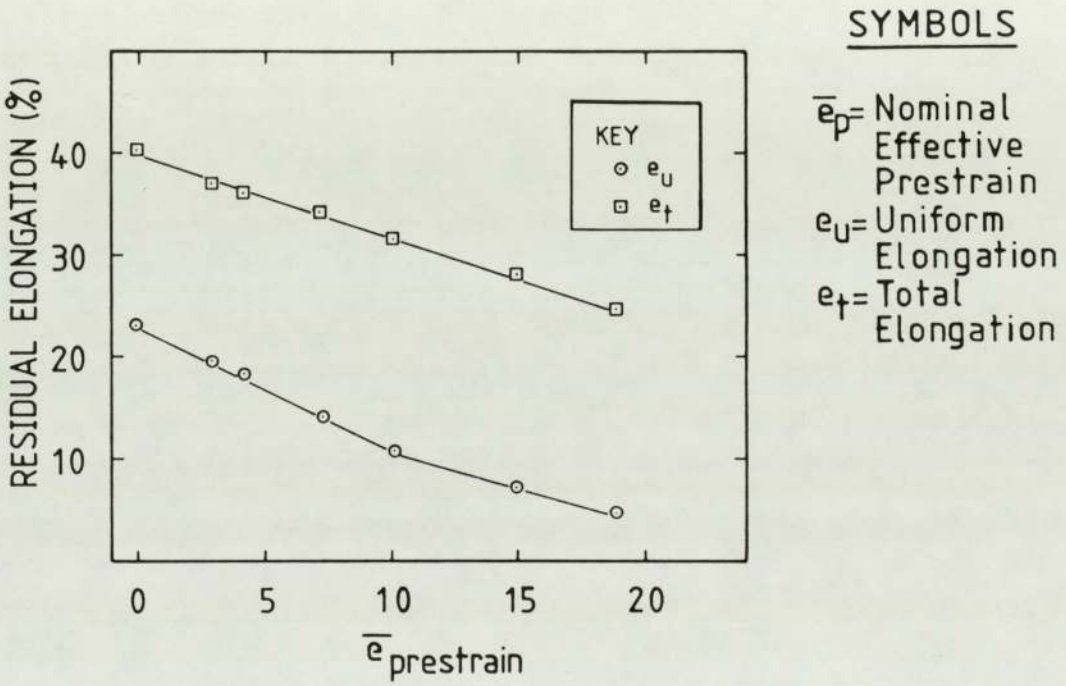

Fig. 29. Steel AK, Uniaxial Prestrain: Tensile Test Results, Stage II Rotated 15 Degrees from the Prestrain Direction.

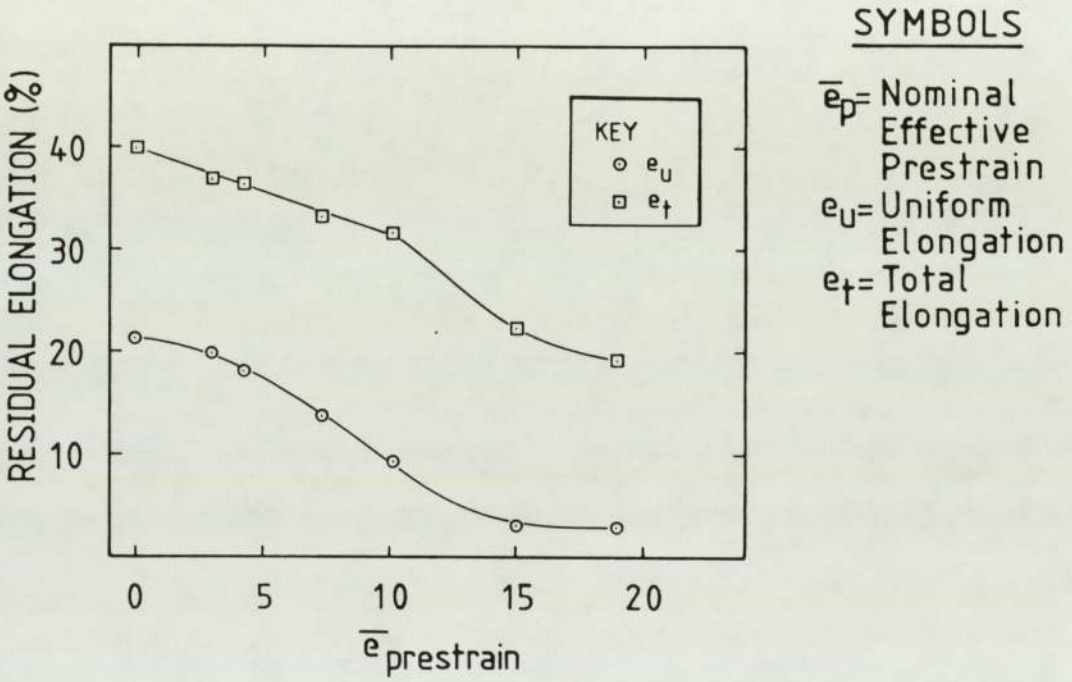

Fig. 30. Steel AK, Uniaxial Prestrain: Tensile Test Results, Stage II Rotated 30 Degrees from the Prestrain Direction.

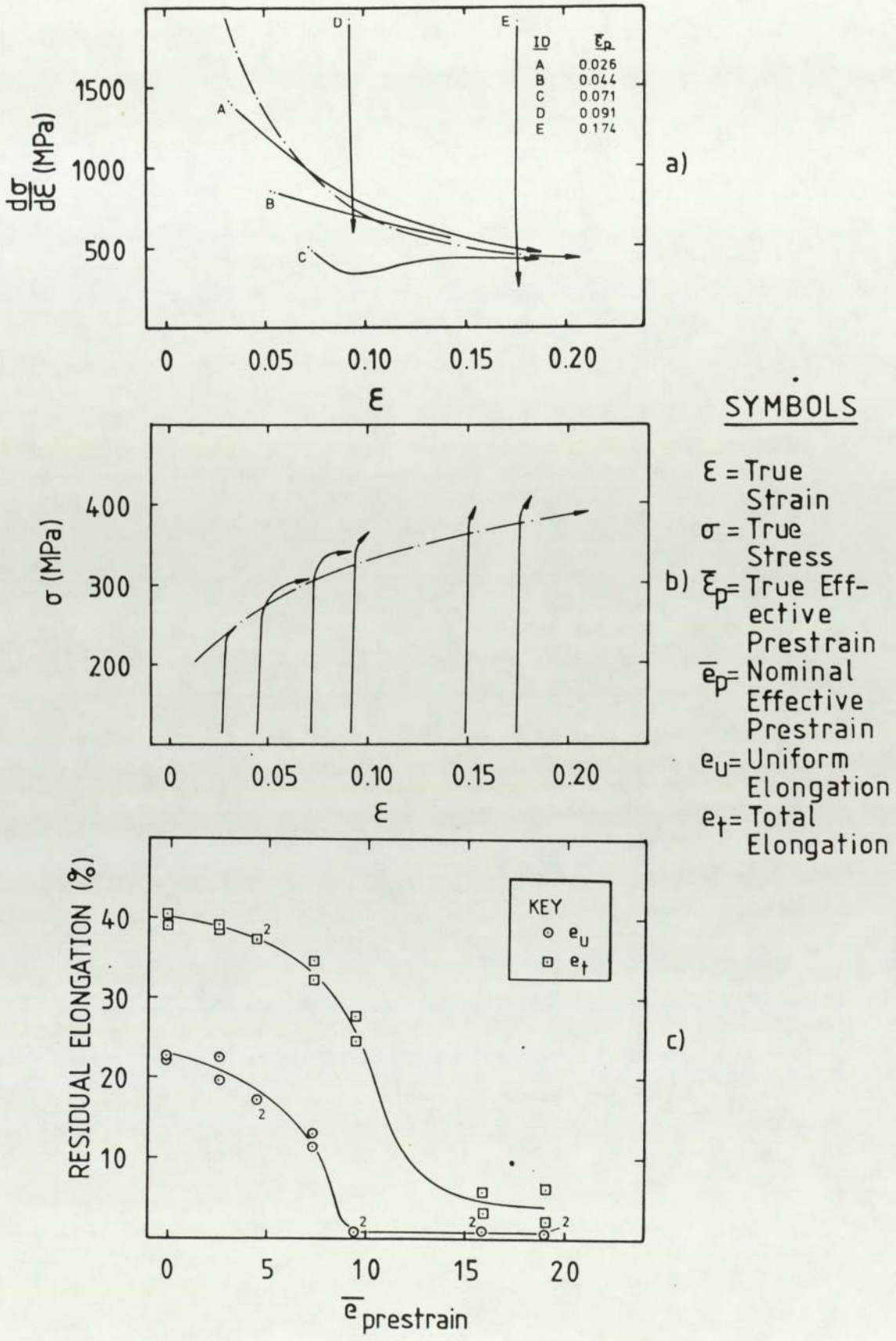

Fig. 31. Steel AK, Uniaxial Prestrain: Tensile Test Results, Stage II Rotated 45 Degrees from the Prestrain Direction. (a) Work-Hardening Curves, (b) True Stress-Strain Curves (Each Offset by the Prestrain), (c) Residual Tensile Elongations. Chain Dotted Lines Represent As-Received Properties.

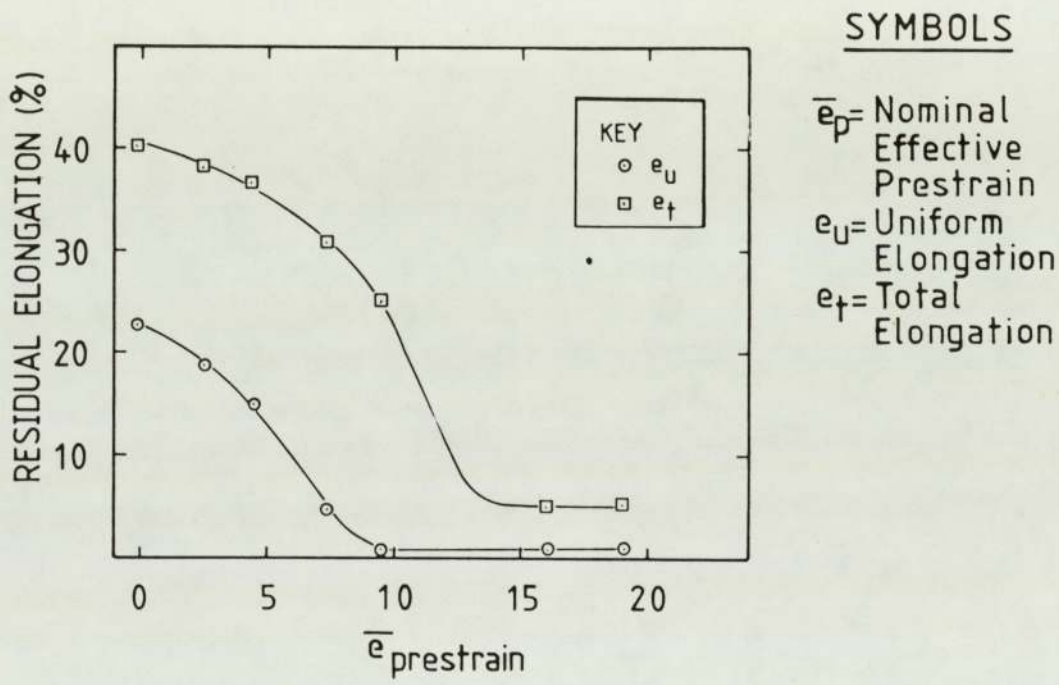

Fig. 32. Steel AK, Uniaxial Prestrain: Tensile Test Results, Stage II Rotated 60 Degrees from the Prestrain Direction.

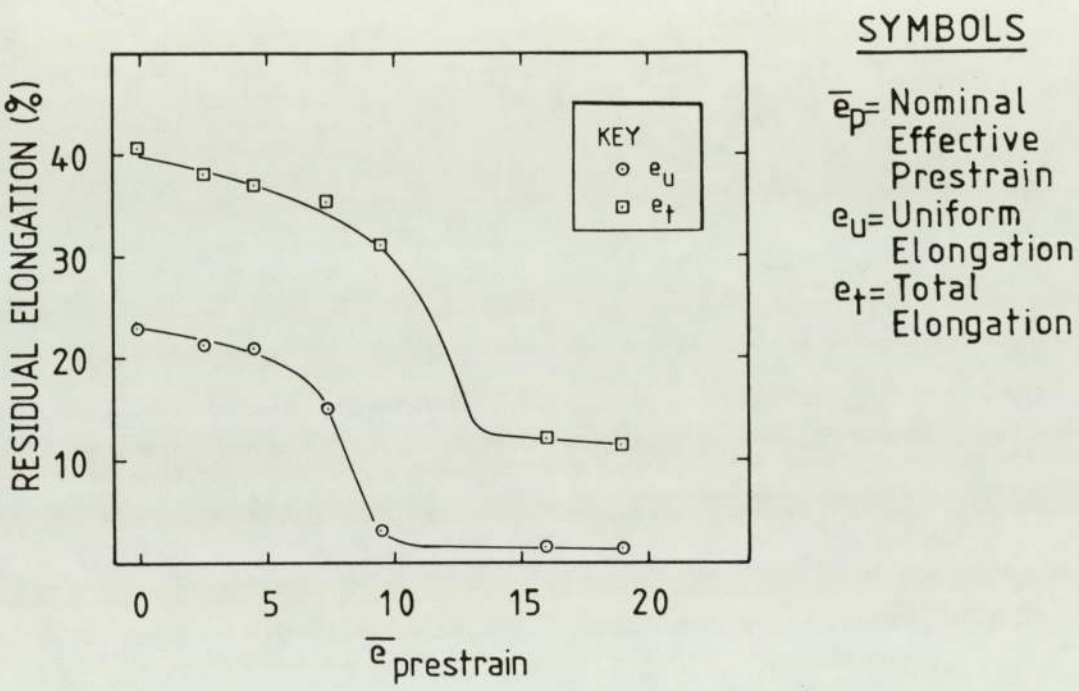

Fig. 33. Steel AK, Uniaxial Prestrain: Tensile Test Results, Stage II Rotated 75 Degrees from the Prestrain Direction.

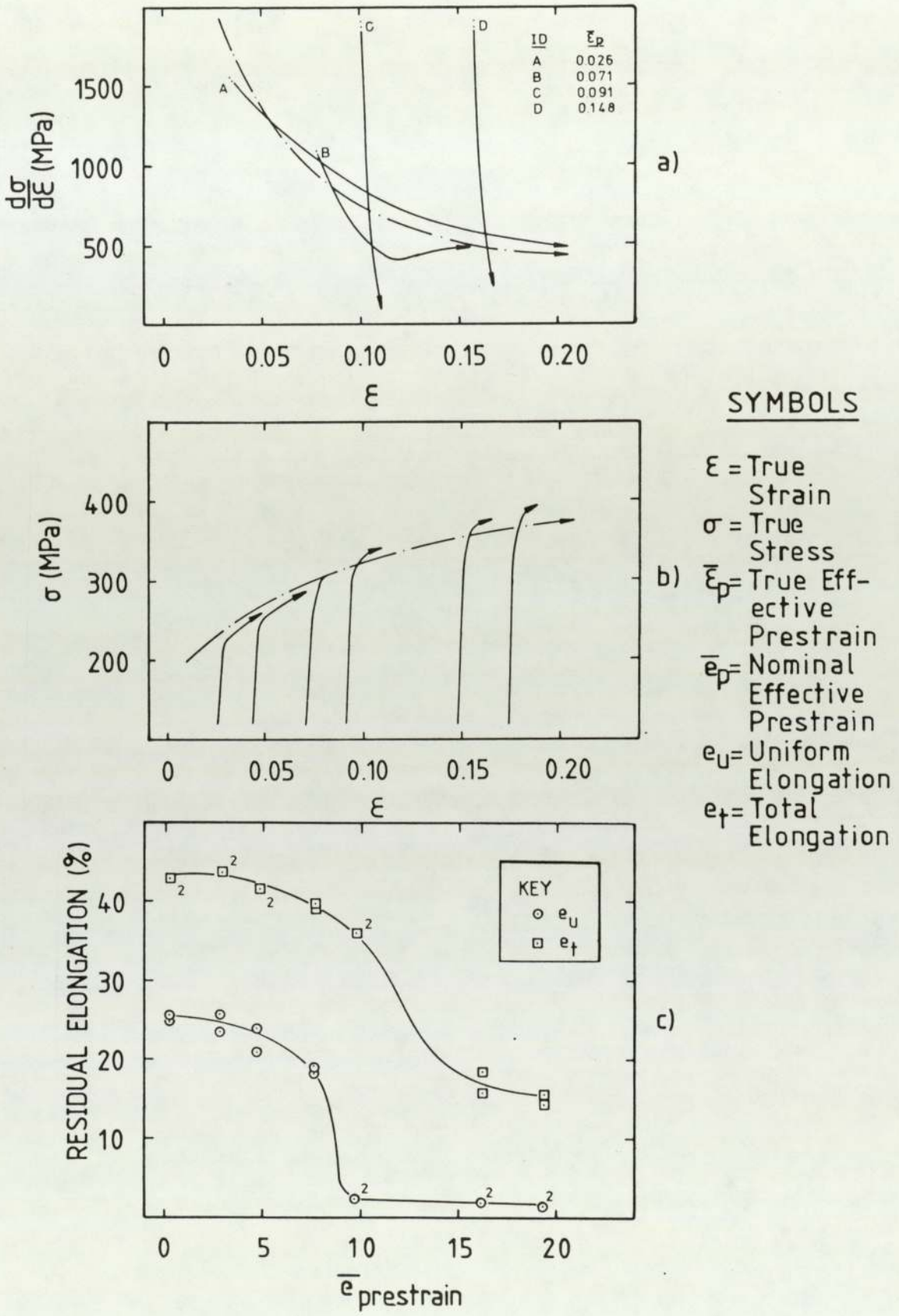

Fig. 34. Steel AK, Uniaxial Prestrain: Tensile Test Results, Stage II Rotated 90 Degrees from the Prestrain Direction. (a) Work-Hardening Curves, (b) True Stress-Strain Curves (Each Offset by the Prestrain), (c) Residual Tensile Elongations. Chain Dotted Lines Represent As-Received Properties.

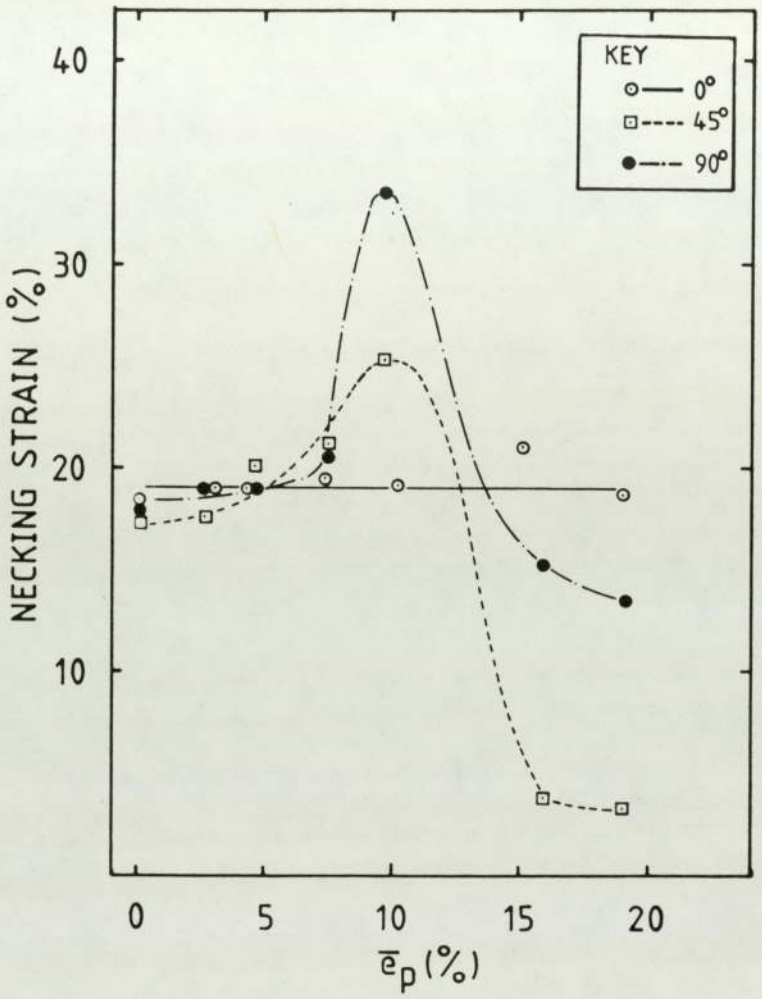

Fig. 35. Steel AK, Uniaxial Prestrain: Variation of Tensile Necking Strains with Prestrain Level and Angle of Separation Between Stage I and II Straining.

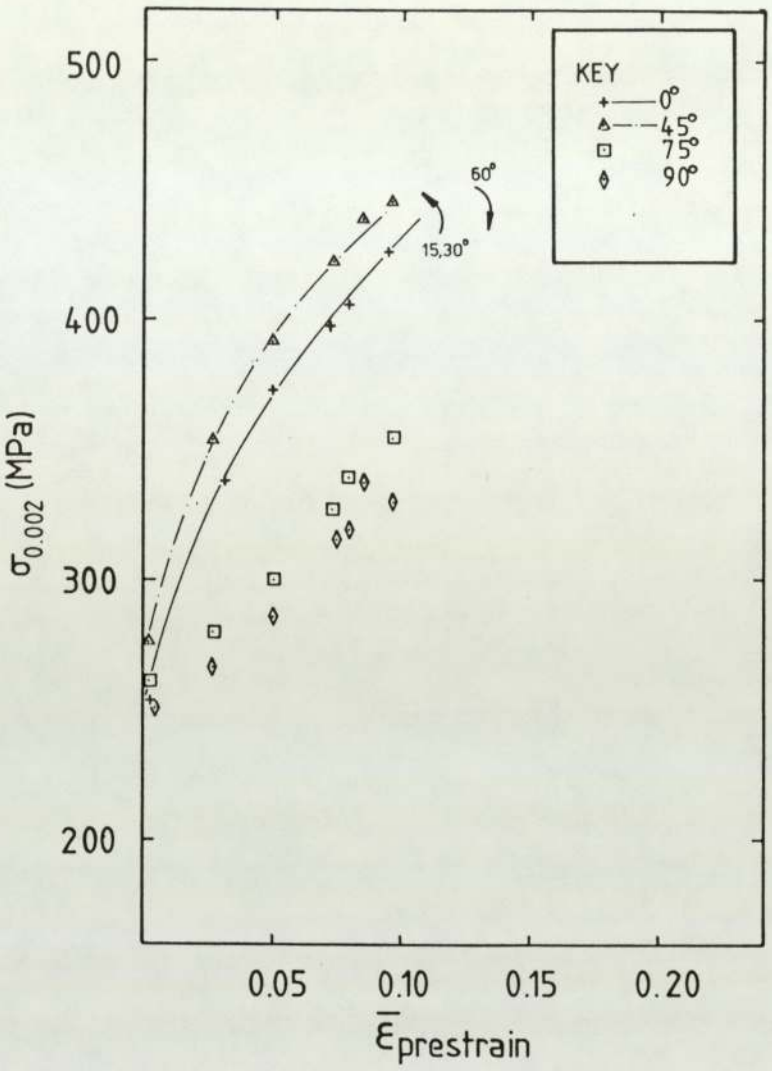

Fig. 36. Steel RP, Uniaxial Prestrain: Variation of True 0.2% Proof Stress with Prestrain Level and Angle of Separation Between Stage I and II Straining.

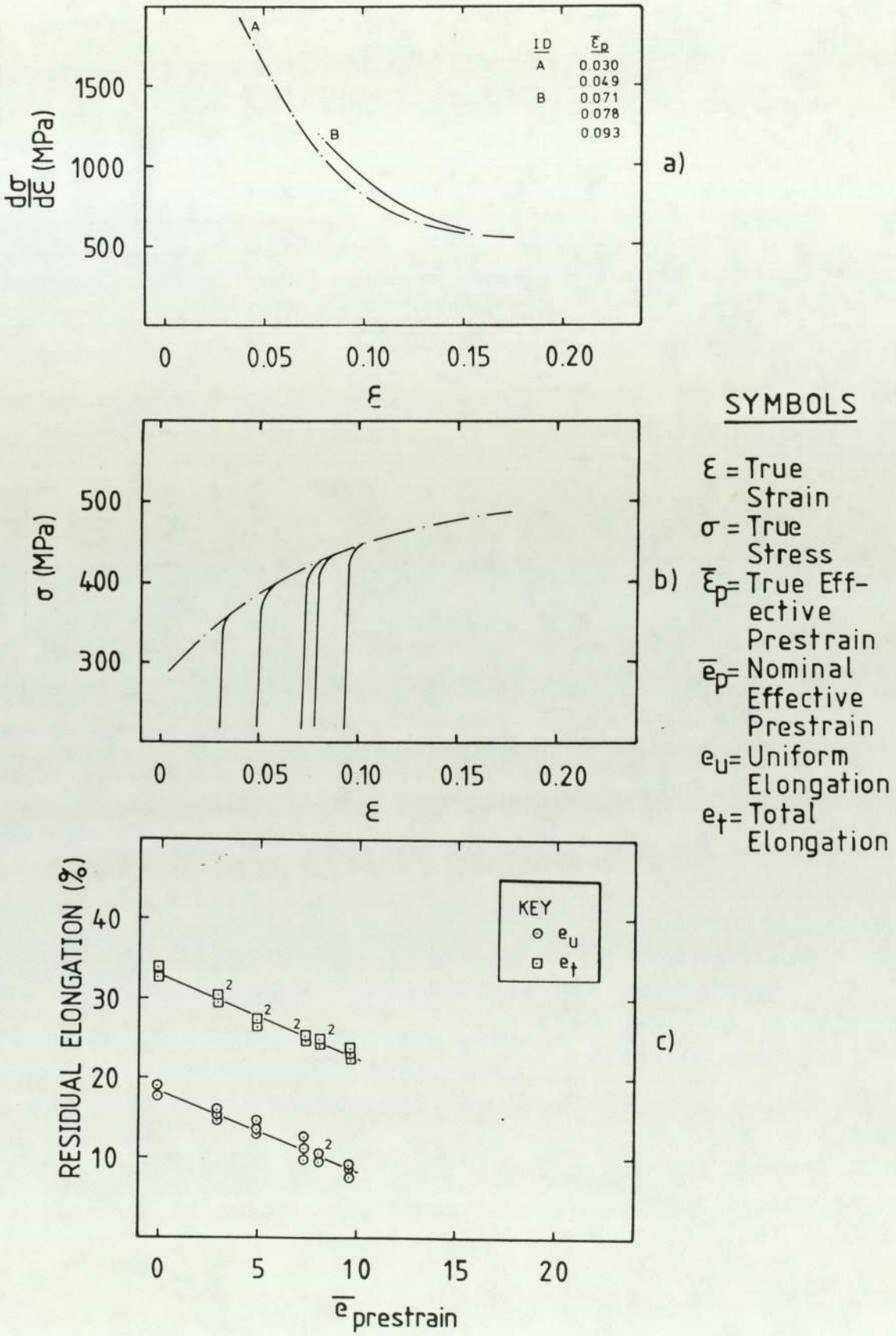

Fig. 37. Steel RP, Uniaxial Prestrain: Tensile Test Results, Stage II Rotated 0 Degrees from the Prestrain Direction. (a) Work-Hardening Curves, (b) True Stress-Strain Curves (Each Offset by the Prestrain), (c) Residual Tensile Elongations. Chain Dotted Lines Represent As-Received Properties.

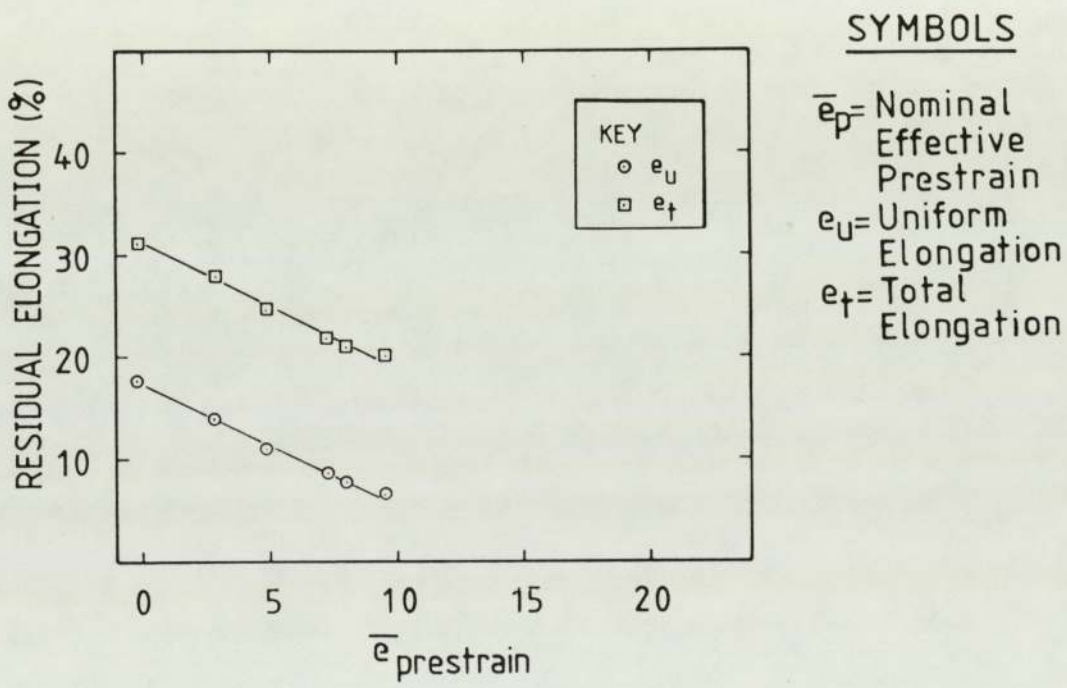

Fig. 38. Steel RP, Uniaxial Prestrain: Tensile Test Results, Stage II Rotated 15 Degrees from the Prestrain Direction.

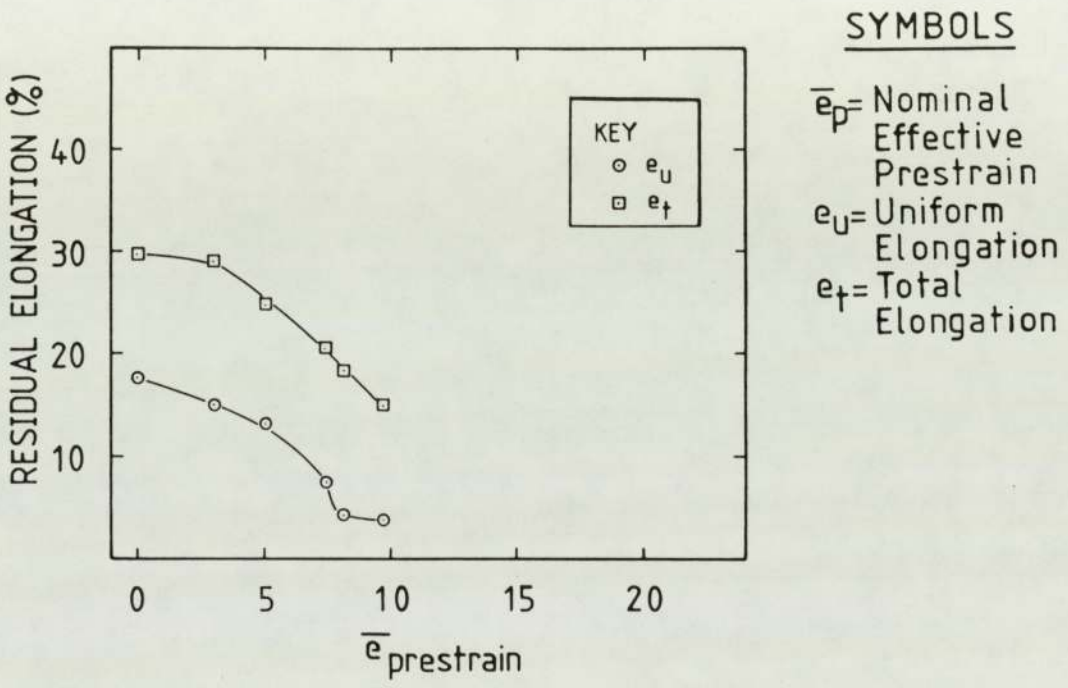

Fig. 39. Steel RP, Uniaxial Prestrain: Tensile Test Results, Stage II Rotated 30 Degrees from the Prestrain Direction.

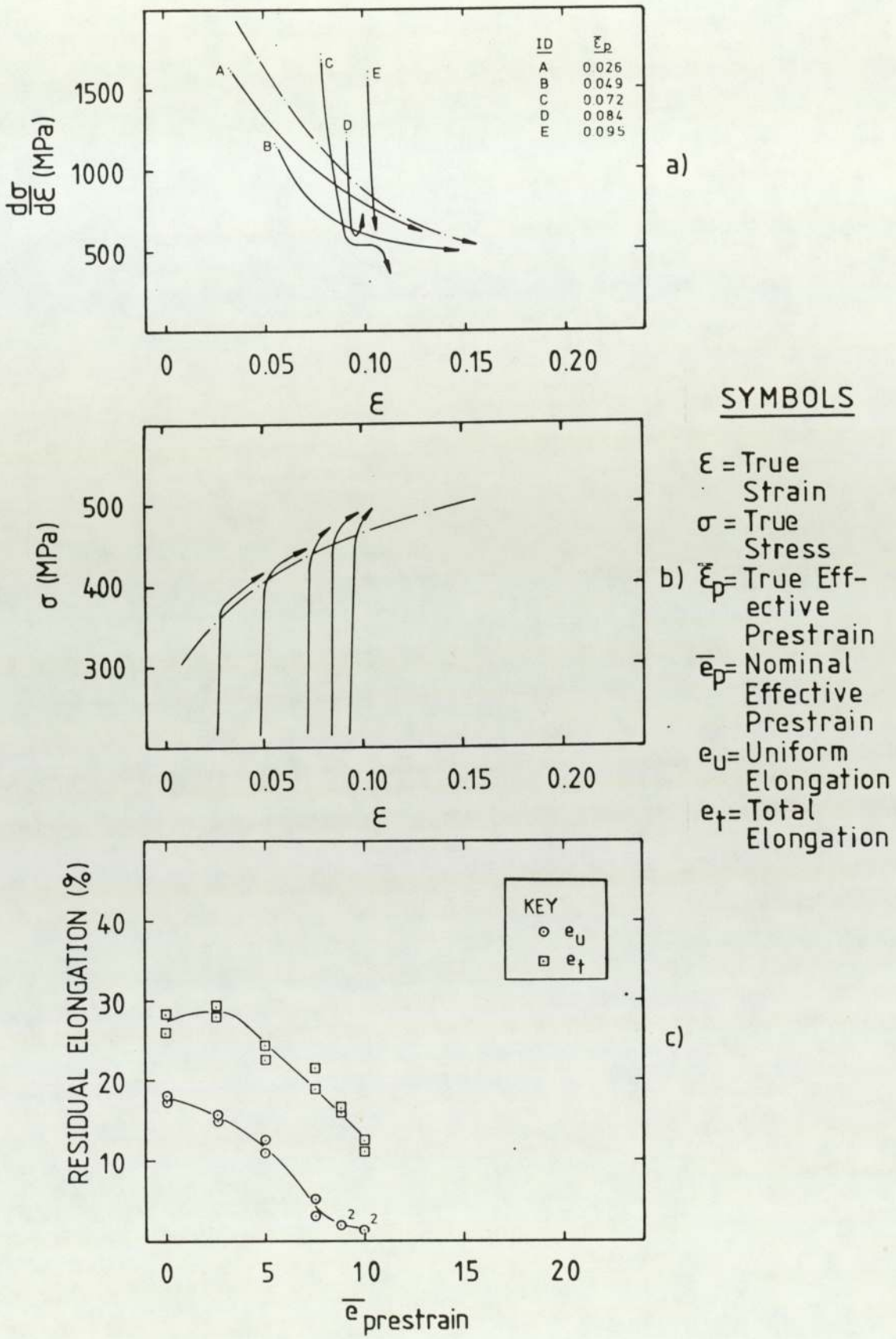

Fig. 40. Steel RP, Uniaxial Prestrain: Tensile Test Results, Stage II Rotated 45 Degrees from the Prestrain Direction. (a) Work-Hardening Curves, (b) True Stress-Strain Curves (Each Offset by the Prestrain), (c) Residual Tensile Elongations. Chain Dotted Lines Represent As-Received Properties.

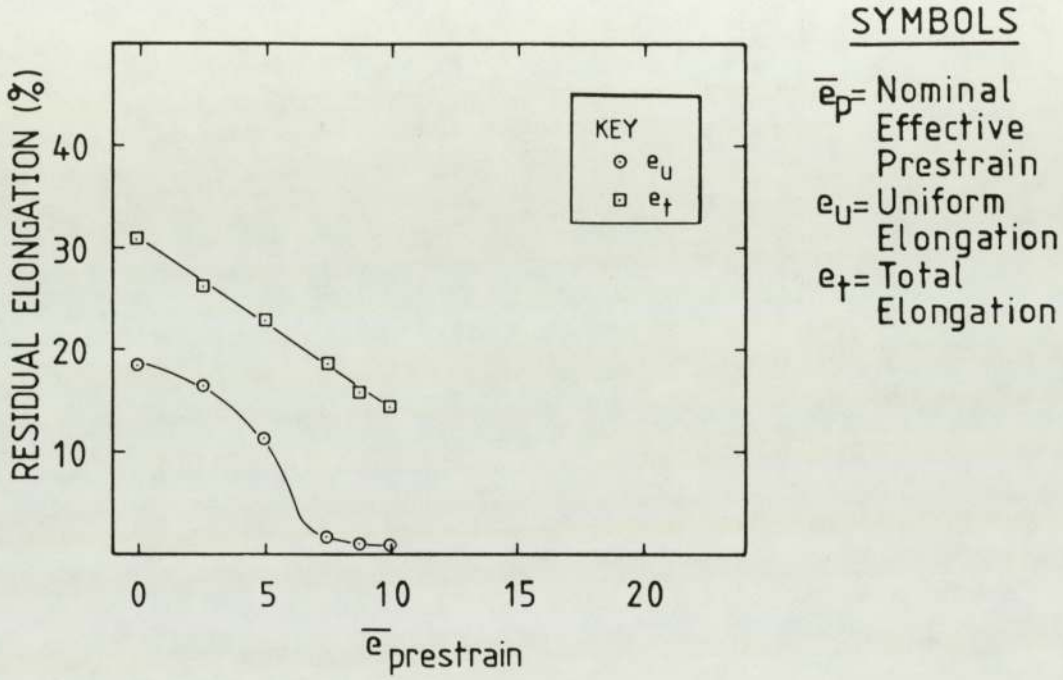

Fig. 41. Steel RP, Uniaxial Prestrain: Tensile Test Results, Stage II Rotated 60 Degrees from the Prestrain Direction.

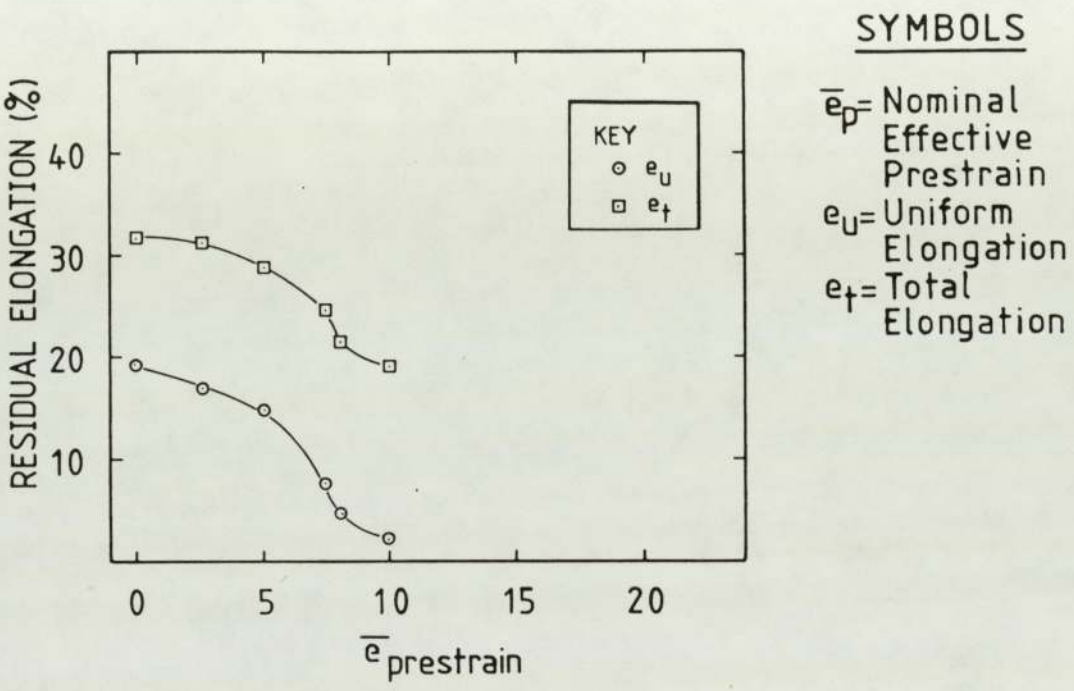

Fig. 42. Steel RP, Uniaxial Prestrain: Tensile Test Results, Stage II Rotated 75 Degrees from the Prestrain Direction.

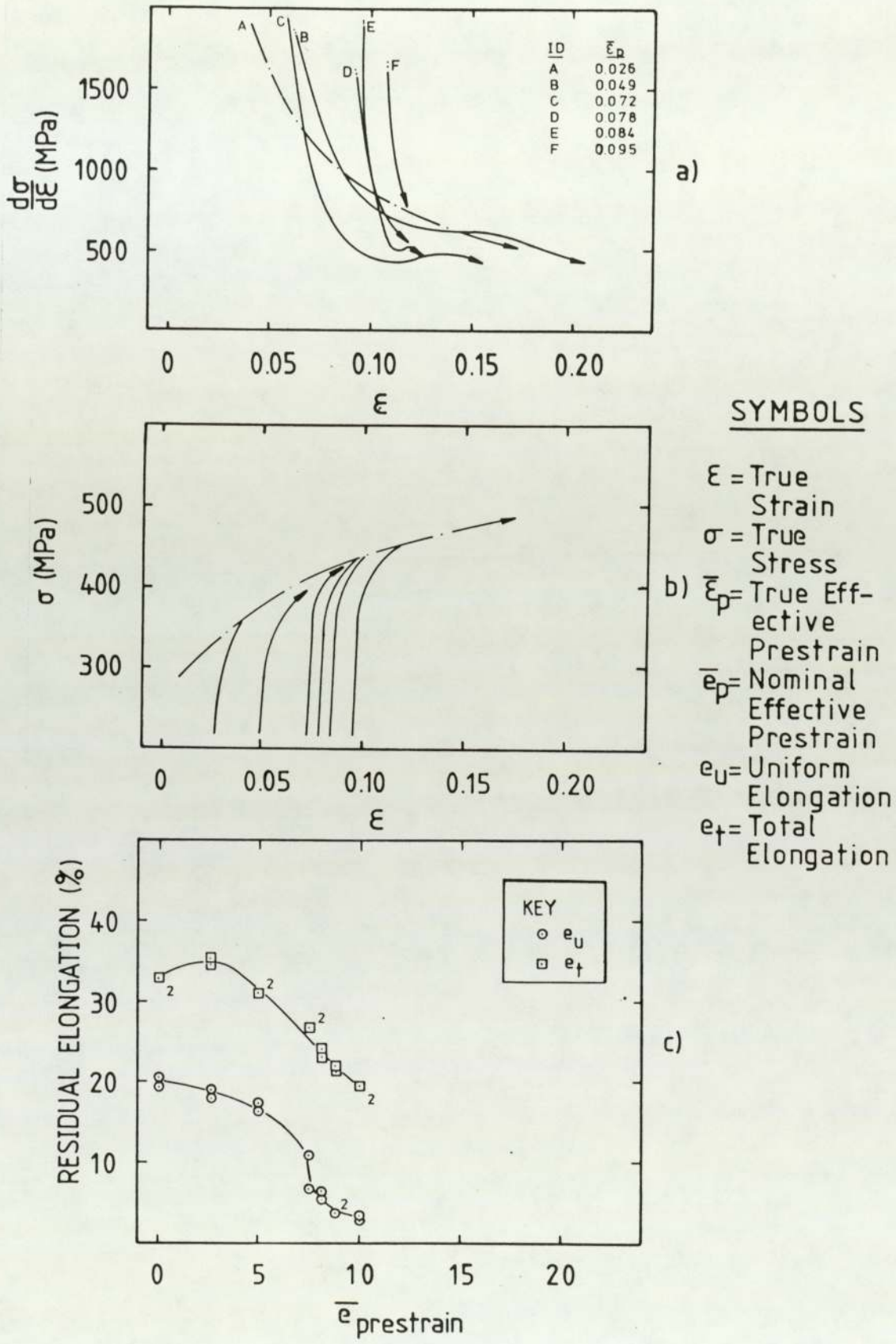

Fig. 43. Steel RP, Uniaxial Prestrain: Tensile Test Results, Stage II Rotated 90 Degrees from the Prestrain Direction. (a) Work-Hardening Curves, (b) True Stress-Strain Curves (Each Offset by the Prestrain), (c) Residual Tensile Elongations. Chain Dotted Lines Represent As-Received Properties.

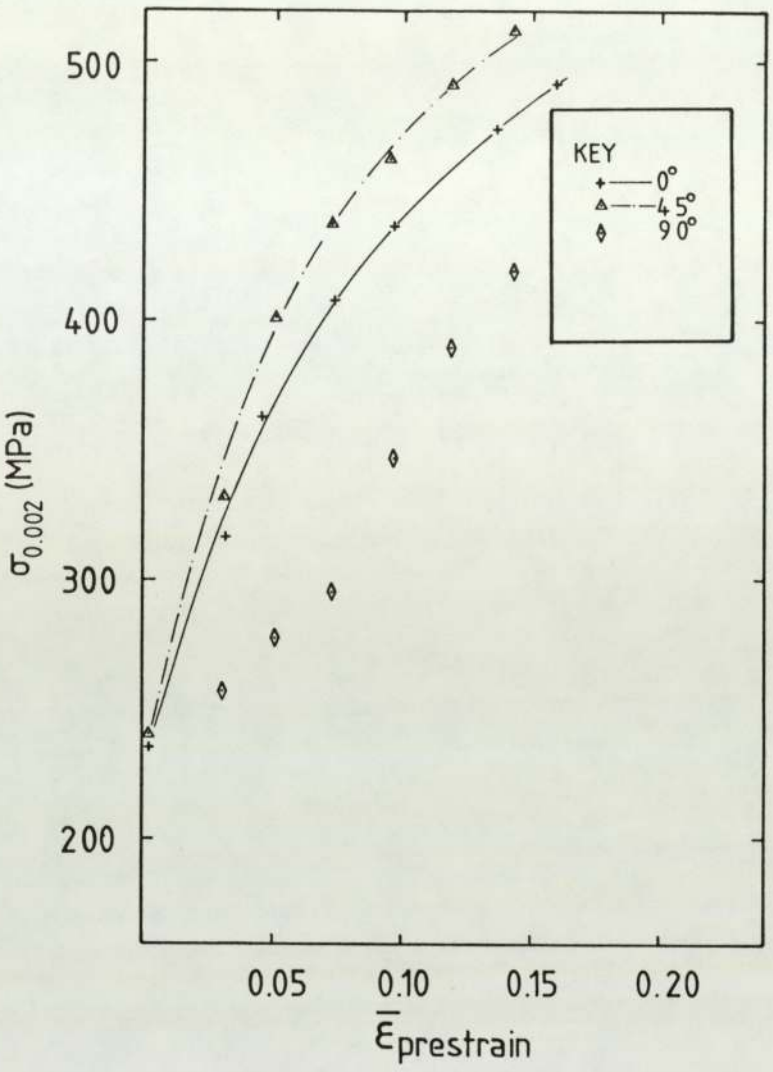

Fig. 44. Steel DP, Uniaxial Prestrain: Variation of True 0.2% Proof Stress with Prestrain Level and Angle of Separation Between Stage I and II Straining.

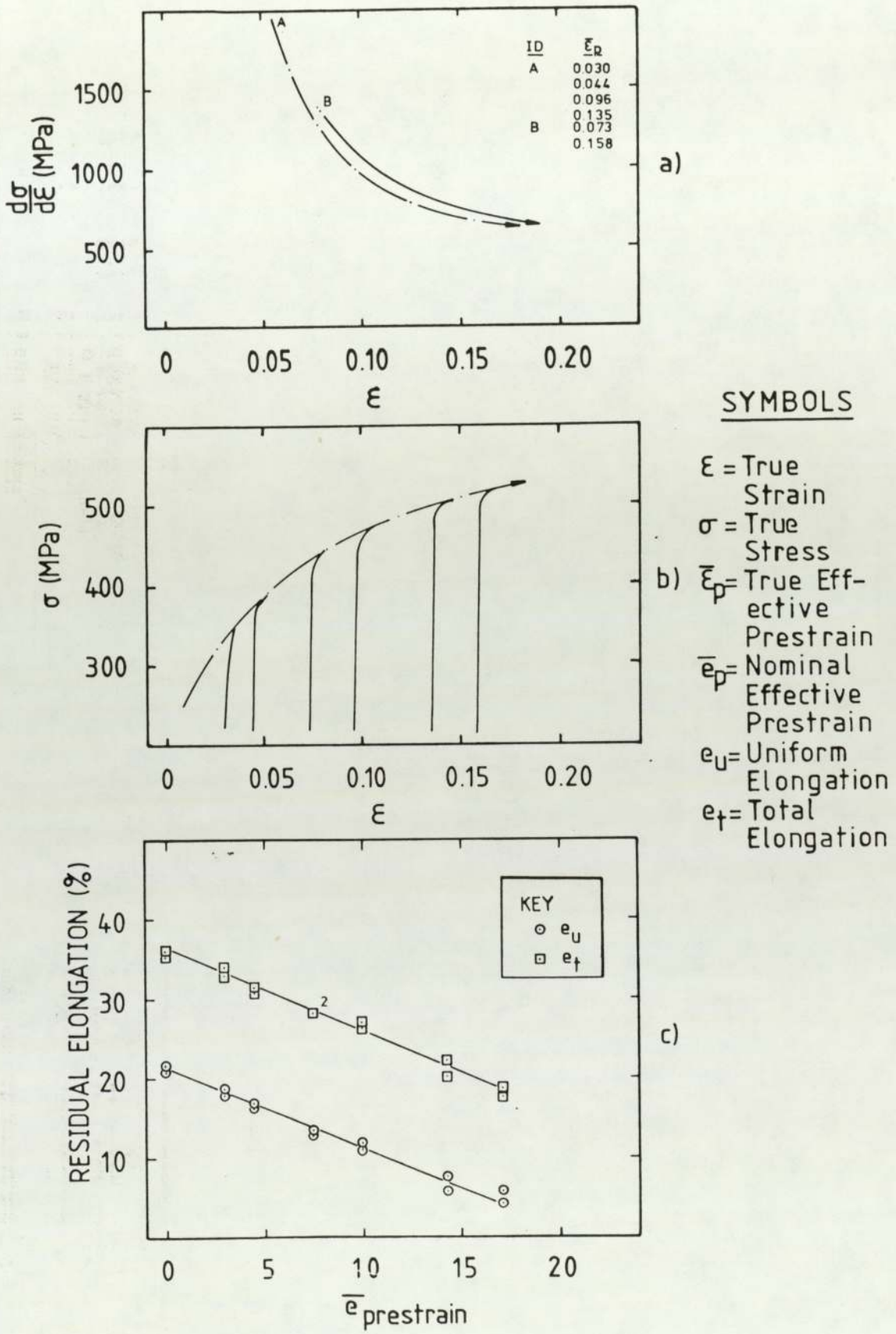

Fig. 45. Steel DP, Uniaxial Prestrain: Tensile Test Results, Stage II Rotated 0 Degrees from the Prestrain Direction. (a) Work-Hardening Curves, (b) True Stress-Strain Curves (Each Offset by the Prestrain), (c) Residual Tensile Elongations. Chain Dotted Lines Represent As-Received Properties.

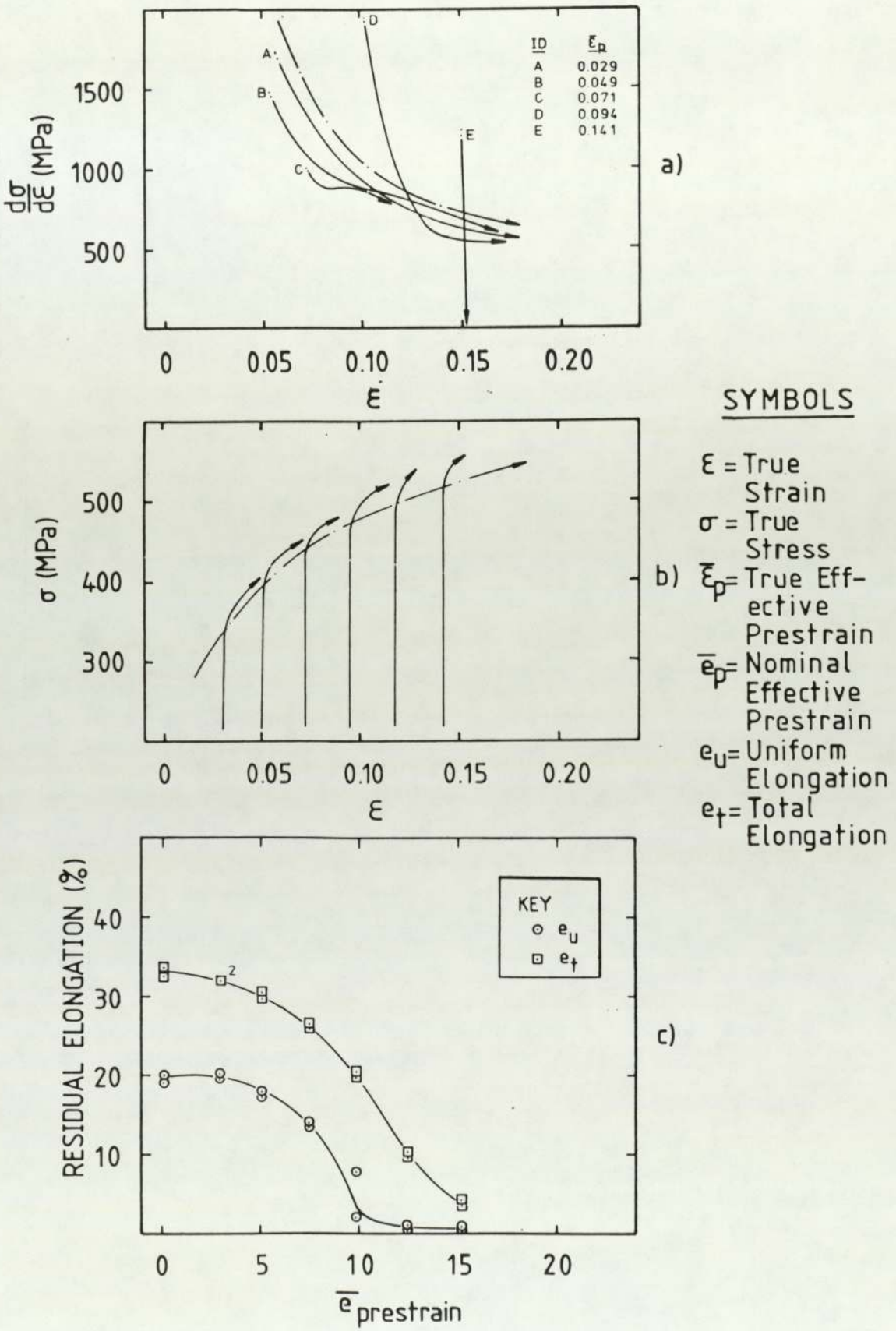

Fig. 46. Steel DP, Uniaxial Prestrain: Tensile Test Results, Stage II Rotated 45 Degrees from the Prestrain Direction. (a) Work-Hardening Curves, (b) True Stress-Strain Curves (Each Offset by the Prestrain), (c) Residual Tensile Elongations. Chain Dotted Lines Represent As-Received Properties.

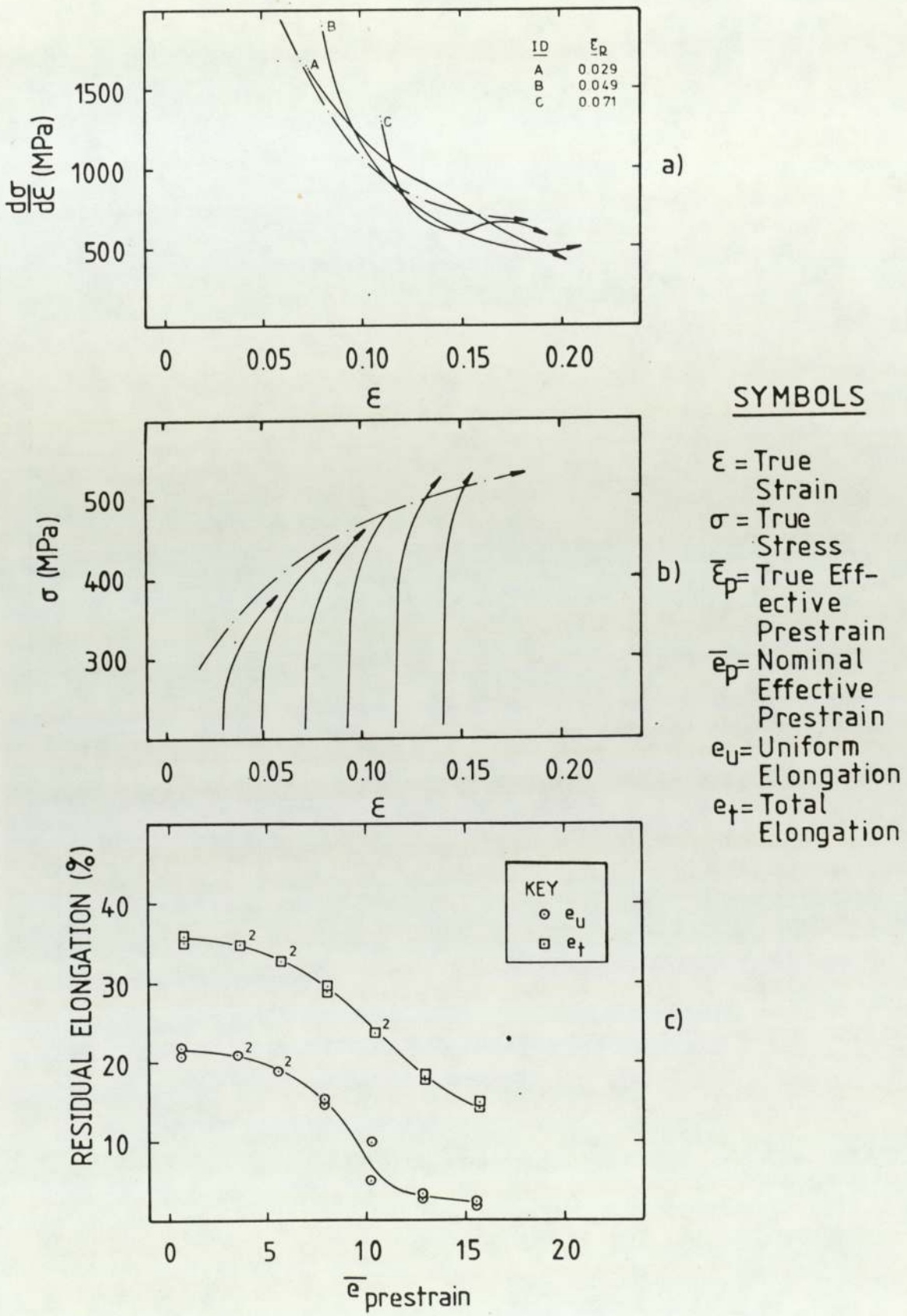

Fig. 47. Steel DP, Uniaxial Prestrain: Tensile Test Results, Stage II Rotated 90 Degrees from the Prestrain Direction. (a) Work-Hardening Curves, (b) True Stress-Strain Curves (Each Offset by the Prestrain), (c) Residual Tensile Elongations. Chain Dotted Lines Represent As-Received Properties.

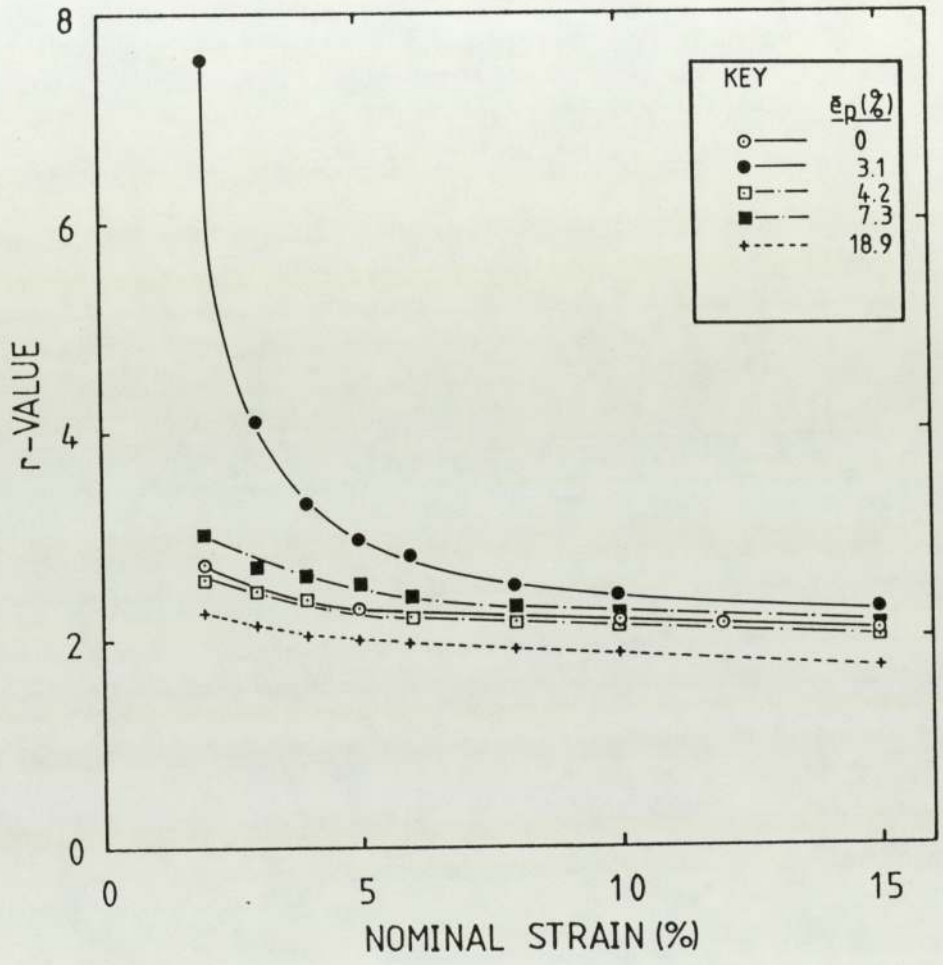

Fig. 48a). Steel AK, Uniaxial Prestrain: Variation of r-Value with Prestrain Level, Stage II Rotated 0 Degrees from the Prestrain Direction.

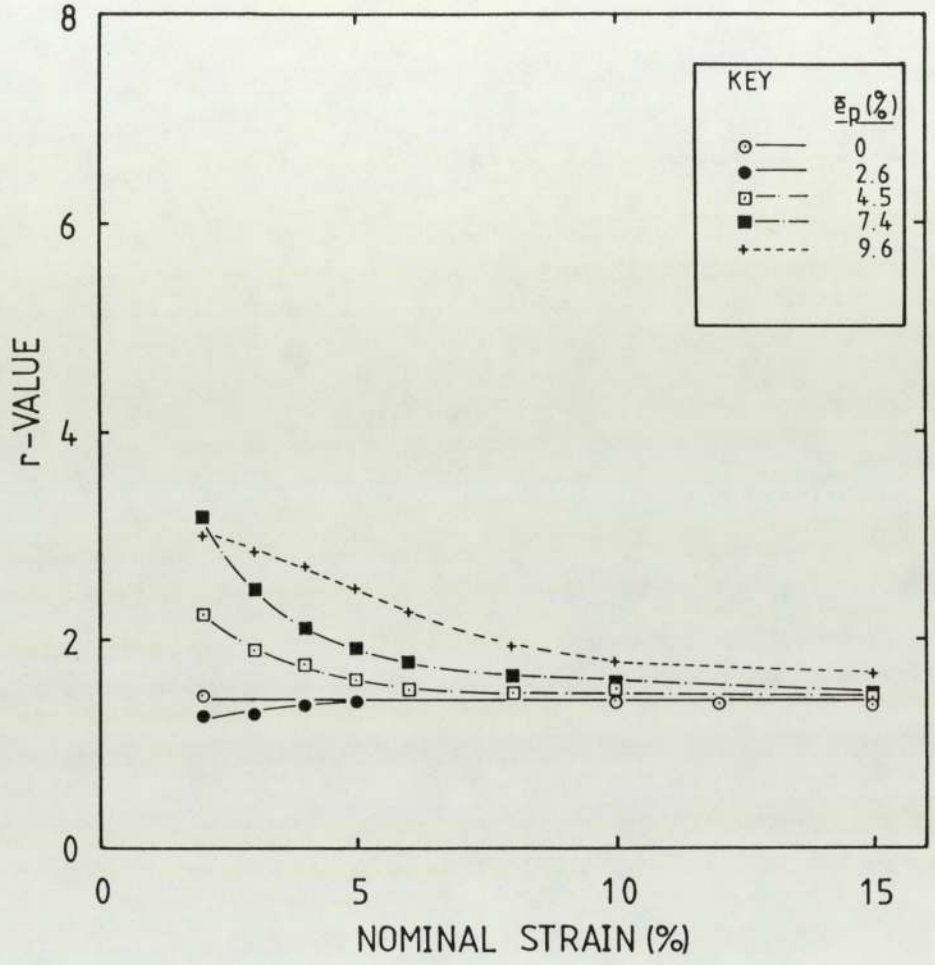

Fig. 48b). Steel AK, Uniaxial Prestrain: Variation of r-Value with Prestrain Level, Stage II Rotated 45 Degrees from the Prestrain Direction.

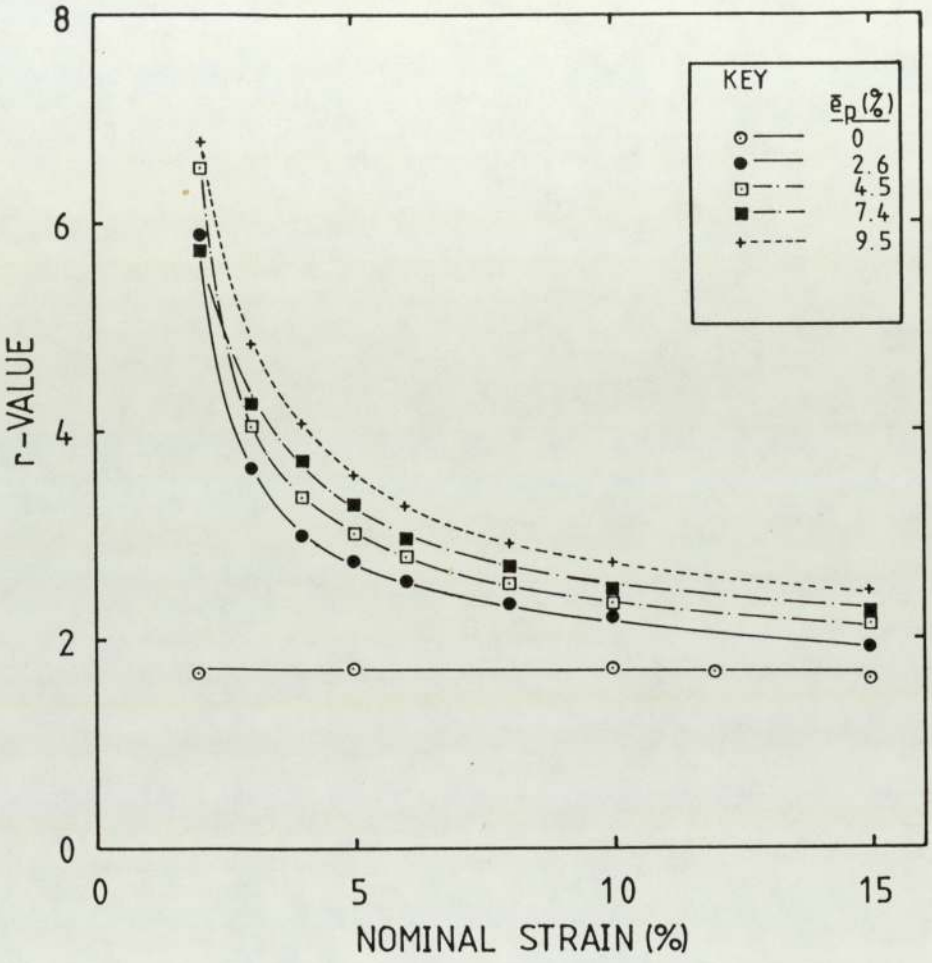

Fig. 48c). Steel AK, Uniaxial Prestrain: Variation of r-Value with Prestrain Level, Stage II Rotated 90 Degrees from the Prestrain Direction.

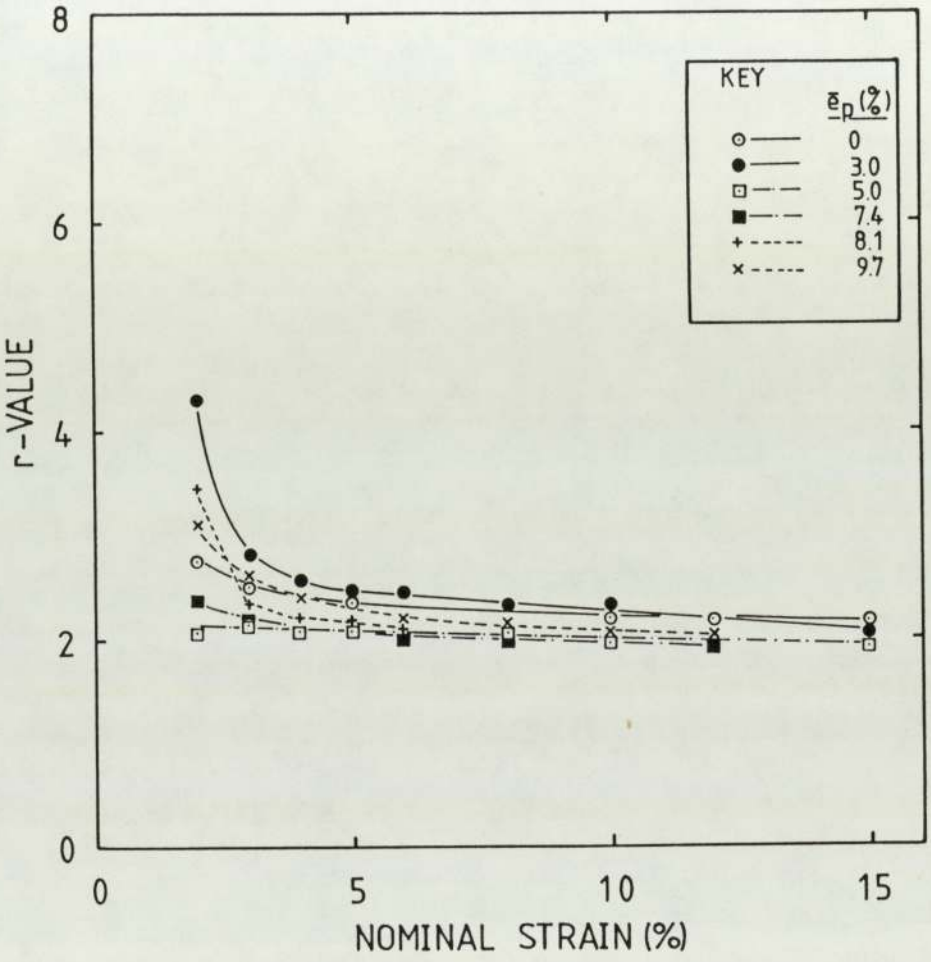

Fig. 49a). Steel RP, Uniaxial Prestrain: Variation of r-Value with Prestrain Level, Stage II Rotated 0 Degrees from the Prestrain Direction.

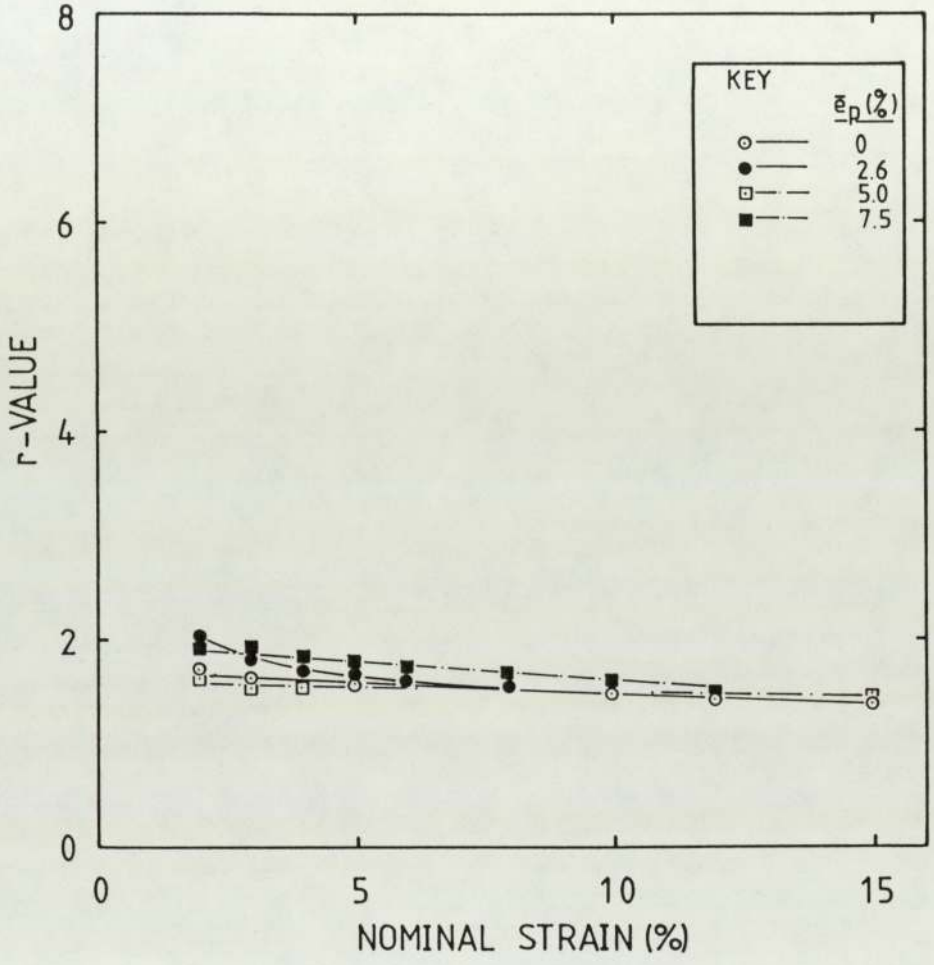

Fig. 49b). Steel RP, Uniaxial Prestrain: Variation of r-Value with Prestrain Level, Stage II Rotated 45 Degrees from the Prestrain Direction.

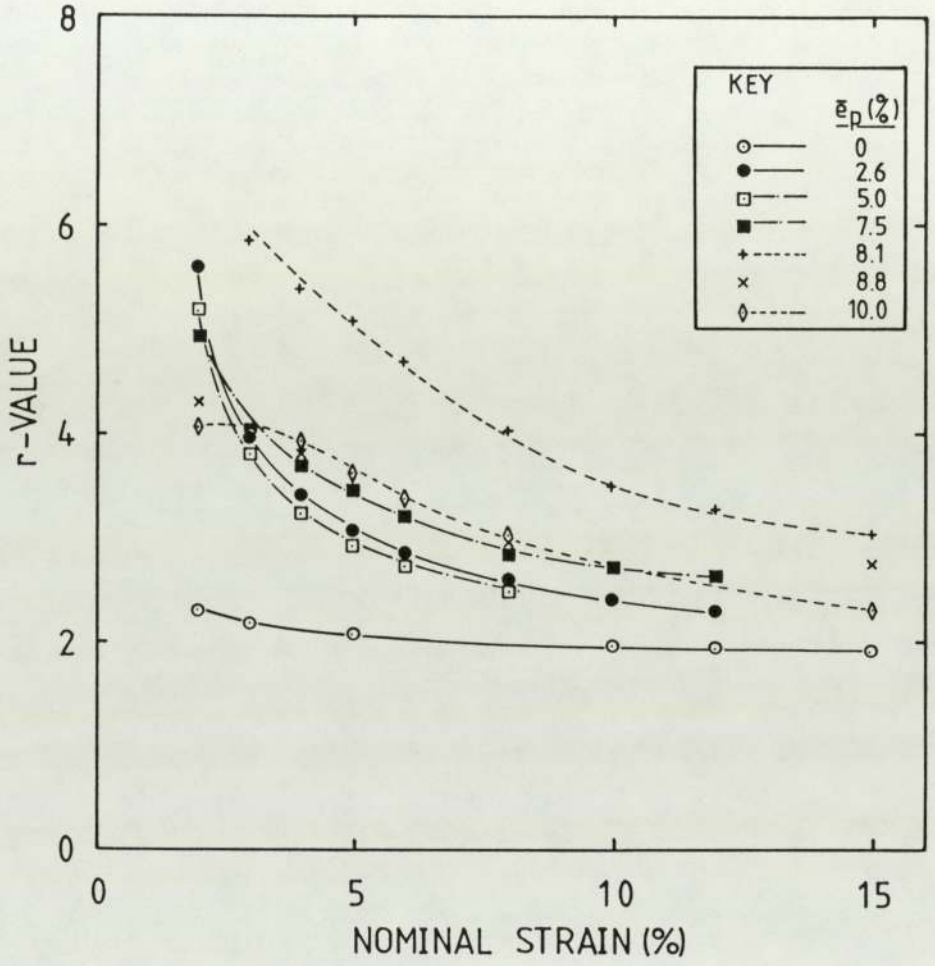

Fig. 49c). Steel RP, Uniaxial Prestrain: Variation of r-Value with Prestrain Level, Stage II Rotated 90 Degrees from the Prestrain Direction.

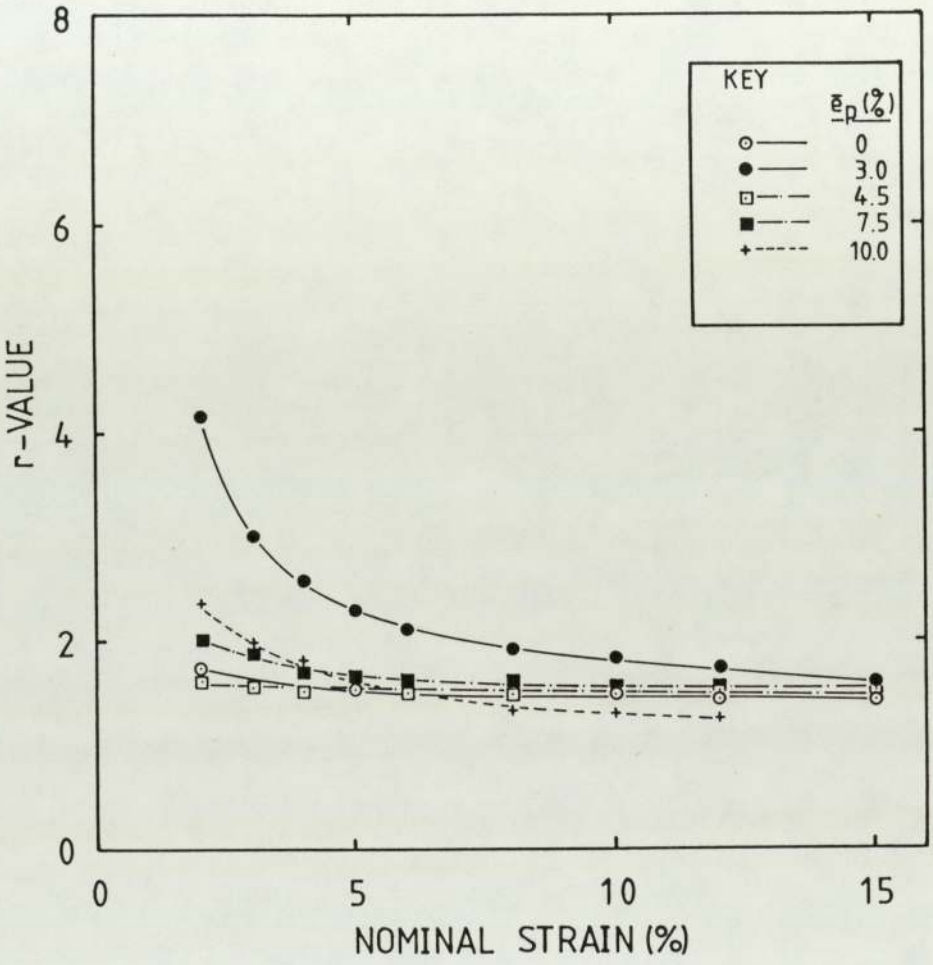

Fig. 50a). Steel DP, Uniaxial Prestrain: Variation of r-Value with Prestrain Level, Stage II Rotated 0 Degrees from the Prestrain Direction.

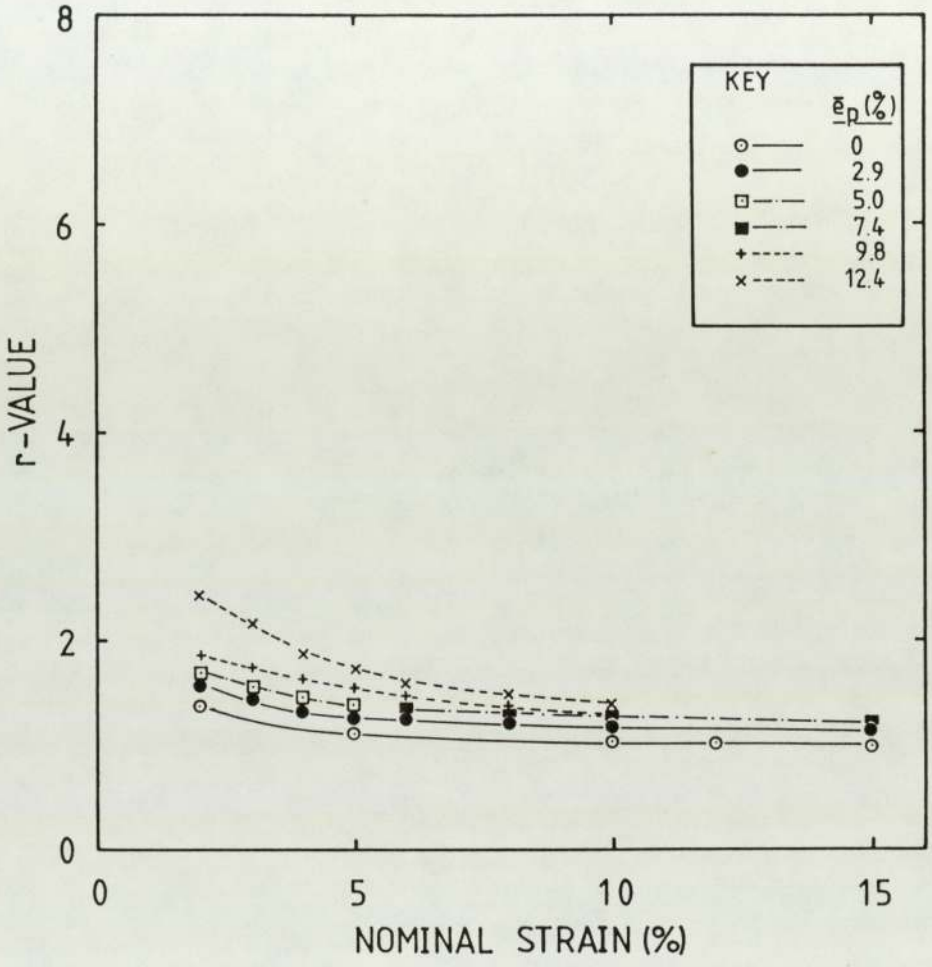

Fig. 50b). Steel DP, Uniaxial Prestrain: Variation of r-Value with Prestrain Level, Stage II Rotated 45 Degrees from the Prestrain Direction.

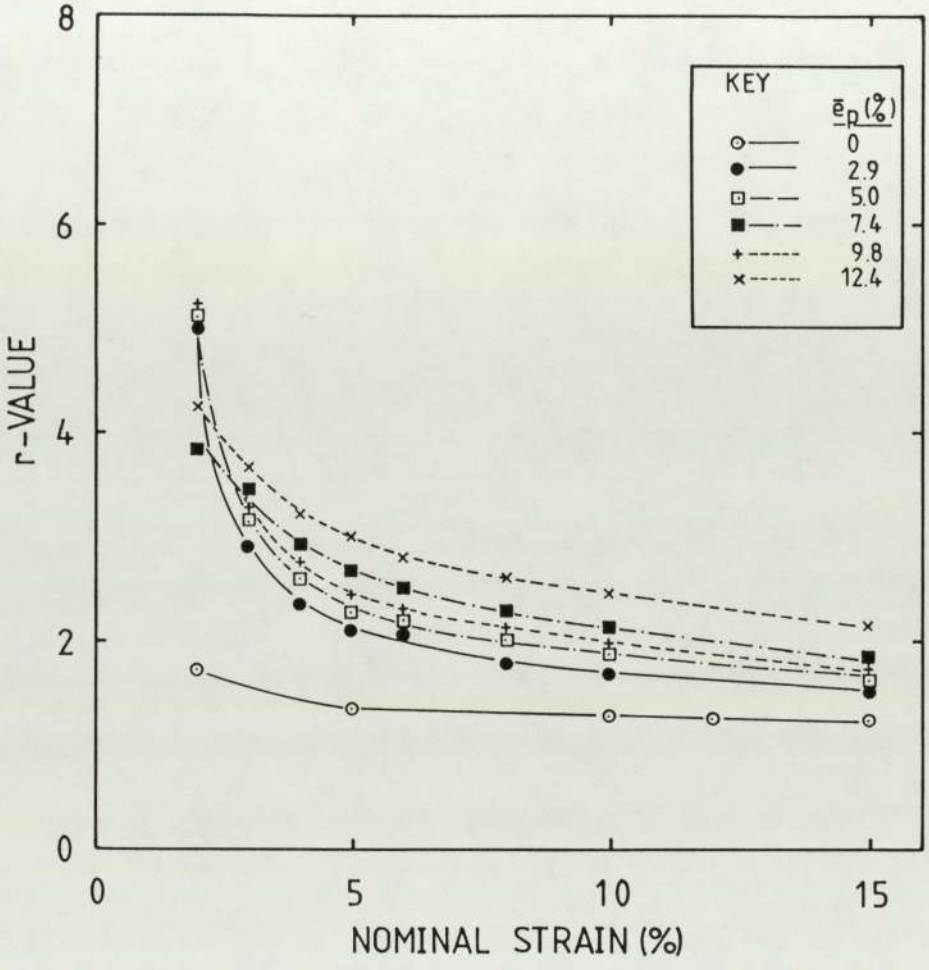

Fig. 50c). Steel DP, Uniaxial Prestrain: Variation of r-Value with Prestrain Level, Stage II Rotated 90 Degrees from the Prestrain Direction.

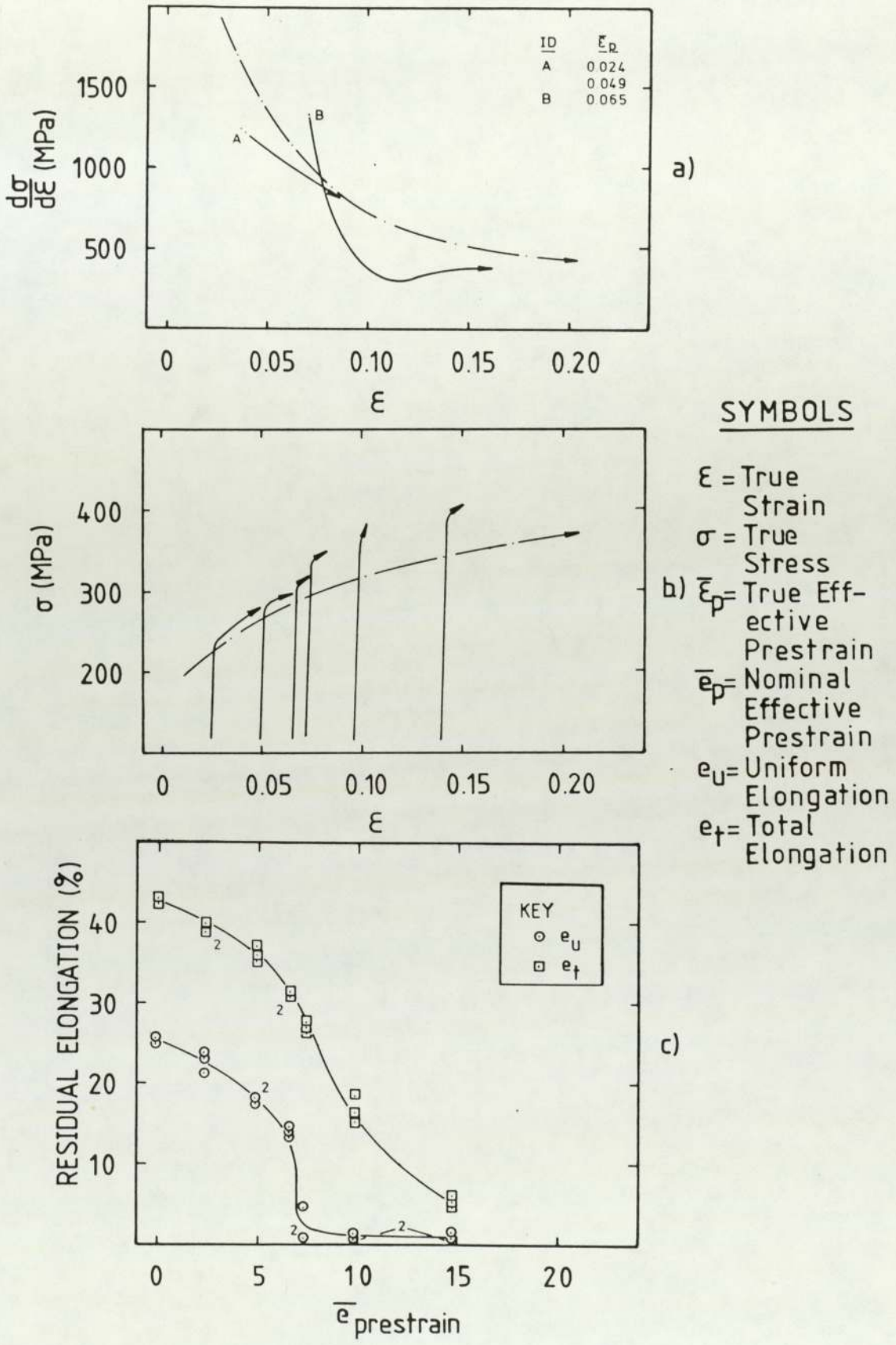

Fig. 51. Steel AK, Biaxial Prestrain: Tensile Test Results, Stage II in the Rolling Direction of the Sheet. (a) Work-Hardening Curves, (b) True Stress-Strain Curves (Each Offset by the Prestrain), (c) Residual Tensile Elongations. Chain Dotted Lines Represent As-Received Properties.

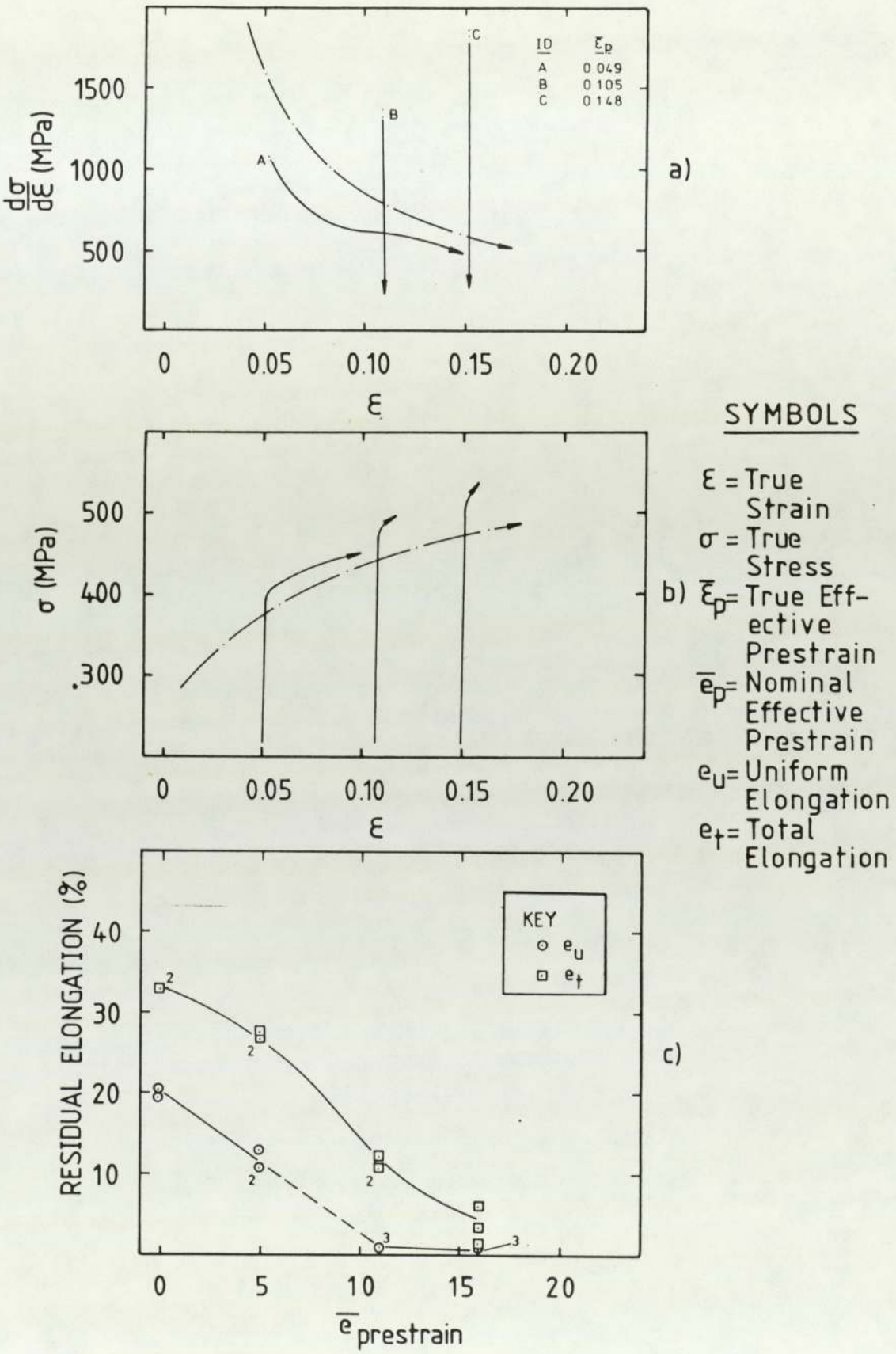

Fig. 52. Steel RP, Biaxial Prestrain: Tensile Test Results, Stage II in the Rolling Direction of the Sheet. (a) Work-Hardening Curves, (b) True Stress-Strain Curves (Each Offset by the Prestrain), (c) Residual Tensile Elongations. Chain Dotted Lines Represent As-Received Properties.

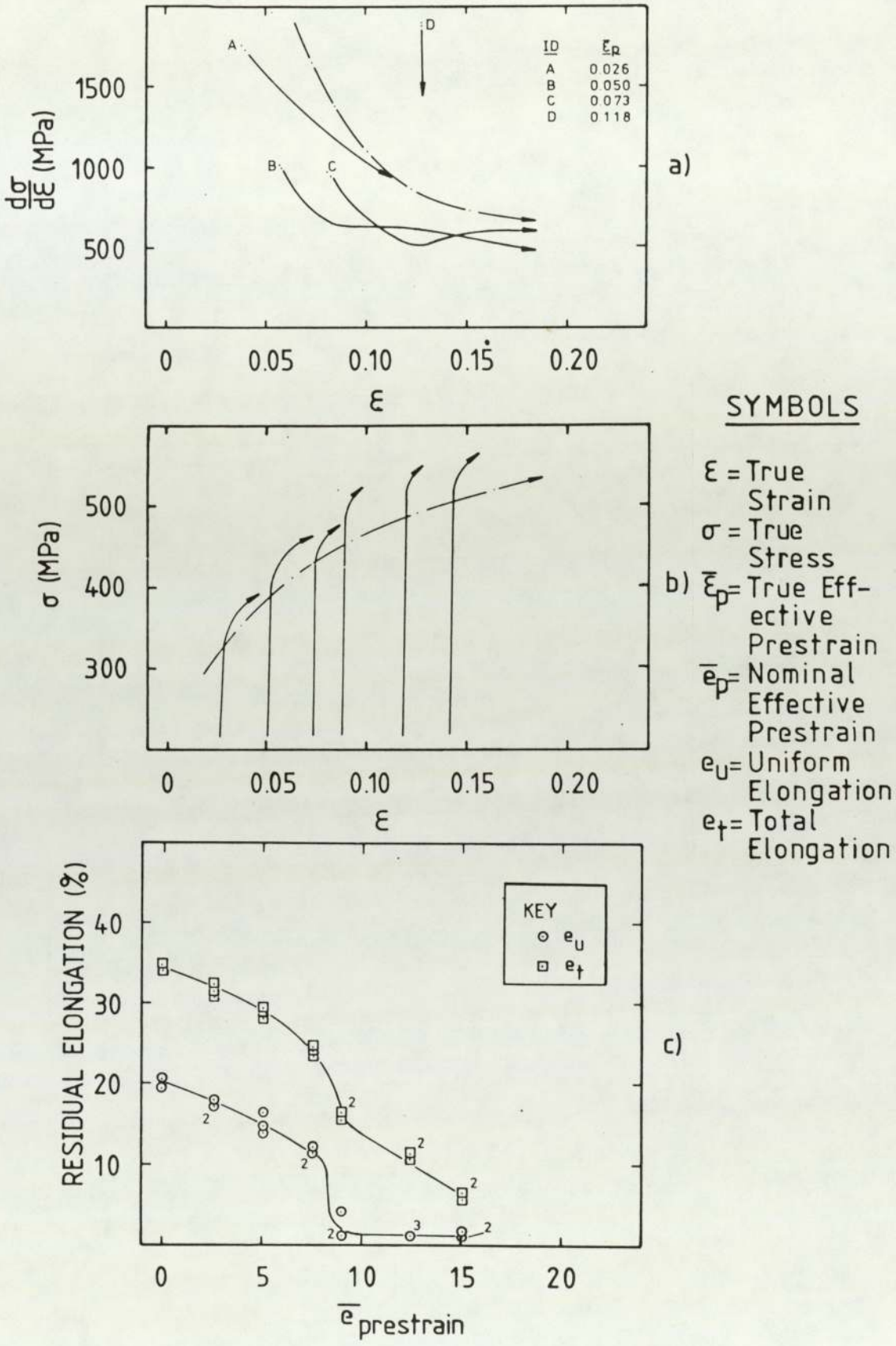

Fig. 53. Steel DP, Biaxial Prestrain: Tensile Test Results, Stage II in the Rolling Direction of the Sheet. (a) Work-Hardening Curves, (b) True Stress-Strain Curves (Each Offset by the Prestrain), (c) Residual Tensile Elongations. Chain Dotted Lines Represent As-Received Properties.

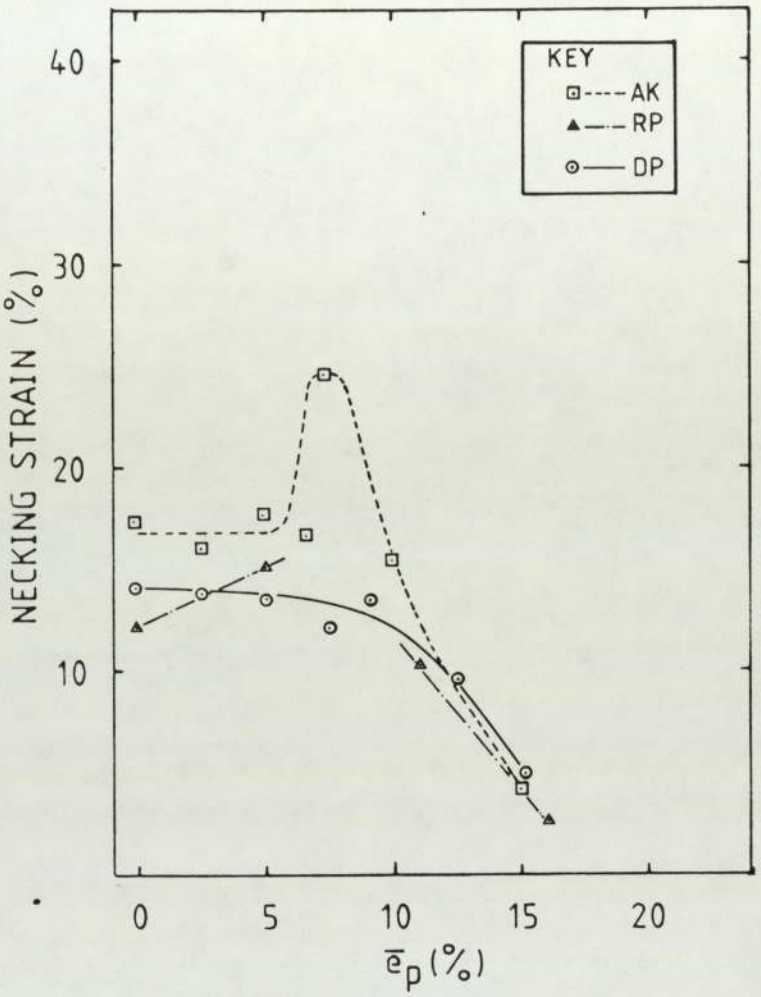

Fig. 54. Steels AK, RP, DP Biaxial Prestrain: Variation of Tensile Necking Strains with Prestrain Level.

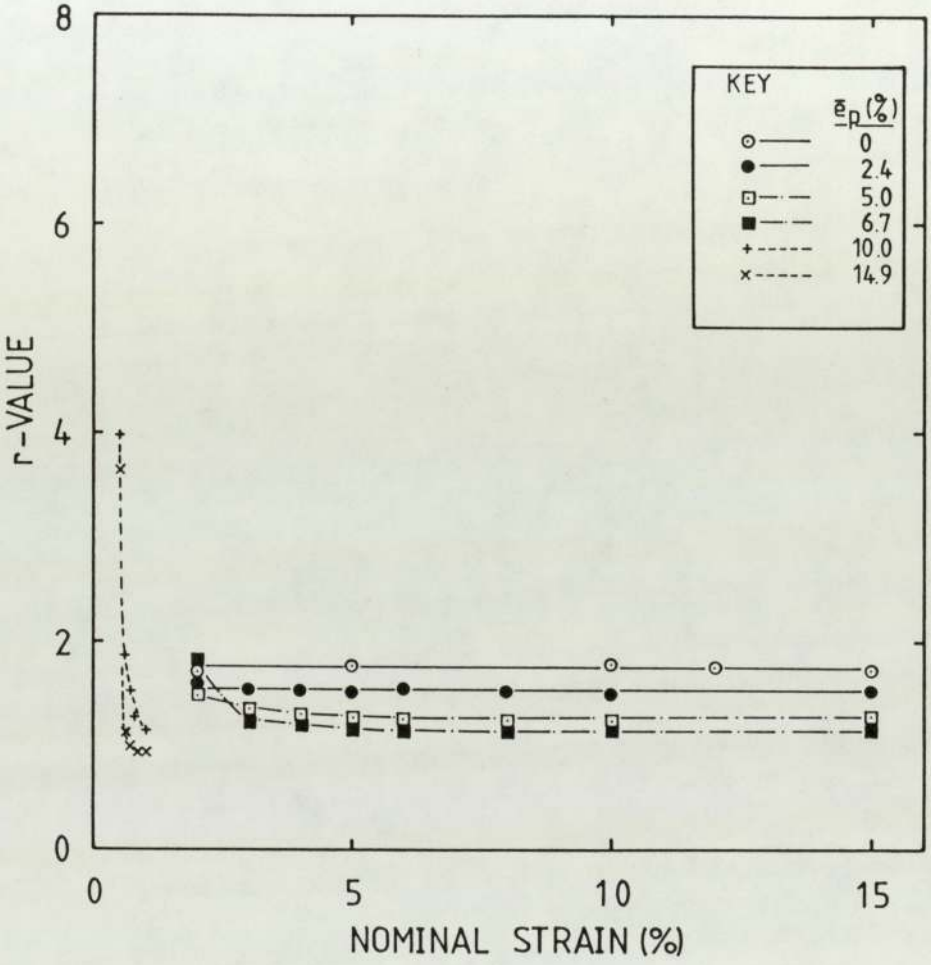

Fig. 55a). Steel AK, Biaxial Prestrain: Variation of r-Value with Prestrain Level, Stage II in the Rolling Direction of the Sheet.

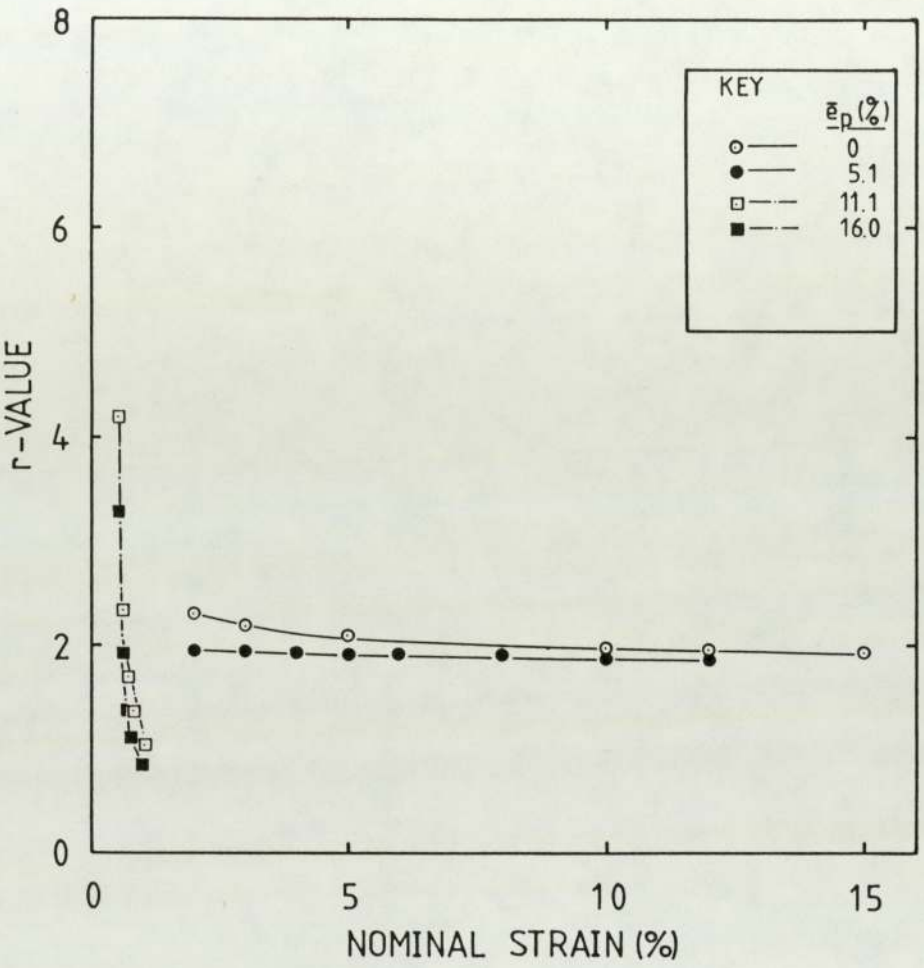

Fig. 55b). Steel RP, Biaxial Prestrain: Variation of r-Value with Prestrain Level, Stage II in the Rolling Direction of the Sheet.

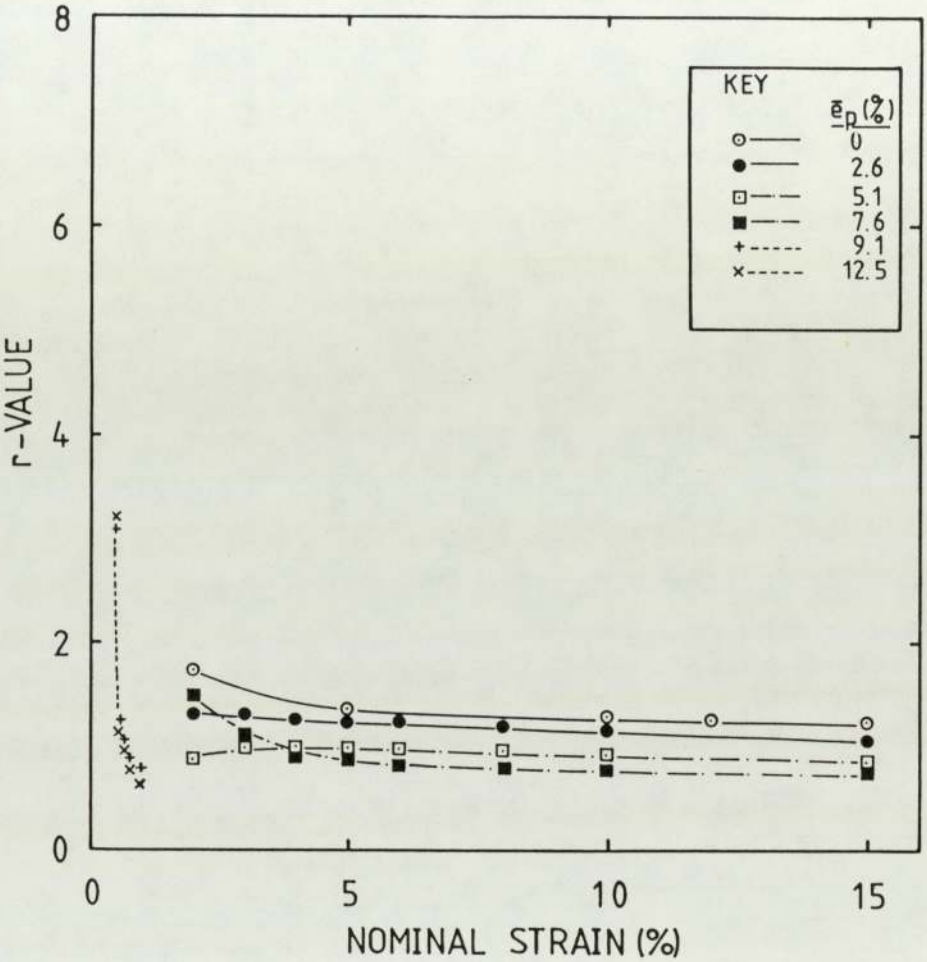

Fig. 55c). Steel DP, Biaxial Prestrain: Variation of r-Value with Prestrain Level, Stage II in the Rolling Direction of the Sheet.

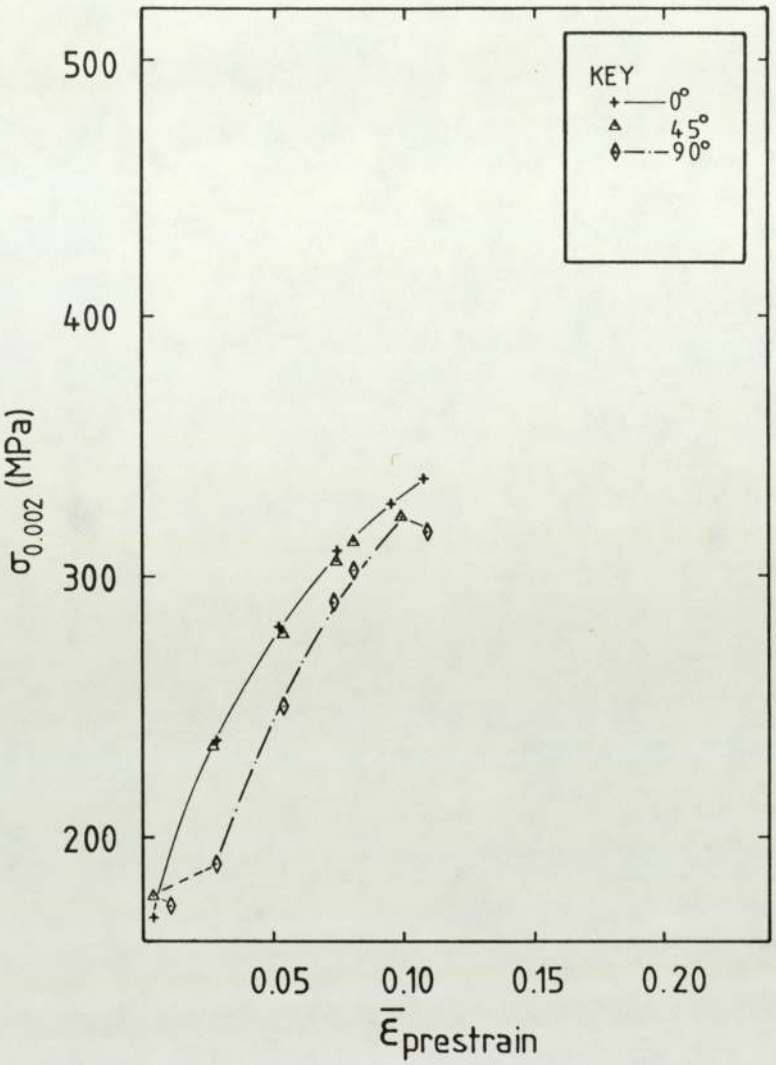

Fig. 56. Steel AK, Plane-Strain Prestrain: Variation of True 0.2% Proof Stress with Prestrain Level and Angle of Separation Between Stage I and II Straining.

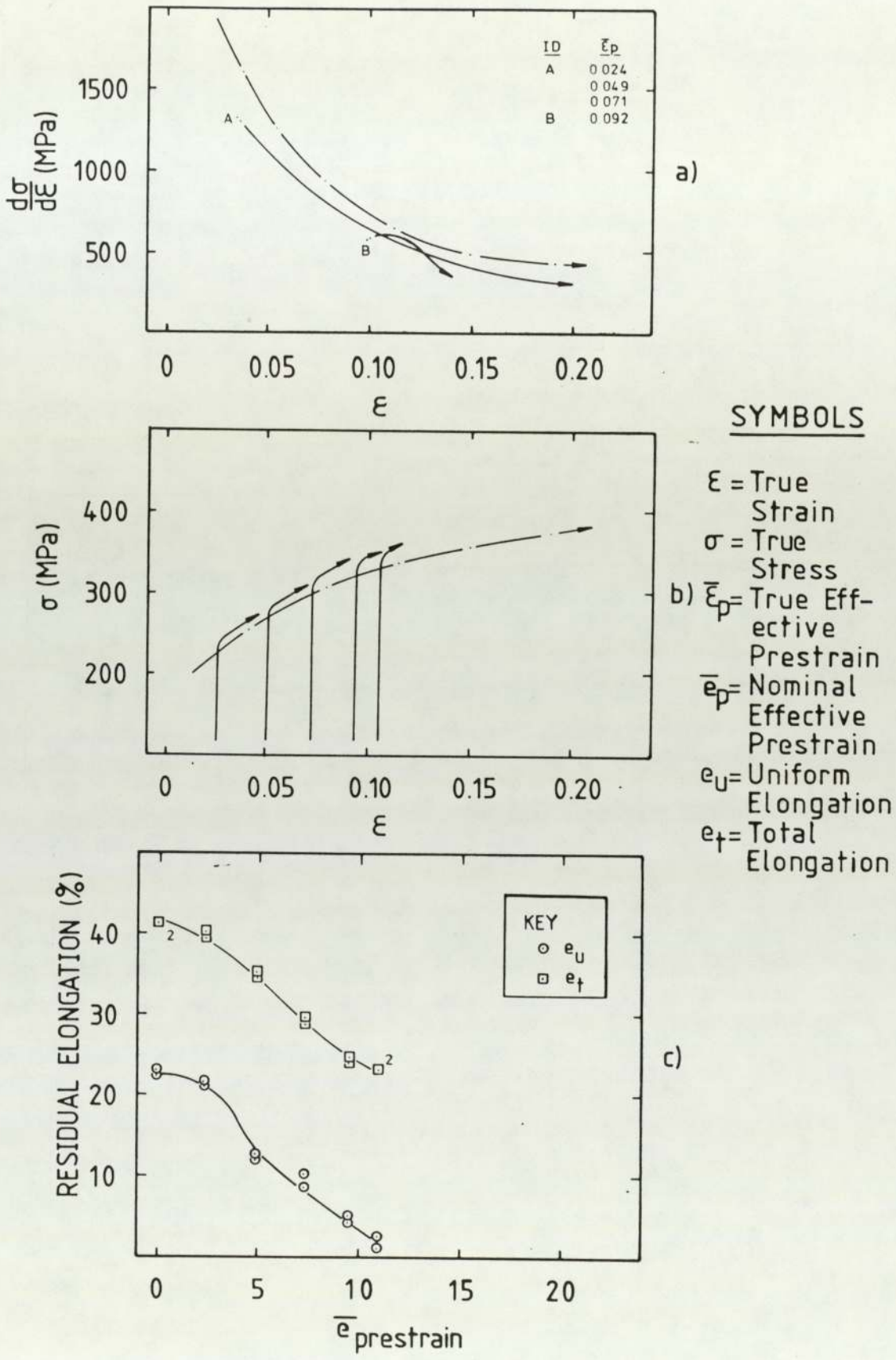

Fig. 57. Steel AK, Plane-Strain Prestrain: Tensile Test Results, Stage II Rotated 0 Degrees from the Prestrain Direction. (a) Work-Hardening Curves, (b) True Stress-Strain Curves (Each Offset by the Prestrain), (c) Residual Tensile Elongations. Chain Dotted Lines Represent As-Received Properties.

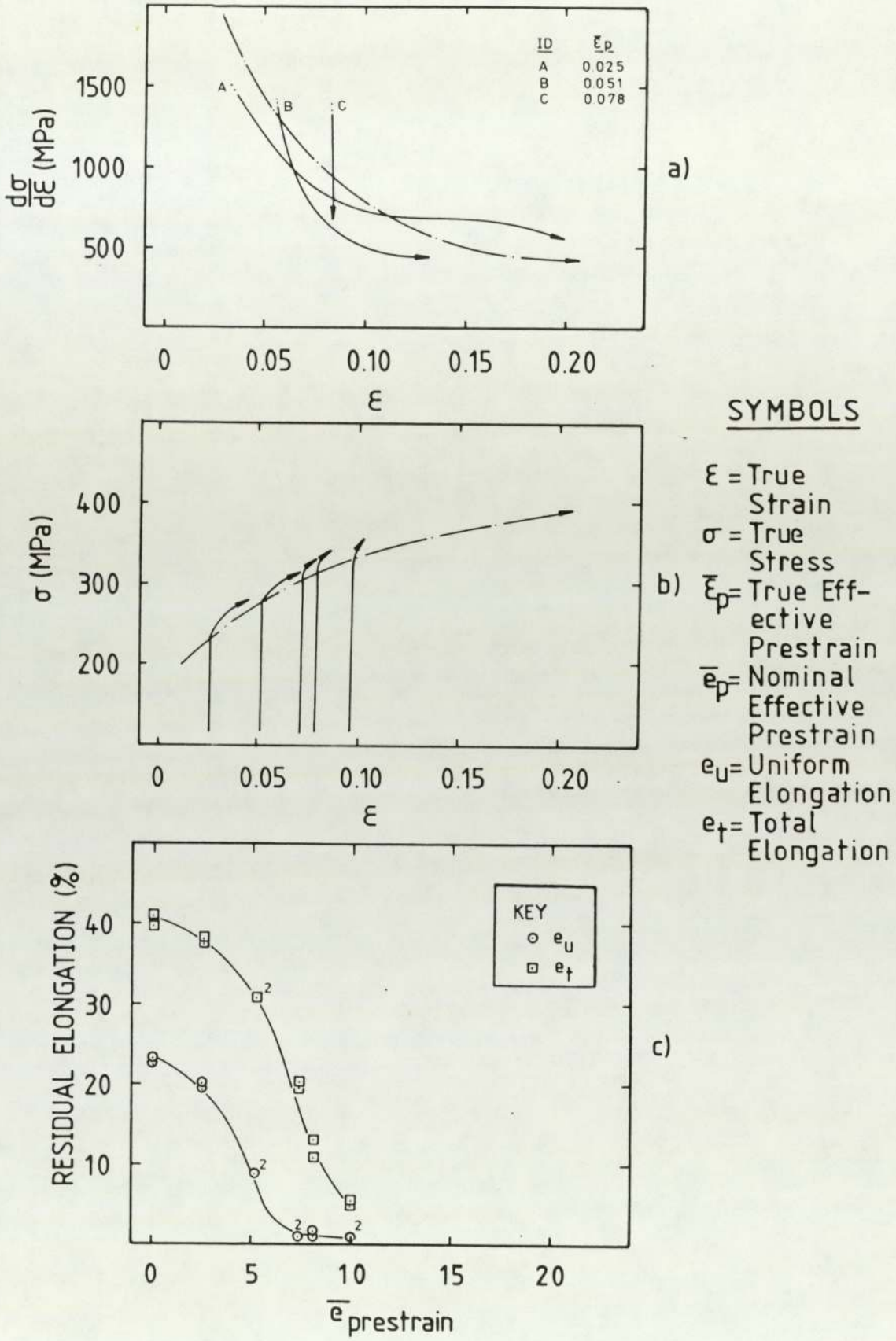

Fig. 58. Steel AK, Plane-Strain Prestrain: Tensile Test Results, Stage II Rotated 45 Degrees from the Prestrain Direction. (a) Work-Hardening Curves, (b) True Stress-Strain Curves (Each Offset by the Prestrain), (c) Residual Tensile Elongations. Chain Dotted Lines Represent As-Received Properties.

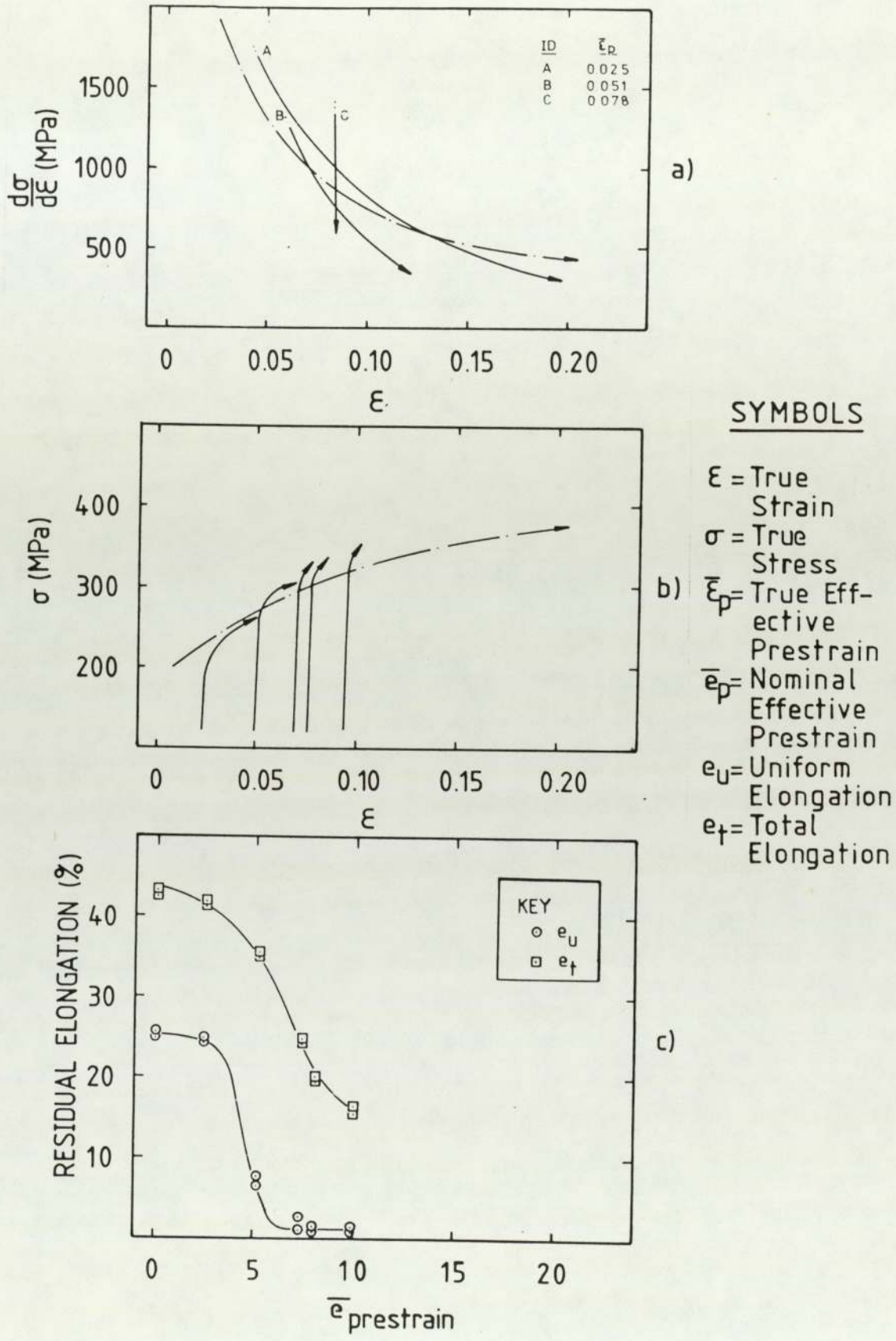

Fig. 59. Steel AK, Plane-Strain Prestrain: Tensile Test Results, Stage II Rotated 90 Degrees from the Prestrain Direction. (a) Work-Hardening Curves, (b) True Stress-Strain Curves (Each Offset by the Prestrain), (c) Residual Tensile Elongations. Chain Dotted Lines Represent As-Received Properties.

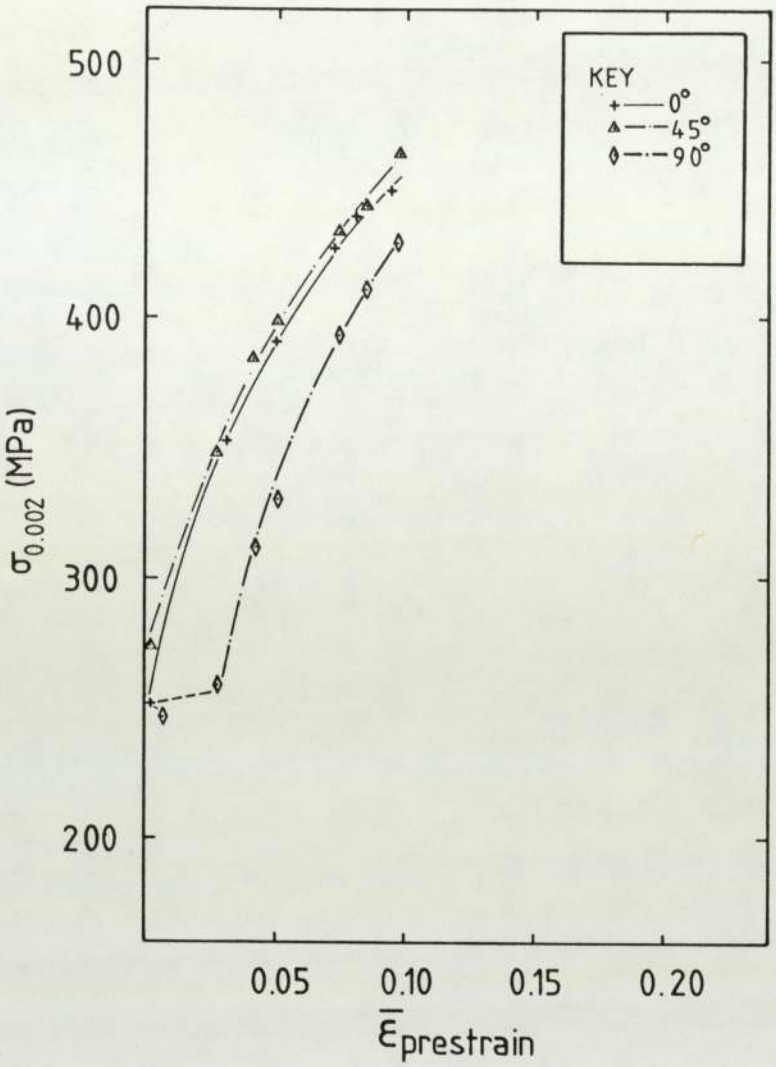

Fig. 60. Steel RP, Plane-Strain Prestrain: Variation of True 0.2% Proof Stress with Prestrain Level and Angle of Separation Between Stage I and II Straining.

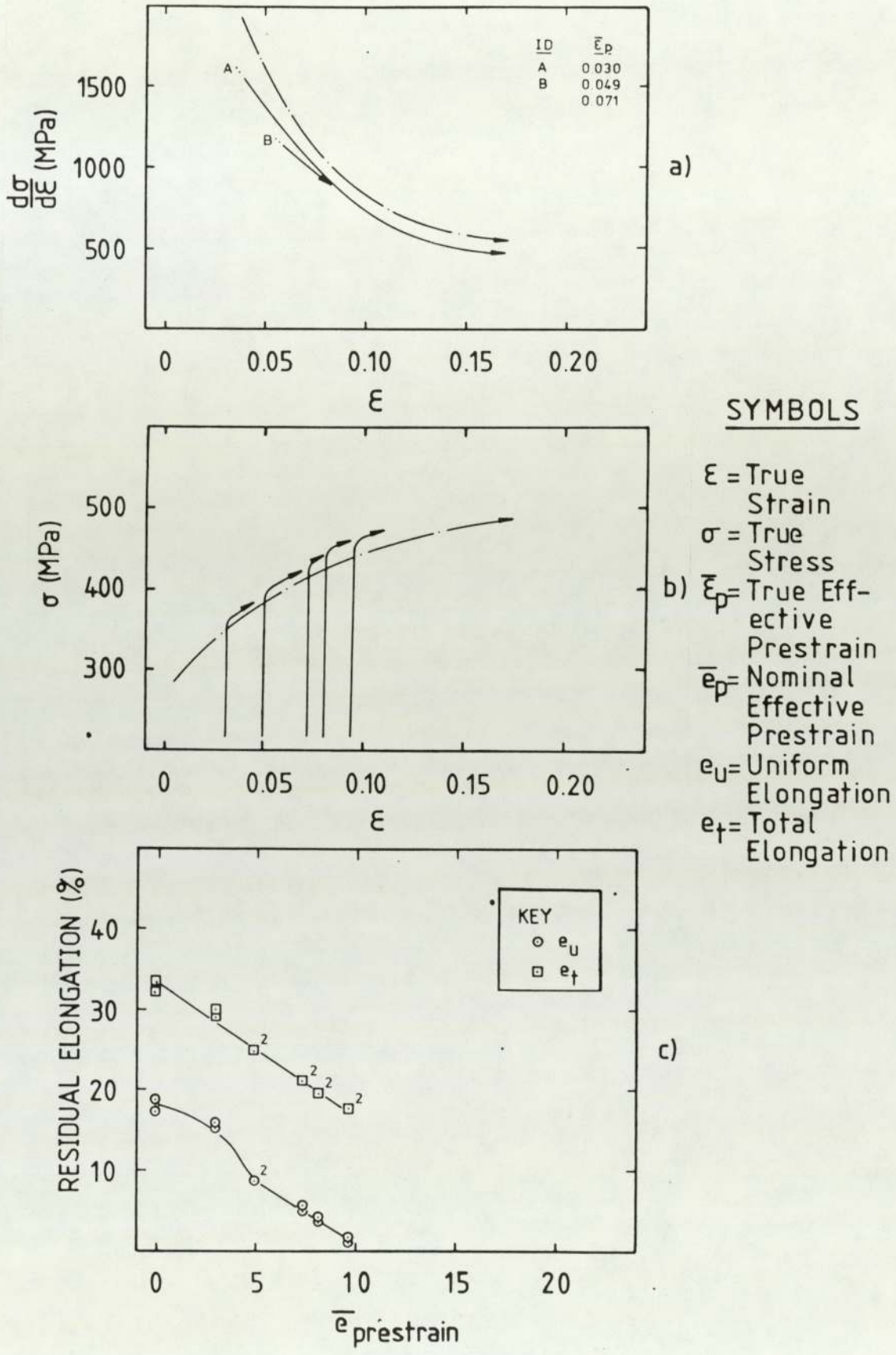

Fig. 61. Steel RP, Plane-Strain Prestrain: Tensile Test Results, Stage II Rotated 0 Degrees from the Prestrain Direction. (a) Work-Hardening Curves, (b) True Stress-Strain Curves (Each Offset by the Prestrain), (c) Residual Tensile Elongations. Chain Dotted Lines Represent As-Received Properties.

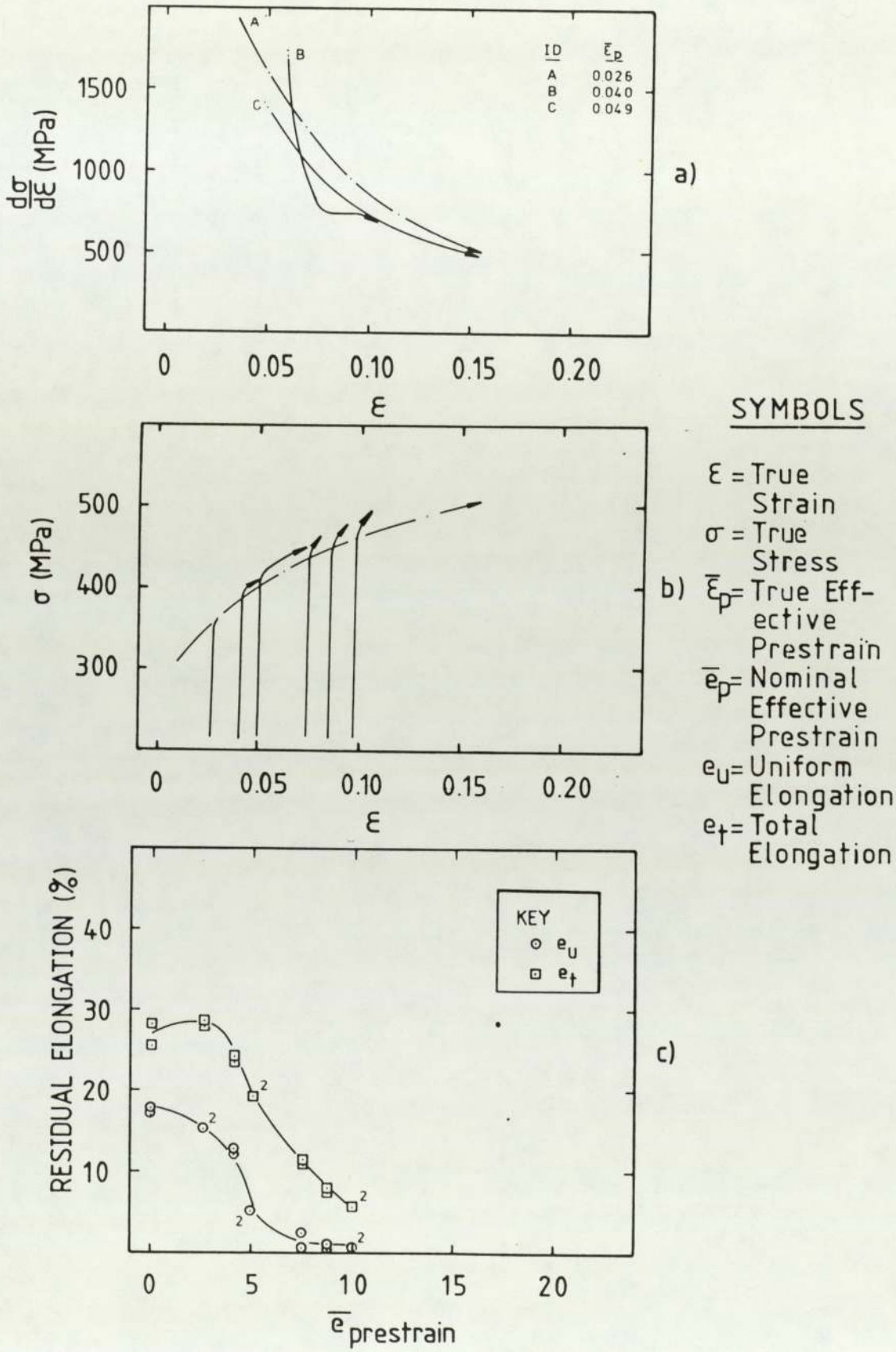

Fig. 62. Steel RP, Plane-Strain Prestrain: Tensile Test Results, Stage II Rotated 45 Degrees from the Prestrain Direction. (a) Work-Hardening Curves, (b) True Stress-Strain Curves (Each Offset by the Prestrain), (c) Residual Tensile Elongations. Chain Dotted Lines Represent As-Received Properties.

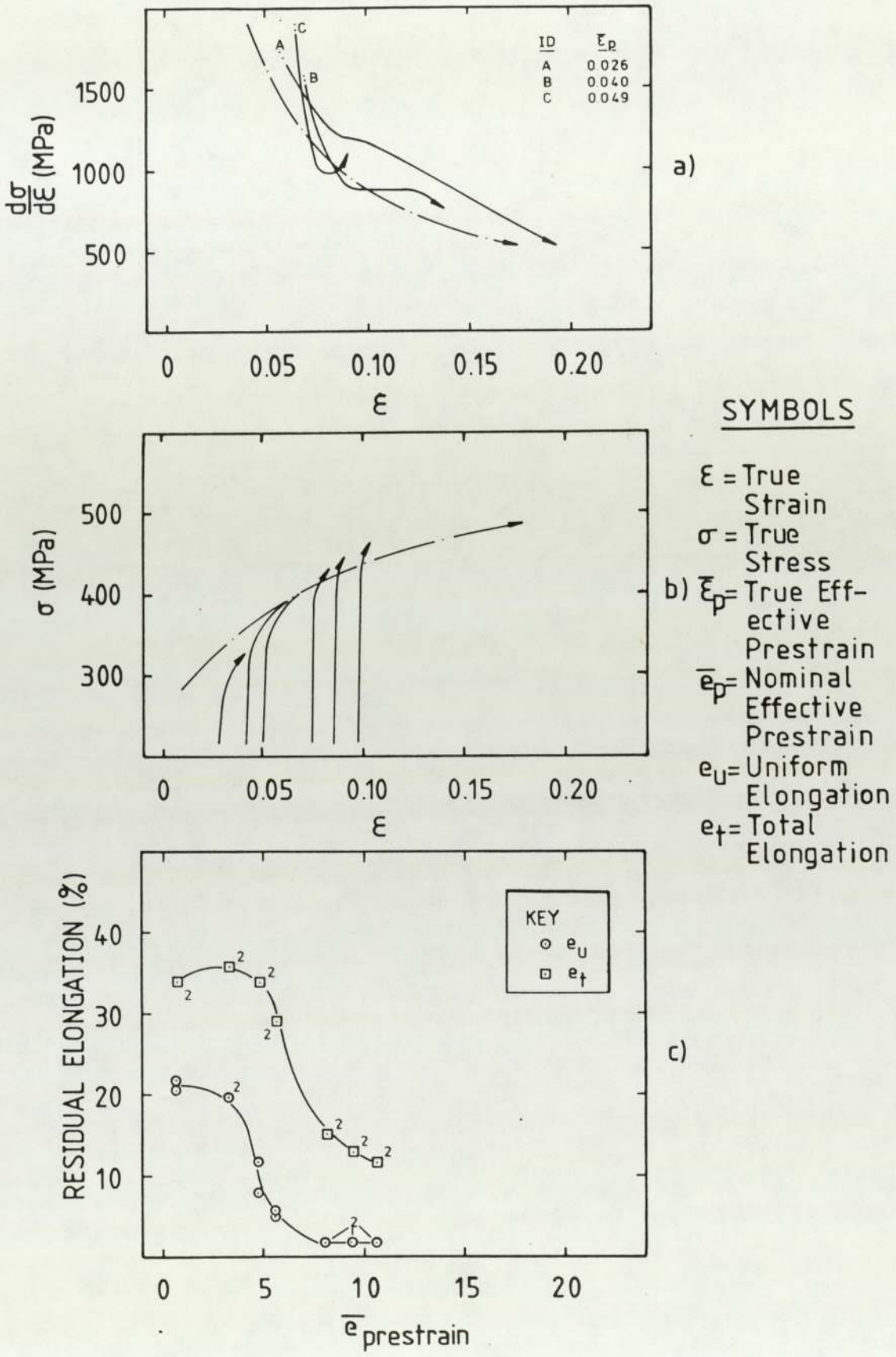

Fig. 63. Steel RP, Plane-Strain Prestrain: Tensile Test Results, Stage II Rotated 90 Degrees from the Prestrain Direction. (a) Work-Hardening Curves, (b) True Stress-Strain Curves (Each Offset by the Prestrain), (c) Residual Tensile Elongations. Chain Dotted Lines Represent As-Received Properties.

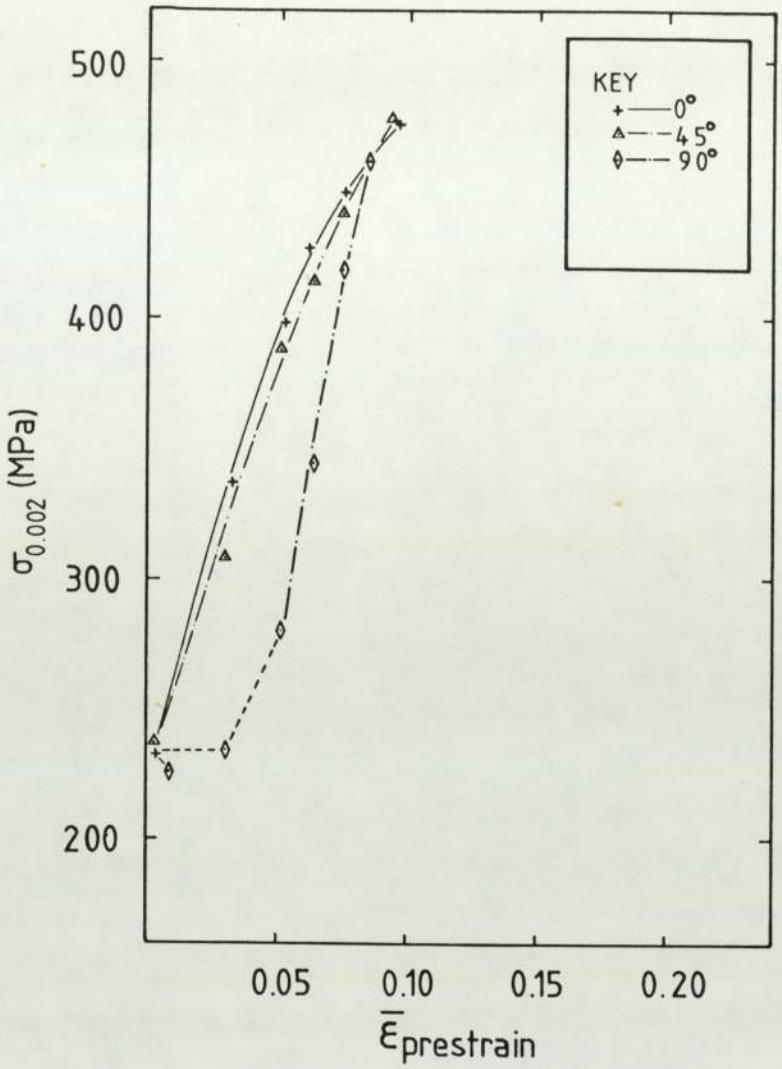

Fig. 64. Steel DP, Plane-Strain Prestrain: Variation of True 0.2% Proof Stress with Prestrain Level and Angle of Separation Between Stage I and II Straining.

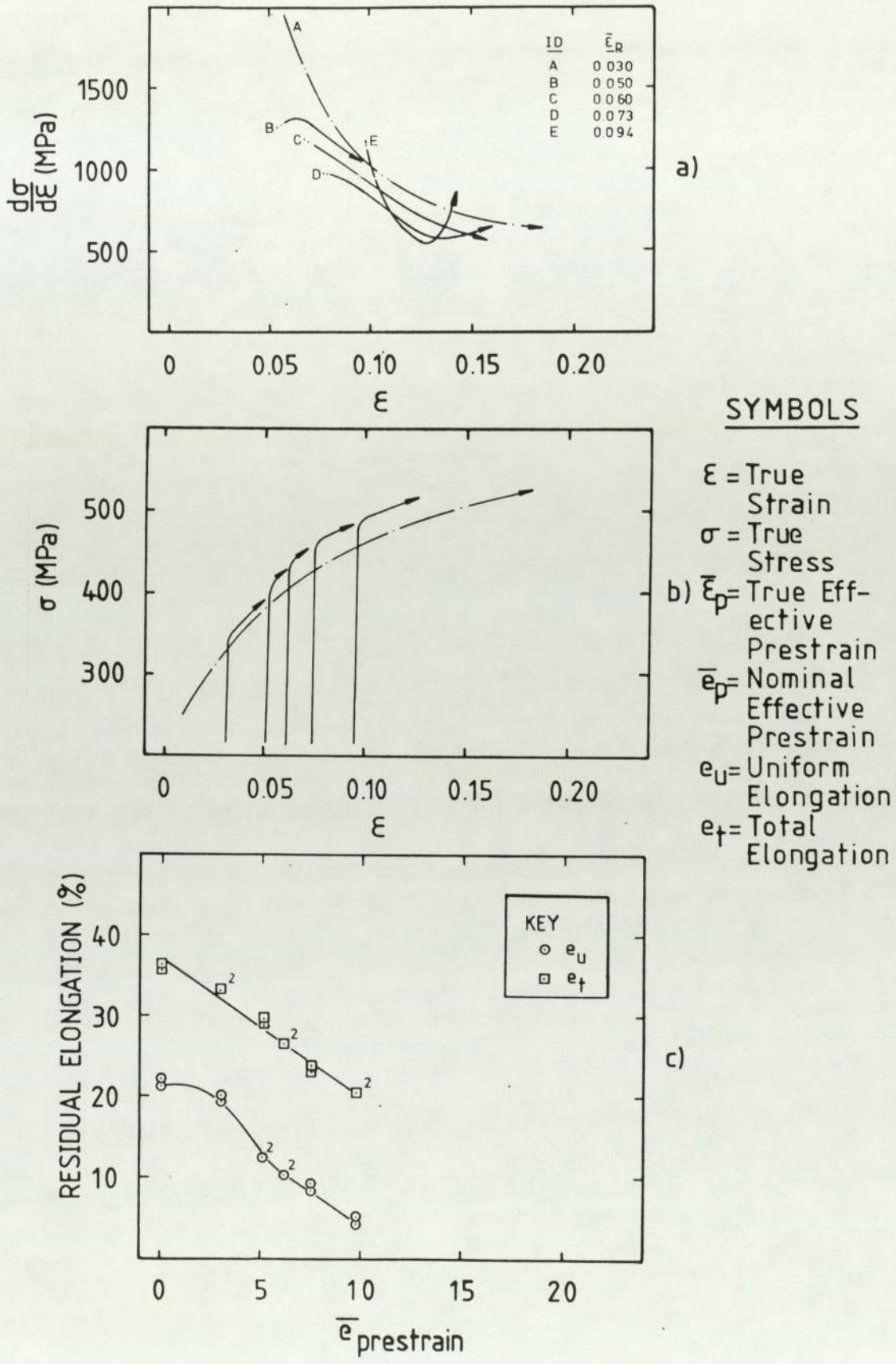

Fig. 65. Steel DP, Plane-Strain Prestrain: Tensile Test Results, Stage II Rotated 0 Degrees from the Prestrain Direction. (a) Work-Hardening Curves, (b) True Stress-Strain Curves (Each Offset by the Prestrain), (c) Residual Tensile Elongations. Chain Dotted Lines Represent As-Received Properties.

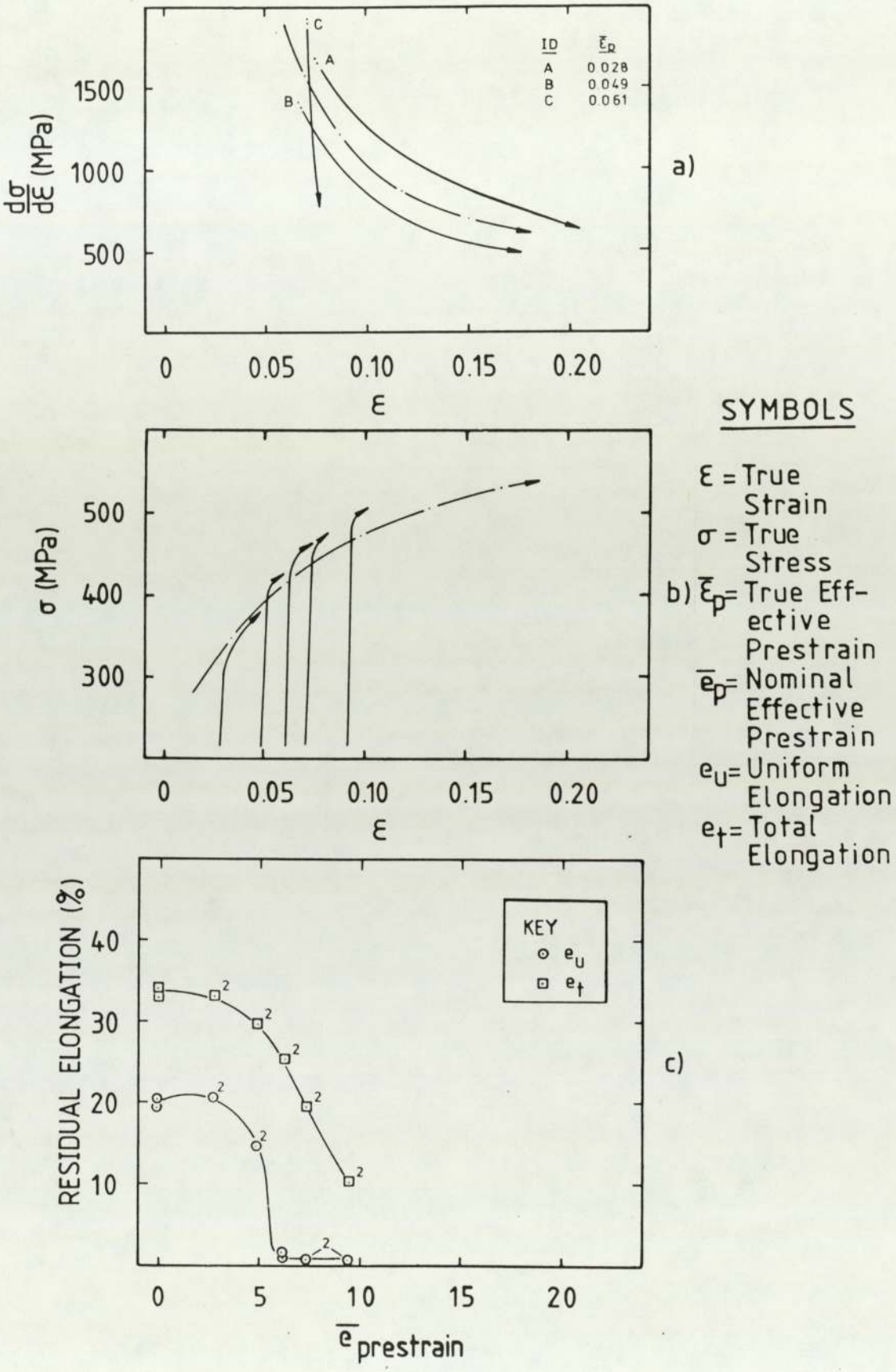

Fig. 66. Steel DP, Plane-Strain Prestrain: Tensile Test Results, Stage II Rotated 45 Degrees from the Prestrain Direction. (a) Work-Hardening Curves, (b) True Stress-Strain Curves (Each Offset by the Prestrain), (c) Residual Tensile Elongations. Chain Dotted Lines Represent As-Received Properties.

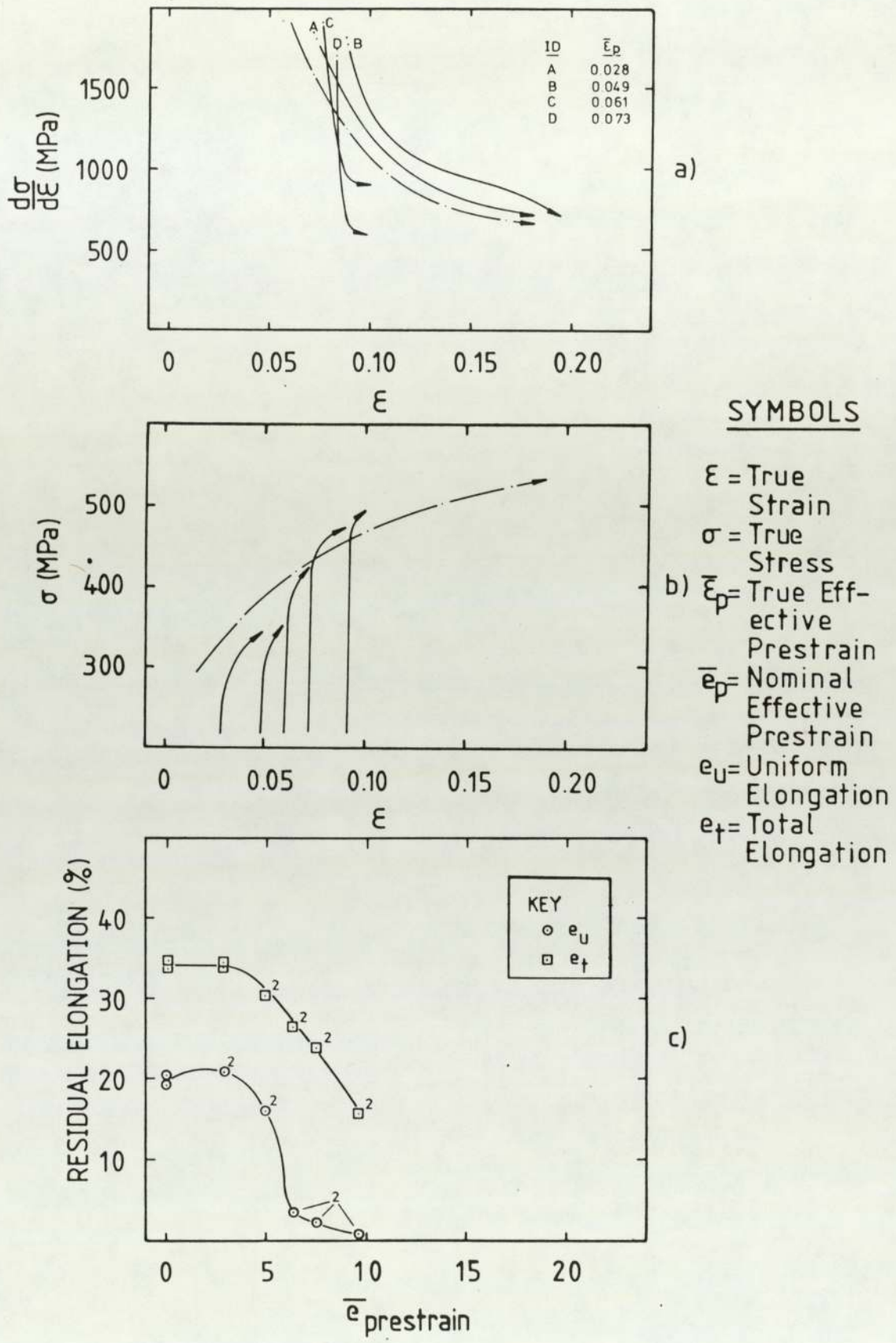

Fig. 67. Steel DP, Plane-Strain Prestrain: Tensile Test Results, Stage II Rotated 90 Degrees from the Prestrain Direction. (a) Work-Hardening Curves, (b) True Stress-Strain Curves (Each Offset by the Prestrain), (c) Residual Tensile Elongations. Chain Dotted Lines Represent As-Received Properties.

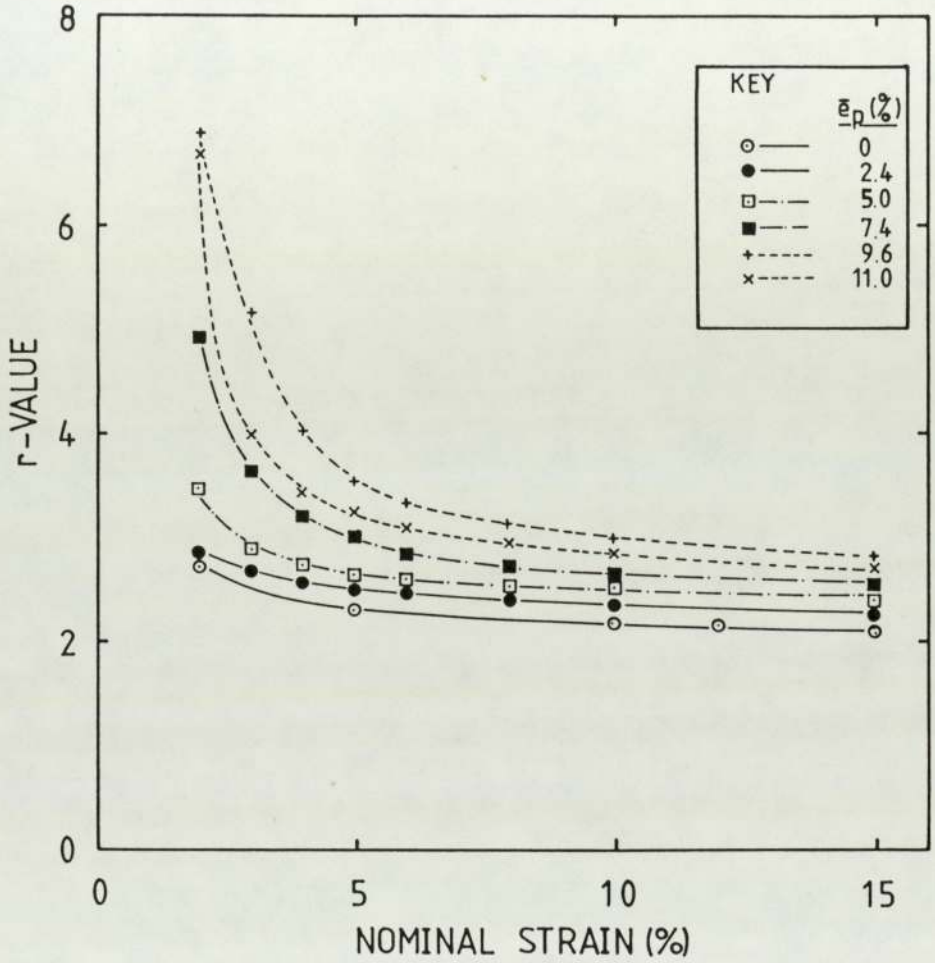

Fig. 68a). Steel AK, Plane-Strain Prestrain: Variation of r-Value with Prestrain Level, Stage II Rotated 0 Degrees from the Prestrain Direction.

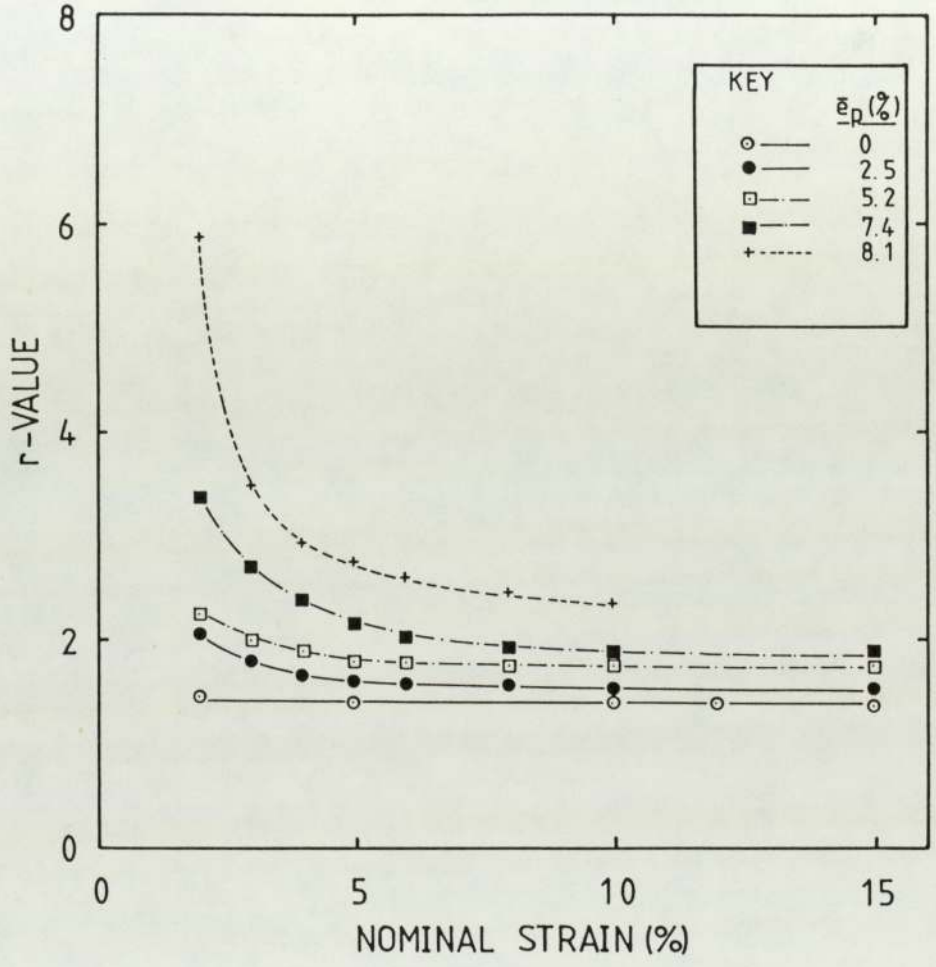

Fig. 68b). Steel AK, Plane-Strain Prestrain: Variation of r-Value with Prestrain Level, Stage II Rotated 45 Degrees from the Prestrain Direction.

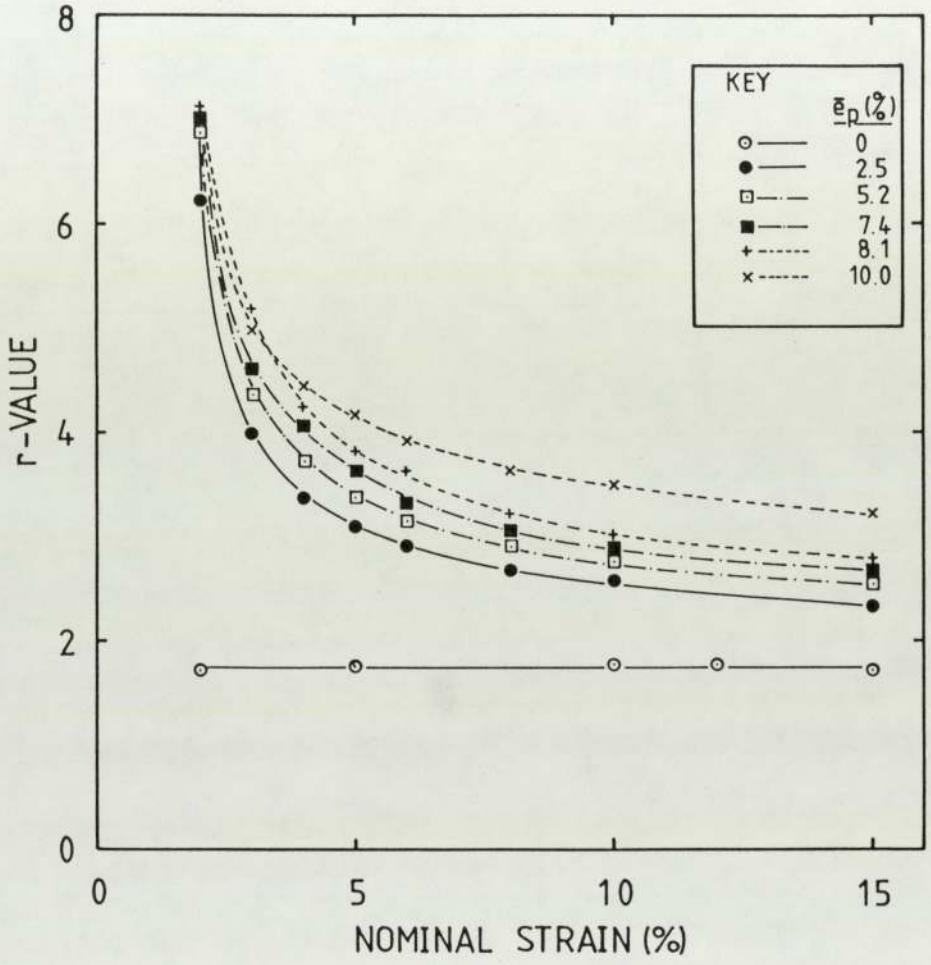

Fig. 68c). Steel AK, Plane-Strain Prestrain: Variation of r-Value with Prestrain Level, Stage II Rotated 90 Degrees from the Prestrain Direction.

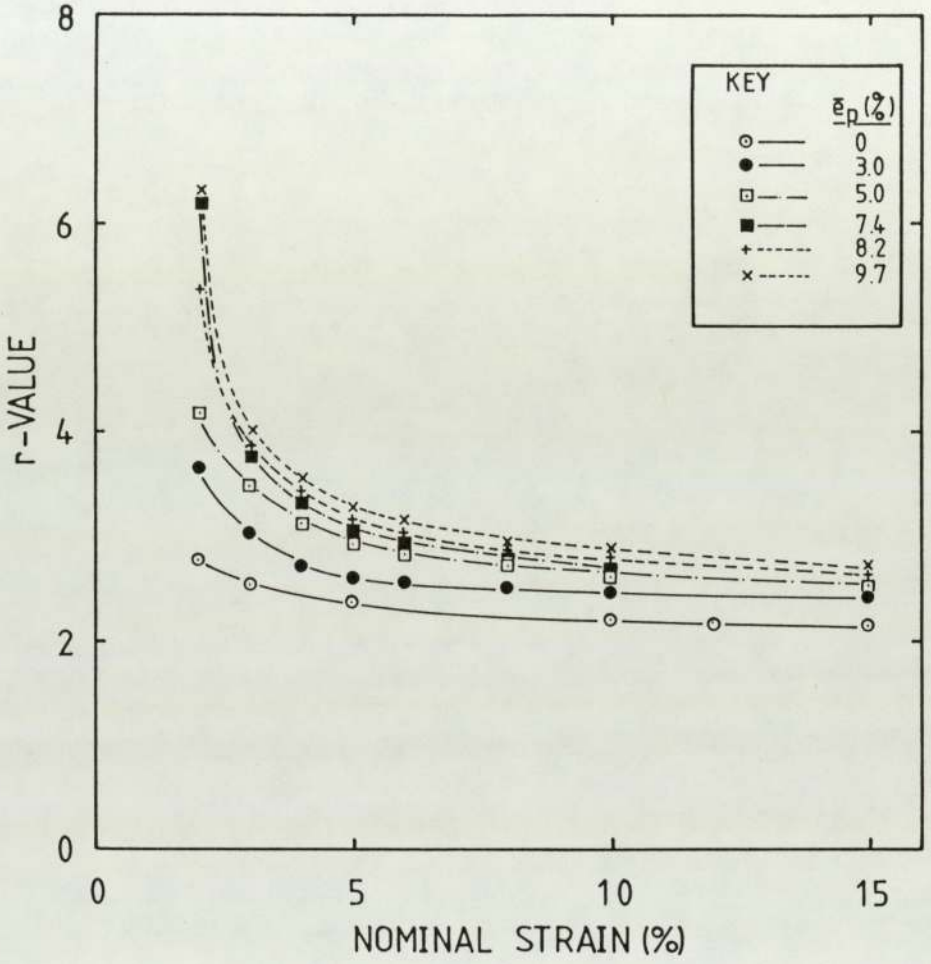

Fig. 69a). Steel RP, Plane-Strain Prestrain: Variation of r-Value with Prestrain Level, Stage II Rotated 0 Degrees from the Prestrain Direction.

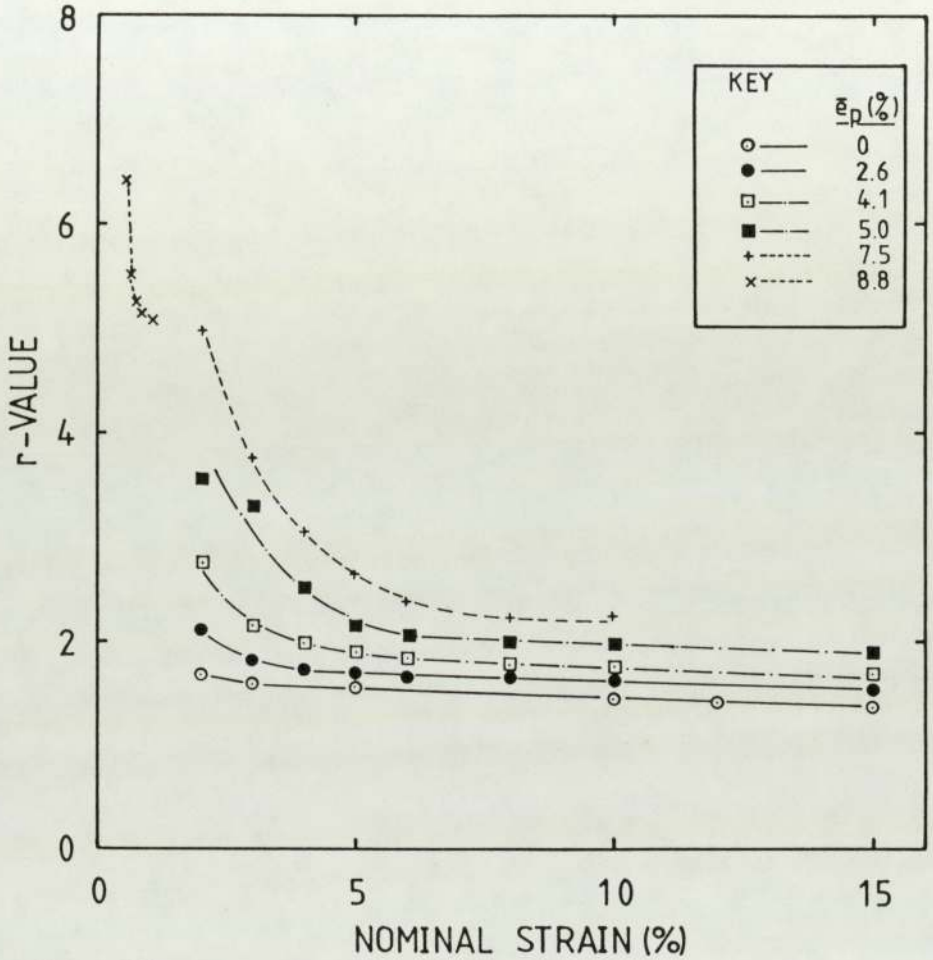

Fig. 69b). Steel RP, Plane-Strain Prestrain: Variation of r-Value with Prestrain Level, Stage II Rotated 45 Degrees from the Prestrain Direction.

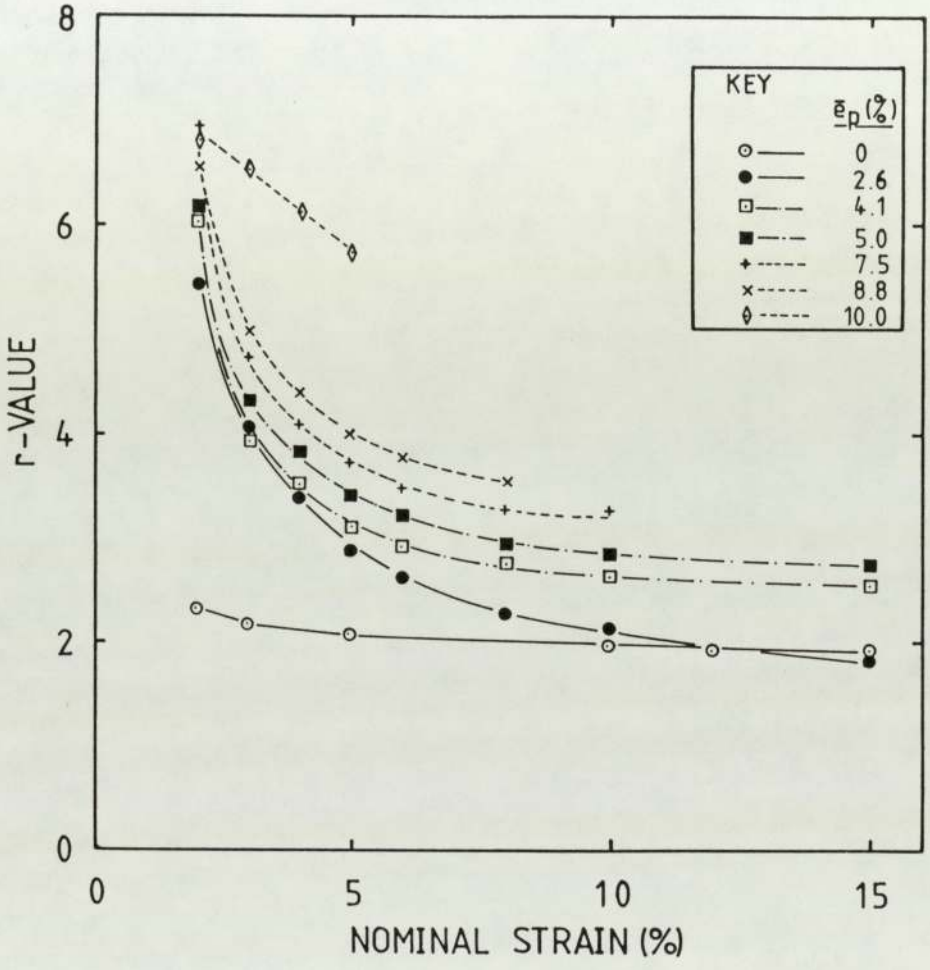

Fig. 69c). Steel RP, Plane-Strain Prestrain: Variation of r-Value with Prestrain Level, Stage II Rotated 90 Degrees from the Prestrain Direction.

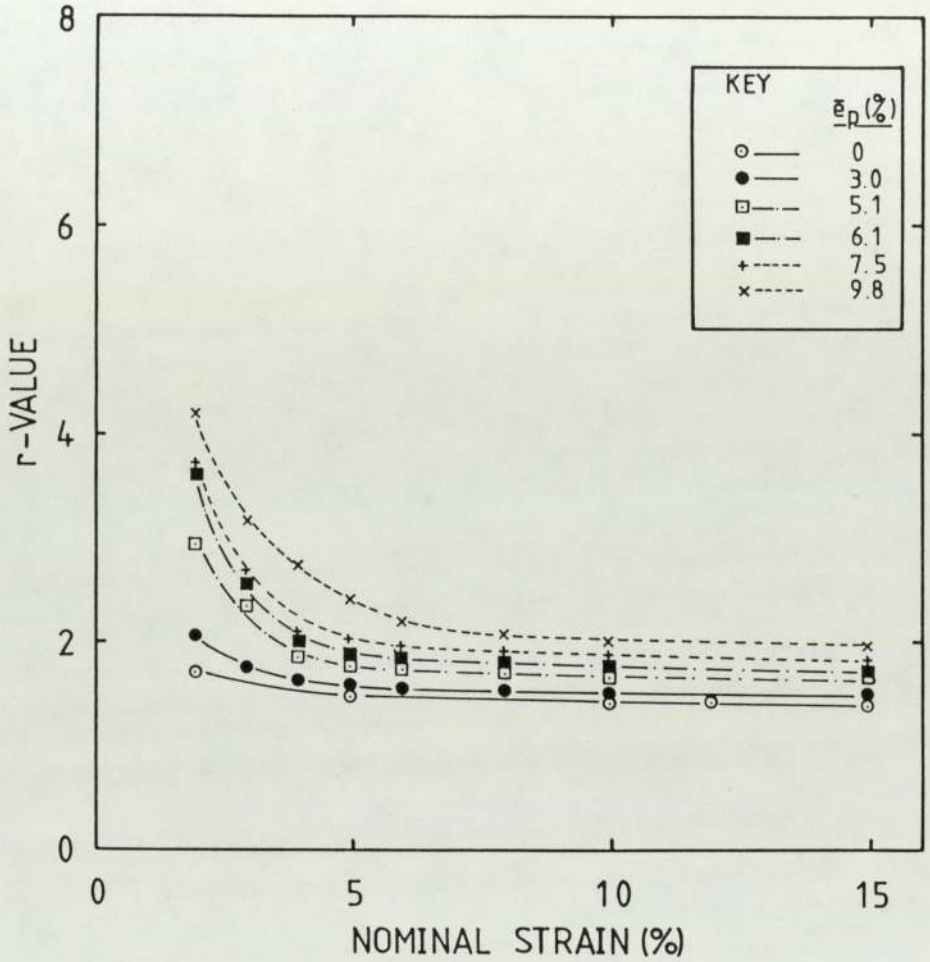

Fig. 70a). Steel DP, Plane-Strain Prestrain: Variation of r-Value with Prestrain Level, Stage II Rotated 0 Degrees from the Prestrain Direction.

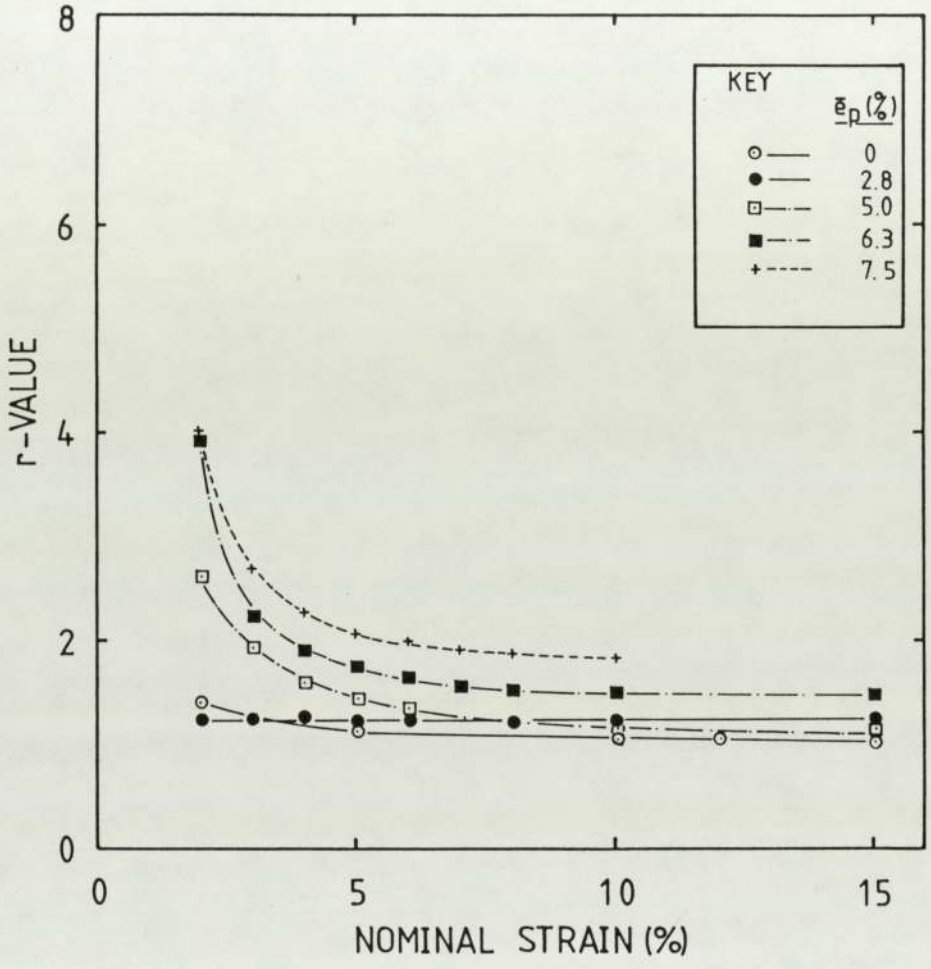

Fig. 70b). Steel DP, Plane-Strain Prestrain: Variation of r-Value with Prestrain Level, Stage II Rotated 45 Degrees from the Prestrain Direction.

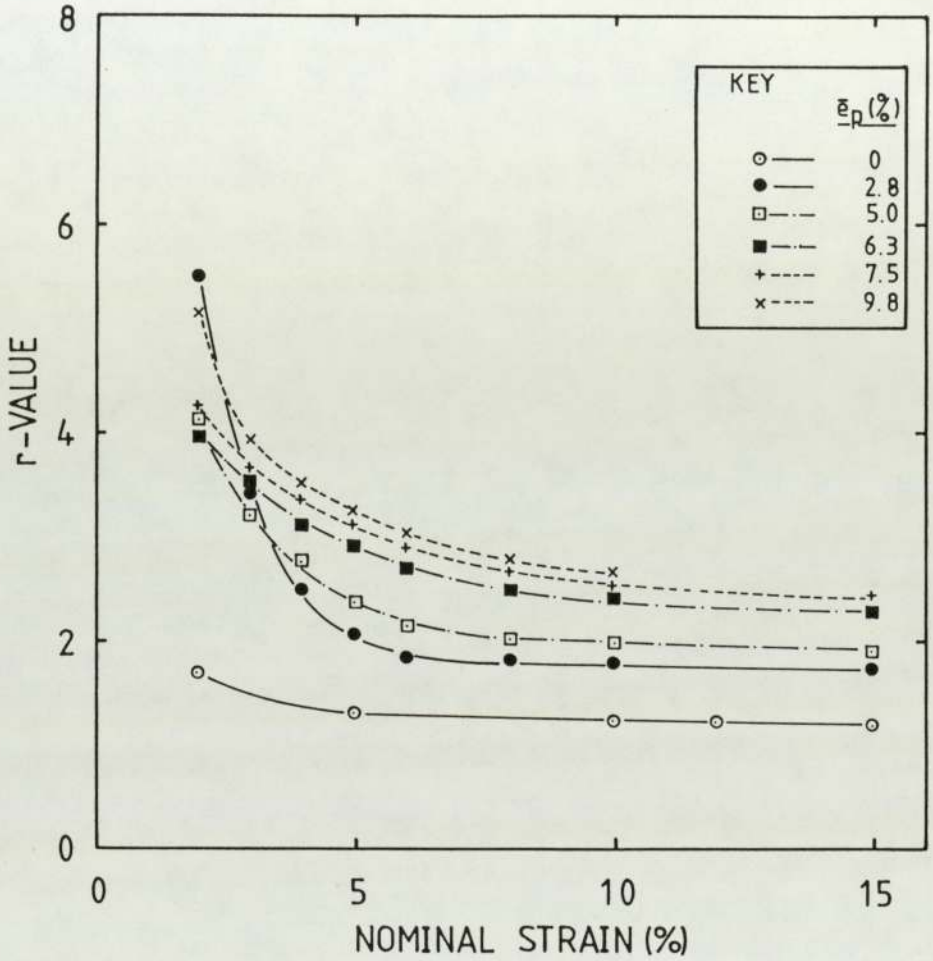

Fig. 70c). Steel DP, Plane-Strain Prestrain: Variation of r-Value with Prestrain Level, Stage II Rotated 90 Degrees from the Prestrain Direction.

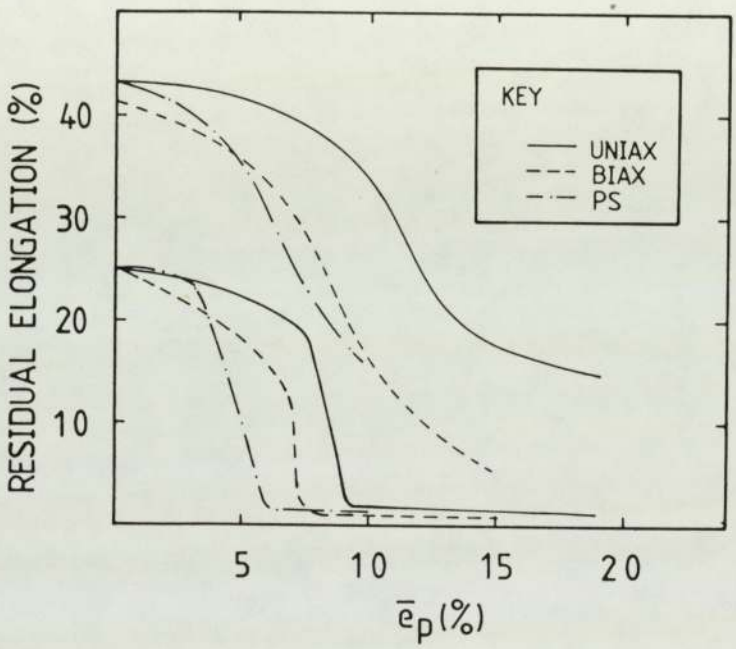

Fig. 71. Comparison of the Effect of Uniaxial, Biaxial and Plane-Strain Prestrains on Stage II Residual Elongations for Steel AK. Stage II Rotated 90 Degrees from the Prestrain Direction.

CHAPTER 4.

Discussion

4.1 Deformation of Body-Centered (BCC) Cubic Metals

The behaviour of a metal after a strain-path change during deformation will be strongly influenced by the dislocation substructure remaining from the previous stage(s). Before the observed phenomena can be adequately explained it is necessary to discuss, in general terms, the evolution of dislocation microstructures in BCC metals such as ferritic steels.

Deformation of metals is the result of slip which initially occurs in the close-packed direction of the lattice. In the case of BCC this is <111>. The dislocations which act as boundaries between slipped and non-slipped regions are constrained to motion on certain planes: edge dislocations can only cause slip on planes defined by the dislocation line and Burger's vector (a/2)<111>:-

{110} and {112} - common

{123} - infrequent

Screw dislocations, on the other hand, can glide on any plane containing a <111> direction (32) and have the capability for cross-slip (due to parallel Burger's vector and dislocation line).

The net result is that BCC metals possess good ductility since there will normally be many more than the five independent slip systems proposed by von Mises (33) in operation.

In a tensile test there is little motion of screw dislocations before yielding. However, macroscopic yielding is caused almost exclusively by mobile screw dislocations (34), which multiply as straining proceeds due to double cross-slip and the operation of Frank-Read sources (as many as 10^{12} dislocations per square centimetre can be found in heavily cold-worked metals). Strain-hardening is the result of the interaction of these mobile dislocations with various barriers:-

a). Interaction with elastic stress-fields around other dislocations.

b). Interactions leading to sessile locks.

c). Formation of dislocation jogs by inter-penetration of dislocations on another slip system (forest-hardening).

d). Pile-ups at grain-boundaries etc.

As the extent of plastic deformation increases, the number of dislocations increases and so there is greater scope for the above interactions. Only at low plastic strains (less than 1% in the tensile test) will relatively straight dislocation lines be observed. With continued straining the tendency is for irregular regions of high dislocation density to form due to the irregular nature of the various obstructions to dislocation motion. By about 3.5% strain these high density clusters have become a network of dense dislocation tangles or cells. Further straining leads to more clearly defined cell-walls, aligned in certain preferred directions. At very high strains (greater than 20%) the formation of shear-bands and associated phenomena become the dominant deformation mechanism (35).

4.2 General Comments Arising From Experimental Results

The results presented here have demonstrated that there is much common ground between the three steels and the three different strain-path changes. This allows the observed behaviour in stage II to be broken down into several distinct, universal stages based on

the elongation versus prestrain data presented. These stages are given below:-

1). Low prestrain regime - often characterised by increased stage II elongation values.
2). Medium prestrain range - characterised by increased flow-stresses and lower elongations.
3). Critical Prestrain range - characterised by an abrupt loss of stage II ductility and very low work-hardening rates.
4). Post-Critical Prestrain - characterised by near constant strains to instability at a very low level.

These four stages are illustrated in Figure 72. The associated changes in the other parameters measured during stage II are discussed as appropriate.

4.3 Low Prestrains - Bauschinger's Hump

Low prestrains (less than 5%) in uniaxial tension and plane-strain have been shown to result in increased residual elongations when tested in uniaxial tension at virtually any angle away from the prestrain direction. Associated with this is a decrease in flow stresses and

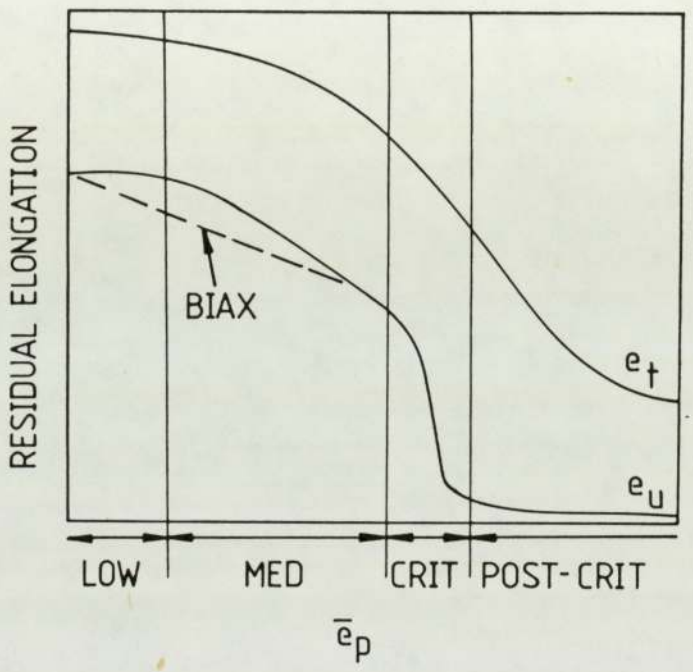

Fig. 72. Schematic Diagram Showing the Four Principal Zones of Behaviour Observed after Prestraining.

a small increase in work-hardening rate. This is analogous to the classical Bauschinger effect observed in tension-compression testing (11), where the second stage of deformation is the reverse of the first. Since it manifests itself as a 'hump' in the stage II elongation curves (see Figs. 62 and 63c) for examples) this shall be referred to as a Bauschinger Hump.

The traditional view has been that this effect originates from the presence of long-range stresses or back-stresses from dislocation pile-ups (36) and the availability of mobile dislocations capable of reversing their flow to suit the externally imposed reversal of stress. Upon reverse loading, these factors allow plastic flow to commence at lower stresses than previously. The annihilation of dislocations during reverse straining (work softening) may also be a contributing factor (35).

However, the Bauschinger effect is usually dependant on a complete load reversal, whereas the present observations indicate that (for the uniaxial and plane strain cases) an orthogonal strain-path change produces the greatest effect. Obviously there must be substantial commonality of slip-planes between the two stages of deformation for this effect to occur.

In the case of biaxial pre-straining there is no observable Bauschinger Hump. The active dislocation sites of the first stage are obviously not capable of assisting the onset of second stage plasticity. More likely, the incompatability of slip-systems leads to conventional work-hardening behaviour caused by the interaction of dislocations with microstructural features (forest dislocations, grain-boundaries etc) and each other. This results in raised flow stresses, reduced work-hardening rates and lower ductilty levels (see Figs. 51-53).

4.4 Medium Prestrains - Latent Hardening

Where a Bauschinger Hump is present it is a transient effect and at medium prestrains, typically greater than 5%, there is a marked increase in flow stresses above the virgin material level accompanied by a decline in the recorded elongation figures (near linear in the case of the strain to instability). This effect, which can be thought of as latent hardening, only manifested with increasing stage II strain, has been reported previously by authors such as Laukonis and Ghosh (19). Figures 27, 36 and 44 clearly indicate the dependence of this effect on the angle between stage I and stage II uniaxial tensile deformation. For

angles up to about 60 degrees from the prestrain direction the yield (proof) stresses increase due to forest hardening caused by stage II dislocations interacting with dislocations left over from the prestrain. Above 60 degrees there is a distinct drop in the measured yield stresses. This may be a result of a partial reversal in the direction of glide of piled-up dislocations under a reduced applied stress (ie: a Bauschinger type effect again) or the activation of secondary slip-systems due to high, localised stresses caused by dislocation interactions with each other and such features as grain-boundaries or cell-walls.

This can be clarified by translating the angle between the prestrain and tensile test direction to a uniform co-ordinate system in strain-space (as shown in Figure 73 and Appendix 4). For a uniaxial tensile prestrain, it can be seen that an angle of about 50 degrees between stages I and II corresponds to orthogonality in strain-space (42). This is consistent with the observations above, since the incompatability between stage I and II slip-systems should be greatest for a 90 degree rotation in strain-space producing the largest latent hardening effect. For angles greater than 90 degrees in strain-space (ie: $>$ 50 degrees between stages I and II) there will be assistance to

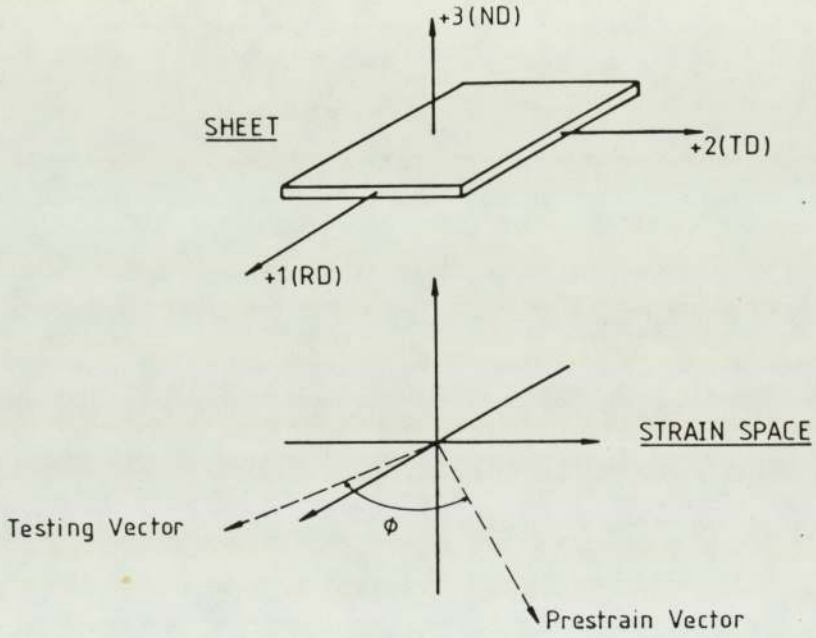

Fig. 73. A Possible Co-ordinate System to Describe the Strain Vectors During Prestraining (Stage I) and Subsequent Tension Testing (Stage II).

stage II flow from the original slip-systems and hence reduced yield stresses.

4.5 Critical Prestrain - Abrupt Loss of Ductility with Increasing Prestrain

The premature instability and loss of ductility observed for all of the steels and all of the prestrain modes is dependent upon two factors. Firstly, there is a loss of work-hardening rate and secondly there is the latent hardening effect. The loss of work-hardening rate has previously been reported by Hutchinson et al (21). In most cases it is only the strain to instability or uniform extension which exhibits a precipitous drop at a certain prestrain level, the total elongation dropping at a higher rate than for virgin material but not undergoing a precipitous drop.

As the stage I strain increases, the dislocation cell structure produced becomes denser and more tangled (24). Hence, at the higher prestrains, stage II straining cannot easily replace the original dislocation network with the one that would allow a continuation of normal strain-hardening behaviour. Although the presence of so many immobile dislocations

will favour high stresses, the work hardening-rate declines due to the reducing number of slip-planes available with sufficient mobile dislocations to contribute to the overall strain-hardening. Any reduction in the number of active slip-systems will result in lower ductility. If less than five are active at any given moment then the strain to instability will be reduced dramatically (33).

4.5.1 Necking Strains

Figure 35. indicates the effect of uniaxial prestrain on the necking strains observed in subsequent tensile tests. The necking strain is defined as the difference in nominal strain to instability and nominal total strain - this is not strictly correct, due to the non-additive nature of engineering strains, but good enough for a qualitative assesment. As can be seen there is a transient rise in the necking strains at the critical prestrain level, followed by a rapid fall. Where the two stages are separated by 45 degrees, the peak is smaller than orthogonal testing, and the final necking strain achieved is very much reduced below even the 90 degree tests.

The transient increase in necking strains is due to deformation continuing after maximum load is reached in the tensile test. Obviously, the overall amount of work-hardening that these steels are capable of is not dramatically reduced as soon as the abrupt loss of uniform straining occurs. This may be due to a partial elimination of the stage I dislocation structure during stage II straining. However, with increasing prestrain, the effectiveness of any such process will rapidly decline. Hence, a more highly tangled dislocation structure will be produced in stage II, and so post-instability straining is reduced.

As noted for the discussion of latent hardening above the forest hardening due to unemployed dislocations from stage I will be greatest for angles close to 50 degrees around the sheet (90 degrees in strain-space). Obviously, in the case of a 45 degree stage II tensile test the dislocation tangles produced by conflicting stage I and II dislocation structures will persist into the post-instability regime giving the low necking strains and high flow stresses observed. On the other hand, the orthogonal tests can more effectively 'undo' the dislocation structure of stage I as prestraining proceeds since the mismatch in slip-system requirements is less severe. This results in less deviation from the non-prestrained behaviour at

the highest prestrain orthogonal tests.

So far the discussion of necking strains has concentrated on the uniaxial and plane-strain cases in which the behaviour is similar for each of the steels. In the biaxial prestrain tests, however, there is a notable difference in behaviour between steels AK and RP, and steel DP: whereas the first two steels behave after biaxial tension in a manner consistent with the uniaxial behaviour, DP does not show any increase in post-instability necking strains since the total elongation curve undergoes an abrupt drop, in step with the uniform curve, at the critical prestrain (see Figs. 53c and 54). Since it is the total elongation curve that is behaving differently, it is worth considering the possibilty that the failure mode in the case of steel DP is affected by the strain-path change in a different way to the other steels, and that microstructural damage may be important.

In commercial alloys containing significant proportions of second-phases, failure in the tensile test is associated with void coalescence and growth in thin bands of highly localised shear (37). These voids are normally associated with decohesion at the interfaces between these particles and the matrix, or by fragmentation: the damage caused by decohesion in

equi-biaxial stretching could be as much as 5 to 10 times that in uniaxial tension (37, 38). Steels AK and RP contain a similar percentage and distribution of second phases whereas DP contains a substantial proportion of martensite islands as a second phase. Rashid (39) has clearly demonstrated that for this class of dual-phase steel, failure results by decohesion of the martensite/ferrite interfaces after severe localised straining, followed by cracking within the martensite islands. Hence, it follows that an equi-biaxial prestrain of a sufficient level would in effect pre-crack the interface. This, coupled with the loss of work-hardening capacity in stage II, leads to a concurrent drop in strain to instability and strain to failure. The net effect is that the continuation of straining beyond instability always observed for steels AK and RP, and for DP after uniaxial and plane-strain prestrain, is not present after biaxial prestraining.

4.6 Post Critical Prestrain - Ductility Plateau

After undergoing the abrupt loss of stability discussed above, all of the steels, after any of the strain-path changes, exhibit a plateau in the strain to instability curve as a function of prestrain level. That is, the strain to instability is independent of prestrain level. The residual strains observed during this period are 1.0% or less nominal strain. None of the tests performed indicated that the curves would rise again, although further tests would be needed to confirm this. At the same time the total elongation curves show a continued descent at a similar rate to that before the premature instability precipice, with only a slight tendency to flatten out. The final strain levels reached for both curves appear to be a minimum at 45 degrees to the prestrain in the uniaxial and plane-strain cases, which has already been shown to approach the orthogonality condition in strain-space.

At the highest prestrains the incompatibility between the slip requirements of stage I and II have resulted in a highly tangled dislocation structure with few active slip-planes compared to a straightforward tensile test. In a situation such as this it would be expected that the strain to instability would continue to decrease with increasing prestrain. Since this

obviously doesn't happen, some physical process must be operating to counteract the loss of work-hardening capacity by supplying fresh sources of mobile dislocations. It is unlikely that stage II straining will be capable of freeing the slip-planes already locked-up when the prestrain structure is so well defined, hence there must either be appreciable cross-slip occurring or the activation of the normally less-favourable slip systems (eg: <111>(123). In either case the new dislocation sources would not be capable of operating over an extended strain range and so an increase in ductility would be very unlikely.

4.7 Severity of Prestrain

As indicated at the end of Chapter 3, the effective prestrain required to produce an abrupt onset of instability reduces as the prestrain mode changes from uniaxial to biaxial to plane-strain, assuming equivalent orientation relative to the prestrain (see Fig. 71). Similarly, after the Bauschinger Hump the measured residual elongations for a given effective prestrain decrease in the same order. Once more, much of the answer lies in the degree of incompatibility of slip-systems between the stages, resulting from the stable dislocation networks created during the initial

stage (although the situation is confused by ignoring anisotropy in calculating the effective prestrain).

The mean free path required for dislocation movement in uniaxial tension is greater than that provided by a biaxial prestrain (24) and so extended straining becomes more difficult as the biaxial cell structure becomes better defined. Similar arguments may well apply to plane-strain prestraining, but there is little in the way of reported observations to back this up.

The role of microstructural damage cannot be ignored either since biaxial prestraining in particular is known to promote void formation (see section 4.5.1). An increased proportion of voids would reduce the load carrying capacity of the specimens below that resulting from the dislocation mechanisms already outlined.

4.8 Plastic Strain-Ratio Dependence on Stage II Strain

The conventional r-value is based upon the total strain accumulated during the tensile test and does not accurately reflect the instantaneous texture present in the material. Re-presenting one of the r-value versus

stage II strain curves in terms of incremental strains (the incremental r-value or r_i is defined as $d\varepsilon_w/d\varepsilon_t$ for each strain increment chosen) reveals that the change in anisotropy producing the rise in r-value at low strains is transient. The effect is almost completely absent after (typically) 3% strain in stage II (see Figure 74 for steel AK tension tested at 90 degrees to a uniaxial prestrain).

The change in anisotropy is most likely to be due to exhaustion of the mobile dislocations left over from the prestrain. It is unlikely that this will significantly influence the overall plastic behaviour.

After biaxial prestraining the r-value is independent of stage II strain until very high prestrains are reached (and even then the accuracy of r-value measurement over the small plastic strains achieved is limited). Increasing prestrain, however, leads to a reduction in r-value which implies that the well defined and equi-axed dislocation cell structure associated with biaxial stretching forces the subsequent work-hardening during the tensile test to be more isotropic than for the other two strain-path changes.

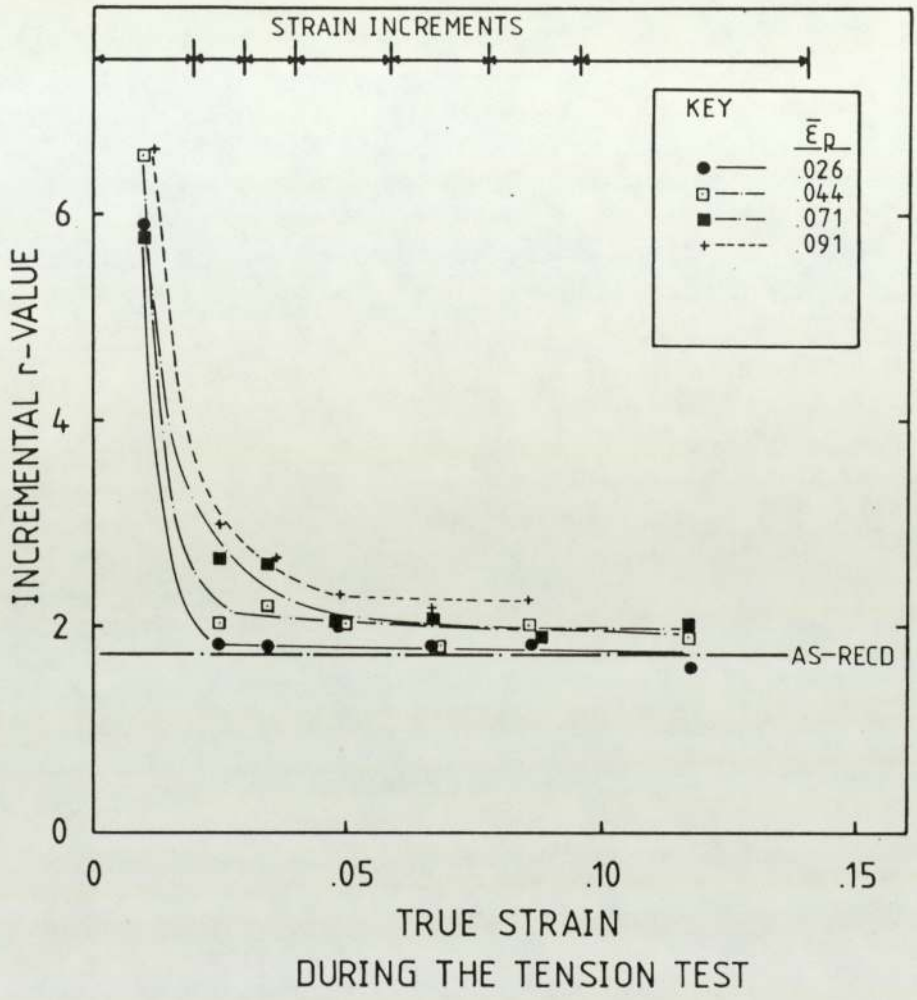

Fig. 74. Steel AK, Uniaxial Prestrain: Variation of Incremental r-Value with Prestrain Level, Stage II Rotated 90 Degrees from the Prestrain Direction (see Fig. 48c for Comparison).

4.9 On the Significance of the Shape of Flow Curves

Due to the limitations of scale it has not been possible to fully illustrate the form of the flow curves, which deviate significantly from the parabolic norm, particularly at high prestrain levels. Since the work-hardening curves have been presented fully it is worthwhile relating them to the flow curves from wich they were derived.

Figures 75a-75c present idealised flow curves and associated work-hardening curves extracted from all of the data presented. There are three clear forms of behaviour, but a given steel/prestrain combination will not necessarily exhibit each one fully.

Figure 75a illustrates the classical situation of a continuous drop in work-hardening rate as the plastic strain increases. The initial rate is very high, but drops in a parabolic fashion to near horizontal at maximum load on the curve obtained during a tension test. In dislocation terms the progressive fall is a result of the reduction in the number of active slip-systems as straining proceeds, which in turn restricts the number of possible dislocation reactions and so reduces the rate of hardening. This behaviour is observed in the non-prestrained tests or

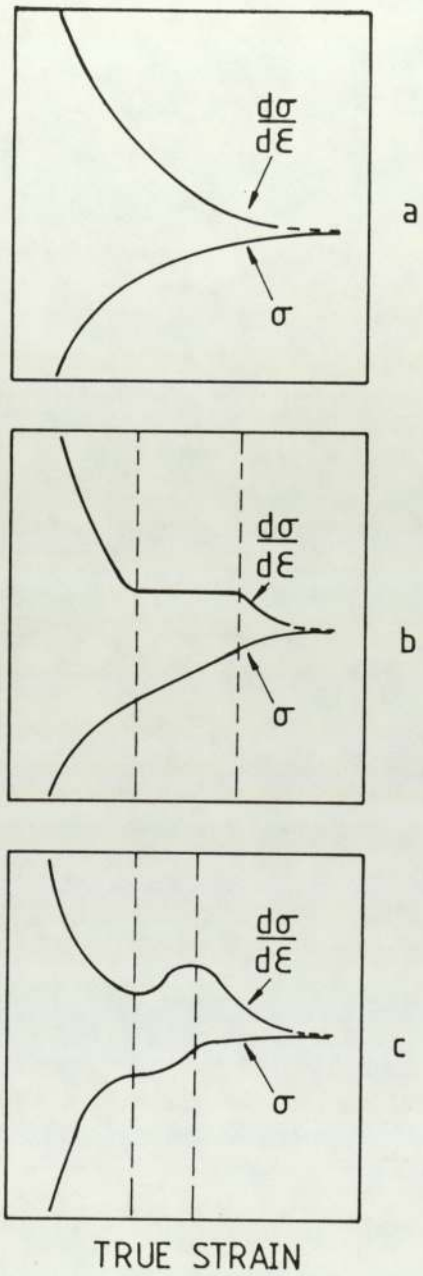

Fig. 75. Idealised Flow Curves and Associated Work-Hardening Rate Curves Observed at:-

a). Zero or Low Prestrains

b). Immediately Prior to or At the Critical Prestrain Level

c). At or Above the Critical Prestrain.

at low prestrains.

As the critical prestrain is approached there is a tendency for the flow curves to develop significant linear portions as shown in Fig.75b. This shows up as a transient region of constant strain-hardening rate before more normal behaviour is resumed. Good examples of this behaviour can be found in Fig. 58 (for plane-strain prestrained AK) and Fig. 43 (for uniaxially prestrained RP). By implication the work-hardening during stage II is progressing in three distinct stages: at low second stage strains, work-hardening capacity is reducing with strain for the reasons given above (but more rapidly). In this first regime, work-hardening is dominated by those dislocations introduced in stage I that are capable of gliding in the second stage (on common slip-planes). As stage II proceeds it is likely that previously inactive slip systems will become sources of mobile dislocations offseting the loss of strain-hardening. Obviously, as the stage II slip systems become dominant there will be partial erasure of the stage I structure and a return to more conventional (reducing) work-hardening behaviour.

With continuing prestraining, some of the work-hardening curves develop true minima, followed by

a return of work-hardening capacity. Finally, there is a return to conventional behaviour with continued stage II straining. This is presented in Fig. 75c and a good example for steel RP after uniaxial prestraining can be found in Fig. 43. In many ways this is very similar to the behaviour observed after static strain-ageing (35). Indeed, the shape of the flow curve itself is reminiscent of the beginnings of a true yield phenomenon. Whether strain-ageing is present or not, the work-hardening behaviour would indicate either unpinning of existing dislocations with continued straining or, more likely, the generation of fresh dislocations either at highly stressed locations within the microstructure (ie: by the activation of normally unfavourable slip-systems at a suitable critical resolved shear stress) or by cross-slip. The dislocations from these secondary dislocation sources would be able to glide relatively unimpeded for a short period of continued deformation resulting in an up-turn in hardening-rate. As these dislocations are immobilised the downward trend is resumed.

CHAPTER 5

Conclusions and Recommendations

5.1 Conclusions

There are two general conclusions arising from this work:-

A). Conventional low C, Al-killed steels, re-phosphorised steels and dual-phase steels all exhibit similar changes in flow behaviour after the strain-path changes investigated. When one considers the different initial strength level, anisotropy, microstructure and hardening mechanism for each of these steels, this is a surprising finding.

B). When dealing with complex strain-paths, it is not adequate to treat each stage as independent of those that precede it. For those cases investigated, this would lead to a dramatic over-estimation of the second stage uniform strain when the first stage strain exceeds a few percent.

Since the behaviour of the three steels and strain-path combinations is sufficiently similar, the following more specific conclusions can be drawn:-

1. The rise in elongation and associated fall in flow stresses, often observed after low prestrains, is believed to share a common mechanism with the Bauschinger effect (hence, the term 'Bauschinger Hump').
2. 'Latent-hardening' results from forest-hardening caused by the interaction of dislocations in stage II with those left over from the prestrain.
3. An abrupt loss of strain to instability with increasing prestrain is associated with a rapid loss of work-hardening capacity. This can be explained by considering a reduction in the number of active slip systems below that required for extensive ductility. As the degree of incompatability between the dislocation structures of stages I and II increases, the number of mobile dislocations on any given slip-plane is reduced until the slip-plane no longer contributes significantly to overall work-hardening.
4. The lowest necking strains observed for uniaxial and plane-strain prestrains occur

when stage II deformation is at 45 degrees to the prestrain direction. This is a result of dislocation tangles persisting into the post-instability regime. When the two stages are orthogonal, there is sufficient commonality of slip-systems to allow more extensive straining after maximum load in the tensile test than observed at 45 degrees.

5. The dual-phase steel does not exhibit any transient increase in necking strains after biaxial prestraining. It is suggested that this may be due to failure of martensite/ferrite interfaces.
6. Near constant strain to instability at the highest prestrains is observed for each of the steels, after each prestrain. This can be explained by the activation of previously unfavourable slip systems and cross-slip of existing mobile dislocations.
7. There is a transient increase in r-value at low stage II strains only after uniaxial and plane-strain prestrain. This is most likely due to exhaustion of mobile dislocations left over from prestraining.
8. Each of the strain-path changes resulted in a disruption of monotonic work-hardening behaviour. Three distinct forms of flow

curves were observed, each associated with the changes in the elongation behaviour outlined above.

9. As a general guide, plane-strain prestrain causes an abrupt drop in strain to maximum load, in a subsequent tensile test, at a lower effective strain than when biaxial prestraining is used. Likewise, uniaxial prestraining disrupts monotonic flow behaviour less severely than after biaxial straining.

5.2 Recommendations for Further Investigation

It is inevitable in any study, no matter how comprehensive, that tangential areas of investigation will be identified which cannot be pursued in the time available. Two such areas have been identified as deserving of further research at the same level as the present investigation.

Firstly, there is the question of void formation at the martensite/ferrite interfaces during biaxial stretching of the dual-phase steel. Since this class of material will increasingly be used in large scale biaxial forming operations, it is necessary to explore

the incidence of microstructural damage rigorously. Not only will this influence forming limits, but also service failures due to fatigue of structural components may result. Since dual-phase steels are used in plate form for pipelines and submarine hulls, any further work should include this product form. Even though the forming operations involved are not the same, the presence of microstructural damage after roll-forming, bending etc should be investigated. A range of prestrain modes and levels would be required, as in the present study. After prestraining, inspection of the blanks is best performed using a Scanning Electron Microscope, there being well established statistical techniques for interpretation of the void counts obtained.

The emphasis of this thesis has been upon the study of flow behaviour after prestraining, as described by tensile test parameters. Although arguments explaining observed behaviour have been presented in terms of dislocation theory, these have been inferred from the mechanical property changes obtained, rather than from observation of changes in dislocation cell structures. These studies are notoriously difficult and reported findings have been inconclusive. Hence, any such investigation would be a major undertaking if reliable results are to be

obtained. Such a study would involve a considerable amount of Transmission Electron Microscope work to study the evolution of dislocation cell structures before, during and after strain-path changes. Identification of active and non-active slip systems is also important. The choice of steel is not too important on the basis of the present findings.

On a much smaller scale than the two pieces of work suggested above, it would be useful to relate the effect of prestraining on r-value to the actual texture changes taking place. This could be done for the uniaxial and/or plane-strain case and for biaxial prestraining. Again, the choice of steel is immaterial. A study based on incomplete pole-figures would be adequate.

APPENDIX 1

Effective Strain Expressions (after von Mises)

The expression for effective strain derived by von Mises (see ref.11, p90) is:-

$$\bar{\varepsilon} = \frac{\sqrt{2}}{3}\sqrt{((\varepsilon_1 - \varepsilon_2)^2 + (\varepsilon_2 - \varepsilon_3)^2 + (\varepsilon_3 - \varepsilon_1)^2)}$$

where $\varepsilon_1, \varepsilon_2, \varepsilon_3$ are true strains in principal directions 1,2 and 3

This equation assumes that the material is fully isotropic.

Uniaxial Tension

The principal strains are:-

ε_1= axial strain

$\varepsilon_2 = \varepsilon_3 = -(\varepsilon_1/2)$ ($\varepsilon_1 + \varepsilon_2 + \varepsilon_3 = 0$ for constancy of volume)

Therefore,

$$\bar{\varepsilon} = \varepsilon_1$$

Biaxial Tension

The principal strains are:-

$\varepsilon_1 = \varepsilon_2$

$\varepsilon_3 = -2\varepsilon_1$

Therefore,

$$\bar{\varepsilon} = 2\varepsilon_1$$

Plane Strain

The principal strains are:-

ε_1

$\varepsilon_2 = 0$

$\varepsilon_3 = -\varepsilon_1$

Therefore,

$$\bar{\varepsilon} = 1.155\varepsilon_1$$

APPENDIX 2

Calculation of Strain-Hardening Rates

The true strain-hardening rate is defined as the rate of change of true stress with true strain ie: it is the slope of the true stress-strain curve at a given value of true strain. This is often presented as an instantaneous work-hardening exponent value (n-value) by means of the following relationship:-

$$n_i = \varepsilon_i \cdot \frac{d\sigma_i}{d\varepsilon_i} \cdot \frac{1}{\sigma_i}$$

Traditionally, the value of strain-hardening rate has been determined graphically from the flow-curve generated during tension testing. This is obviously very time consuming for large numbers of curves and prone to appreciable errors of measurement. However, before such data can be numerically differentiated it is necessary to smooth the values of the ordinate so that any errors in the data are minimised.

There are many techniques available for

performing this smoothing, but among the simpler are those involving the fitting of a least-squares polynomial to a small number of succesive data pairs (rather than over the entire range): as the fitted curve passes between the data points, smoothing occurs. Each recorded value of the ordinate is replaced with a smoothed value based on a polynomial of degree m relevant to a subrange of 2m+1 points centered, where possible, on the value to be smoothed. Obviously, it is necessary to modify this method at the ends of the range. Evaluating the derivative at each smoothed point is simple since the fitted curve is of known form.

If a parabola (degree 2) is chosen as the smoothing function, five successive data points are needed to calculate a smoothed value: the program presented here performs this form of smoothing on up to 50 pairs of true stress - true strain data taken from a flow curve (note: the strain values need not be equi-spaced). The program presented here is written in UCSD Pascal for the Apple II microcomputer and is based on a BASIC original running on a Tektronix 4052A workstation. The program has been re-written for inclusion in this thesis since Pascal is a better algorithm description language than BASIC. Please note that the error trapping of this version is minimal and

there is no provision for editing data after entry: it is strongly recommended that such features should be incorporated in any versions for use by anyone but the author of the program.

```
      PROGRAM PARABOLIC (INPUT,OUTPUT);

(*************************************************)
(* Function: 5 Point Parabolic Smoothing of      *)
(*           True Stress-Strain Data for Eval-   *)
(*           uation of Work-Hardening Rates.     *)
(* Input   : True Strain, True Stress            *)
(* Output  : True Strain, Smoothed Stress,       *)
(*           Derivative, Instantaneous n-Value   *)
(* Limits  : Max. 50 Data Pairs                  *)
(*                                               *)
(* Language: Apple Pascal (UCSD 1.1)             *)
(* Accuracy: 4 Byte Reals (6 decimal places      *)
(*                                               *)
(* Author  : T. Davis                            *)
(*                                               *)
(* Comments: Based on Tektronix BASIC Version    *)
(*************************************************)

CONST

  Mindata =  5;
  Maxdata = 50;


VAR

  Truestrain, Truestress : ARRAY[1..Maxdata]
                                   OF REAL;
  S                      : ARRAY[1..7] OF REAL;
  Datapoints             : INTEGER;
  I, J, K, Jj, Jm        : INTEGER;
  Aa, Ah                 : REAL;
  T1, T2, T3, T4, T5     : REAL;
  Dterm, Smoothstress,
  Deriv, Ninst           : REAL;


PROCEDURE CLEARVARS;

(* SET ALL VARIABLES, ARRAYS TO ZERO *)

BEGIN

  FOR i:=1 TO Maxdata DO
  BEGIN
    Truestrain[i]:=0.0; Truestress[i]:=0.0
  END;
```

```
  Datapoints:=0; I:=0; J:=0; K:=0; Jj:=0; Jm:=0;
  Aa:=0.0; Ah:=0.0;
  T1:=0.0; T2:=0.0; T3:=0.0; T4:=0.0; T5:=0.0;
  Dterm:=0.0; Smoothstress:=0.0; Deriv:=0.0;
  Ninst:=0.0

END; (* CLEARVARS *)


PROCEDURE GETDATA;

(* GET STRESS-STRAIN DATA FROM KEYBOARD *)

BEGIN

  WHILE Datapoints(Mindata do
  BEGIN
    WRITELN('How many data pairs ()4): ');
    READLN(Datapoints)
  END;
  WRITELN('OK, now enter the stress-strain data:-');
  FOR I:=1 TO Datapoints DO
  BEGIN
    WRITE('DATA PAIR ',I:3,': ');
    READ(Truestrain[i],Truestress[i])
  END;
  WRITELN('OK, the data is in....')

END; (* GETDATA *)


PROCEDURE SMOOTHIT;

(* PERFORM SMOOTHING, CALCULATE DERIVATIVE ETC *)

BEGIN

(* SET UP THE NORMAL EQUATIONS AND SOLVE *)

  FOR I:=1 TO Datapoints DO
  BEGIN

    Jm:=3;
    IF I)Datapoints THEN Jm:=I-Datapoints+5;
    IF I(3 THEN Jm:=I;

    FOR K:=1 TO 7 DO S[K]:=0.0;

    FOR J:=1 TO 5 DO
```

```
    BEGIN

      Jj:=I+J-Jm;
      Ah:=Truestrain[Jj]-Truestrain[I];
      Aa:=Ah;

      FOR K:=1 TO 4 DO
      BEGIN
        S[K]:=S[K]+Aa;
        Aa:=Aa*Ah
      END;

      Aa:=Truestress[Jj];

      FOR K:=5 TO 7 DO
      BEGIN
        S[K]:=S[K]+Aa;
        Aa:=Aa*Ah
      END

    END;

    T1:=S[2]*S[4]-S[3]*S[3];
    T2:=S[2]*S[3]-S[1]*S[4];
    T3:=S[1]*S[3]-S[2]*S[2];
    T4:=5*S[4]-S[2]*S[2];
    T5:=S[1]*S[2]-5*S[3];

    (* CALCULATE MATRIX DETERMINANT *)
    Dterm:=5*T1+S[1]*T2+S[2]*T3;
    (* CALCULATE SMOOTHED VALUE OF TRUE STRESS *)
    Smoothstress:=(T1*S[5]+T2*S[6]+T3*S[7])/Dterm;
    (* CALCULATE THE DERIVATIVE AT THIS TRUE STRAIN *)
    Deriv:=(T2*S[5]+T4*S[6]+T5*S[7])/Dterm;
    (* CALCULATE THE INSTANTANEOUS N-VALUE *)
    Ninst:=Truestrain[i]*Deriv/Truestress[i];

    WRITELN(Truestrain[i]:6:4,'        ',
            Smoothstress:5:1,'       ',
            Deriv:6:1,'    ',
            Ninst:5:3)

  END

END; (* SMOOTHIT *)


BEGIN (* MAIN PROGRAM SEGMENT *)

  CLEARVARS;
```

```
  GETDATA;

  WRITELN('TRUE STRAIN  SMOOTH STRESS',
          'DERIVATIVE  INST-N');
  WRITELN('**************************',
          '********************');
  WRITELN(' ');

  SMOOTHIT;

  WRITELN(' ');
  WRITELN('ALL DONE.')

END.  (* OF PROGRAM.  *)
```

Figure 76 compares the performance of the parabolic smoothing program with:-

a). Instantaneous n-values calculated by the Zwick tensile machine.

b). The overall n-value obtained by the parabolic work-hardening law.

c). Instantaneous n-values obtained by numerical differentiation, but using cubic-splines with variable knots and re-splining for smoothing rather than a least squares parabola. This program is more complex than that included here and runs on the Aston University Harris H800 super-minicomputer.

NB: A discussion of cubic-splines is beyond the scope of this thesis, but splining can be thought of as a piecewise approximation technique using blending functions that ensure continuity at the joins between each piece or curve. A set of control points on or off the curves are required (the former are called knots) to control the form of the curves and ensure continuity.

The steel used for this example was AK in the

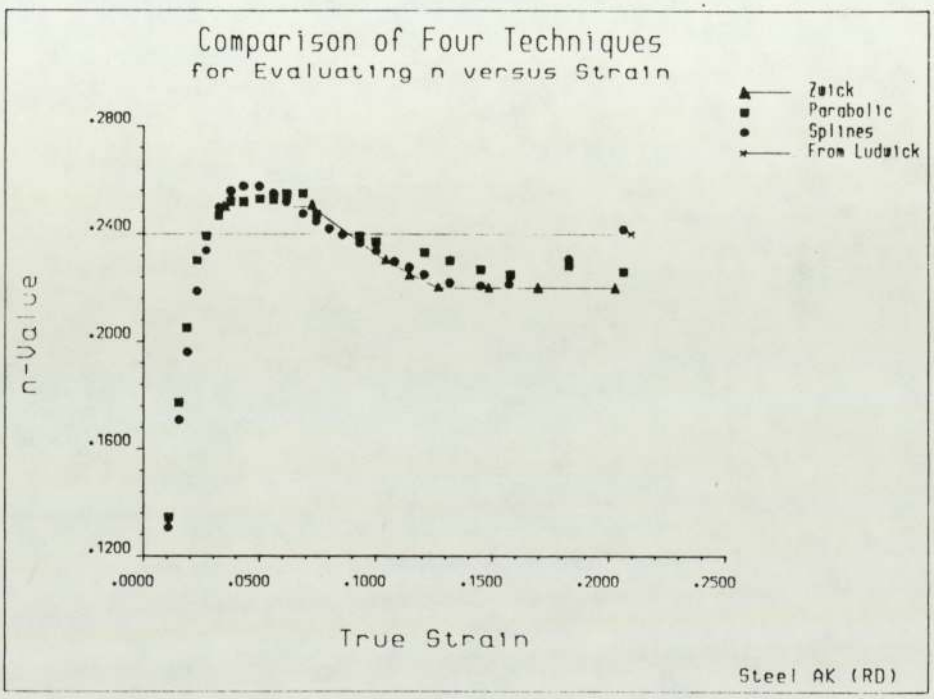

Fig. 76. Comparison of Four Techniques for Evaluating the Variation of n-Value with Strain in the Tensile Test (Refer to Text for Details). There is Good Agreement Between the Three Methods Used to Evaluate Instantaneous n-Values.

rolling direction. As can be clearly seen, the assumption of constant n against strain is erroneous: independent of the method of evaluation, n is a function of strain. An initially very low n-value increases to a peak at 0.04 to 0.05 true strain, then falls off to a near constant value after 0.13 strain (but lower than that predicted by Ludwick-Holloman). The numeric techniques provide a greater range of n-values than the Zwick and but agreement is good between the results. The cubic-spline method provides a smoother curve than the parabolic program, but care must be taken at the ends of the data range. When this exercise is repeated for highly cold-worked samples the splining technique gives better results than the parabolic method.

APPENDIX 3

Errors

All results generated experimentally or by computation are subject to errors from a variety of sources. In the main body of the thesis the tolerances on measured parameters, such as the distance between gauge marks, have been indicated where appropriate. While these give some indication of the precision of experimental values, it is important to appreciate that these errors can be compounded by mathematical operations and by natural variations in the population being sampled.

There are three main categories of errors:-

1). Inherent or measurement errors.
2). Random or statistical errors.
3). Truncation and round-off errors.

Errors of measurement are generally dependent upon the inherent precision of the mensuration equipment and the ease with which a measurement can be carried out. For example, the extensometry used on the Zwick tensile machine, from which r-values were

obtained, has the following resolution:-

Length extension = $\pm$0.01 mm

Width extension = $\pm$0.0005 mm

If the r-value is measured and calculated by the indirect method given in ASTM E517-74, then the error in the final value is given by the formula below (assuming that the original gauge lengths are without error):-

$$\text{Error in } r = \left(\frac{r + 1}{ef} \right) \left(r.\frac{le}{lf} + (r + 1).\frac{we}{wf} \right)$$

where ef = strain at which r is measured

lf, wf = final measured length and width (mm)

le, lf = expected error in measurement of length and width (mm)

Substituting some typical values into this equation gives (for length and width gauge lengths of 50mm and 12.70mm respectively):-

If r = 2 at 15% strain, then error is $\pm$0.01

If r = 2 at 2 % strain, then error is $\pm$0.08

This error can be doubled if the original gauge

lengths are subject to the same errors as the final measurements.

As well as inherent errors, there will be statistical scatter when sampling from a homogeneous population. Traditionally, this scatter is divided into two classes: assignable causes and random fluctuations. Assignable causes are such things as differences between operators, load-frames and the like, which can be eradicated eventually (if desired). Random effects, however, are fundamental to the statistical nature of the universe.

Examining the mechanical property data presented in this thesis, the following sample standard deviations have been calculated:-

Proof stress	s =	6.46 MPa
Elongation	s =	0.55 %
r-value	s =	0.05 at 15% strain
		0.90 at 2% strain

As a rough guide, 99.7% of a normal population should lie within three standard deviations either side of the mean: obviously, interpretation of r-values measured at low strains must be undertaken with caution.

Truncation and round-off errors are commonly encountered when using numerical methods to solve problems. When an infinite mathematical process (such as approximating Pi) is terminated in a finite number of steps, a truncation error is introduced: this type of error is not significant for the present study. Round-off errors, however, are likely to be a problem when any iterative computational procedure is used (such as that outlined in Appendix 2). When performing calculations by hand or using a computer, real numbers can only be represented by a finite number of significant digits. The rounding operations applied to the mantissa in order to satisfy this representation will introduce small errors into the calculation. These rounding errors can propagate through repeated calculations, compounding the error at each step. There are some simple rules for minimising this type of error:-

1). Avoid subtraction of nearly equal numbers.
2). When adding or subtracting numbers, always use the smallest numbers first.
3). Minimise the number of arithmetic operations.

Many computer languages have 'double precision' real numbers available; these should be used whenever round-off errors are expected.

APPENDIX 4

Co-ordinate System in Strain Space

Consider a uniaxial tensile prestrain (stage I) followed by tension testing at some angle ϕ to the prestrain direction. The stage I axes are taken as the reference set, although this will not influence the outcome.

The strain tensor for stage I straining is:-

$$\varepsilon_I = \begin{vmatrix} 1 & 0 & 0 \\ 0 & -0.5 & 0 \\ 0 & 0 & -0.5 \end{vmatrix}$$

Assuming an isotropic material and unit strain in the prestrain direction.

The strain tensor for stage II will be identical to the one above with respect to the new axes. However, we need to transform it back to the same axes as for stage I:-

$$\varepsilon'_{II_{ij}} = a_{ik}\, a_{jl}\, \varepsilon_{II_{kl}}$$

where a is the rotation matrix:-

$$a = \begin{vmatrix} \cos\phi & \sin\phi & 0 \\ -\sin\phi & \cos\phi & 0 \\ 0 & 0 & 1 \end{vmatrix}$$

Hence, for example:-

$$\varepsilon'_{II_{11}} = \cos^2\phi - \tfrac{1}{2}\sin^2\phi + 0$$

etc.

It is now necessary to normalise the stage I strain tensor and the stage II tensor (rotated to the same axes as the prestrain):-

$$\varepsilon_{I_{ij}}\, \varepsilon_{I_{ij}} = 1 \quad \text{and} \quad \varepsilon'_{II_{ij}}\, \varepsilon'_{II_{ij}} = 1$$

ie: ε_{ij} and ε^*_{ij}

Hence, the angle separating the two strain vectors is given by:-

$$\alpha = \cos^{-1}\, \varepsilon_{ij}\, \varepsilon^*_{ij}$$

If α is 90 degrees then this corresponds to the greatest change in active slip-systems. An angle of 180 degrees means complete reversal of slip (ie: the Bauschinger effect).

APPENDIX 5

Tables 6 to 50 (Refer to Chapter 3)

True Prestrain	True Flow Stress in MPa						
	Angle Relative to Prestrain in Degrees						
	0	15	30	45	60	75	90
0	170	169	183	178	176	175	177
0.0257	-	-	-	244	233	217	206
0.0296	235	223	241	-	-	-	-
0.0411	248	248	271	-	-	-	-
0.0440	-	-	-	263	250	226	217
0.0705	283	284	307	-	-	-	-
0.0714	-	-	-	317	297	235	233
0.0908	-	-	-	316	308	275	266
0.0962	304	303	325	-	-	-	-
0.1398	327	332	348	-	-	-	-
0.1484	-	-	-	367	361	-	286
0.1731	350	350	364	-	-	-	-
0.1740	-	-	-	395	382	325	313

Table 6. Steel AK : Effect of TD Uniaxial Prestrain on the True Flow Stress Determined in Subsequent Uniaxial Tensile Tests at Various Angles to the Prestrain. The Flow Stress is the True 0.2% Proof Stress in the Tensile Test.

Nominal Prestrain (%)	Uniform Elongation (Nominal %)						
	Angle Relative to Prestrain in Degrees						
	0	15	30	45	60	75	90
0	22.7	23.0	21.2	22.4	22.9	23.1	24.6
	23.3	-	-	22.8	-	-	25.2
2.6	-	-	-	22.6	18.8	21.5	25.4
	-	-	-	19.8	-	-	23.3
3.0	20.4	19.6	19.7	-	-	-	-
	21.9	-	-	-	-	-	-
4.2	19.8	18.3	17.9	-	-	-	-
	19.0	-	-	-	-	-	-
4.5	-	-	-	17.4	15.0	21.2	23.8
	-	-	-	17.4	-	-	20.8
7.3	15.0	14.1	13.6	-	-	-	-
	15.9	-	-	-	-	-	-
7.4	-	-	-	13.1	4.5	15.1	18.9
	-	-	-	11.5	-	-	18.0
9.5	-	-	-	0.8	0.6	3.1	2.0
	-	-	-	0.8	-	-	2.1
10.1	12.2	10.8	9.1	-	-	-	-
	13.8	-	-	-	-	-	-
15.0	8.0	7.3	2.8	-	-	-	-
	7.5	-	-	-	-	-	-
16.0	-	-	-	0.5	0.6	1.5	1.9
	-	-	-	0.7	-	-	1.7
18.9	6.1	4.9	2.6	-	-	-	-
	6.7	-	-	-	-	-	-
19.0	-	-	-	0.6	0.5	1.3	1.5
	-	-	-	0.6	-	-	1.4

Table 7. Steel AK : Effect of TD Uniaxial Prestrain on the Uniform Elongation Determined in Subsequent Uniaxial Tensile Tests at Various Angles to the Prestrain.

Nominal Prestrain (%)	Total Elongation (Nominal %)						
	Angle Relative to Prestrain in Degrees						
	0	15	30	45	60	75	90
0	41.3	40.6	39.9	40.5	40.1	40.8	42.2
	41.5	-	-	39.1	-	-	42.9
2.6	-	-	-	39.3	38.4	38.2	43.5
	-	-	-	38.6	-	-	43.1
3.0	40.5	37.1	36.9	-	-	-	-
	39.9	-	-	-	-	-	-
4.2	38.6	36.2	36.4	-	-	-	-
	39.2	-	-	-	-	-	-
4.5	-	-	-	37.3	37.3	37.1	41.5
	-	-	-	37.4	-	-	41.1
7.3	35.0	34.2	33.0	-	-	-	-
	34.9	-	-	-	-	-	-
7.4	-	-	-	34.5	30.8	35.6	38.7
	-	-	-	32.3	-	-	39.1
9.5	-	-	-	24.6	25.1	31.3	35.5
	-	-	-	27.5	-	-	35.7
10.1	32.4	31.6	31.6	-	-	-	-
	32.0	-	-	-	-	-	-
15.0	28.7	28.1	22.5	-	-	-	-
	28.8	-	-	-	-	-	-
16.0	-	-	-	3.1	4.8	12.1	18.3
	-	-	-	5.7	-	-	15.6
18.9	25.1	24.7	19.0	-	-	-	-
	25.3	-	-	-	-	-	-
19.0	-	-	-	6.1	5.0	11.6	14.3
	-	-	-	2.1	-	-	15.3

Table 8. Steel AK : Effect of TD Uniaxial Prestrain on the Total Elongation Determined in Subsequent Uniaxial Tensile Tests at Various Angles to the Prestrain.

True Prestrain	True Flow Stress in MPa						
	Angle Relative to Prestrain in Degrees						
	0	15	30	45	60	75	90
0	254	265	279	276	266	261	254
0.0257	-	-	-	355	349	280	268
0.0296	339	345	345	-	-	-	-
0.0488	374	378	390	393	403	299	286
0.0714	398	410	415	-	-	-	-
0.0723	-	-	-	423	417	328	317
0.0779	406	416	419	-	-	340	320
0.0843	-	-	-	440	430	-	339
0.0926	426	430	435	-	-	-	-
0.0953	-	-	-	446	440	355	331

Table 9. Steel RP : Effect of TD Uniaxial Prestrain on the True Flow Stress Determined in Subsequent Uniaxial Tensile Tests at Various Angles to the Prestrain. The Flow Stress is the True 0.2% Proof Stress in the Tensile Test.

Nominal Prestrain (%)	Uniform Elongation (Nominal %)						
	Angle Relative to Prestrain in Degrees						
	0	15	30	45	60	75	90
0	19.0	17.9	17.3	17.0	18.6	19.0	19.4
	17.8	-	-	17.6	-	-	20.4
2.6	-	-	-	14.6	16.6	16.8	18.7
				15.2	-	-	17.6
3.0	15.9	14.1	14.6	-	-	-	-
	14.8	-	-	-	-	-	-
	15.1	-	-	-	-	-	-
5.0	14.7	11.2	13.0	10.6	11.3	14.7	17.4
	13.4	-	-	12.2	-	-	16.2
	12.7	-	-	-	-	-	-
7.4	12.5	8.9	7.1	-	-	-	-
	11.2	-	-	-	-	-	-
	9.8	-	-	-	-	-	-
7.5	-	-	-	4.8	1.8	7.6	10.9
	-	-	-	2.9	-	-	6.7
8.1	9.5	7.6	3.9	-	-	4.5	5.2
	10.8	-	-	-	-	-	6.5
	10.6	-	-	-	-	-	-
8.8	-	-	-	1.8	1.0	-	3.7
	-	-	-	1.5	-	-	3.5
9.7	9.2	6.7	3.6	-	-	-	-
	7.6	-	-	-	-	-	-
	8.9	-	-	-	-	-	-
10.0	-	-	-	1.0	1.1	2.1	2.6
	-	-	-	1.1	-	-	3.2

Table 10. Steel RP : Effect of TD Uniaxial Prestrain on the Uniform Elongation Determined in Subsequent Uniaxial Tensile Tests at Various Angles to the Prestrain.

Nominal Prestrain (%)	Total Elongation (Nominal %)						
	Angle Relative to Prestrain in Degrees						
	0	15	30	45	60	75	90
0	32.5	31.6	29.4	25.8	31.0	31.5	32.7
	33.9	-	-	28.0	-	-	32.5
2.6	-	-	-	27.7	26.4	31.2	35.1
				28.9	-	-	34.4
3.0	29.4	28.3	28.9	-	-	-	-
	30.2	-	-	-	-	-	-
	29.9	-	-	-	-	-	-
5.0	27.1	25.0	24.8	24.0	23.0	28.7	30.8
	26.6	-	-	22.3	-	-	30.8
	26.3	-	-	-	-	-	-
7.4	25.1	22.0	20.3	-	-	-	-
	25.1	-	-	-	-	-	-
	24.7	-	-	-	-	-	-
7.5	-	-	-	21.3	18.7	24.6	26.7
	-	-	-	18.5	-	-	26.5
8.1	24.7	21.3	18.1	-	-	21.4	22.9
	24.5	-	-	-	-	-	23.9
	24.4	-	-	-	-	-	-
8.8	-	-	-	15.8	16.1	-	21.4
	-	-	-	16.1	-	-	21.7
9.7	22.4	20.2	14.8	-	-	-	-
	23.5	-	-	-	-	-	-
	22.8	-	-	-	-	-	-
10.0	-	-	-	10.9	14.5	19.1	19.1
	-	-	-	12.0	-	-	19.4

Table 11. Steel RP : Effect of TD Uniaxial Prestrain on the Total Elongation Determined in Subsequent Uniaxial Tensile Tests at Various Angles to the Prestrain.

True Prestrain	True Flow Stress in MPa		
	Angle Relative to Prestrain in Degrees		
	0	45	90
0	235	239	235
0.0286	-	332	259
0.0296	317	-	-
0.0440	363	-	-
0.0488	-	401	279
0.0714	-	438	296
0.0723	408	-	-
0.0935	-	463	349
0.0953	436	-	-
0.1169	-	491	391
0.1354	474	-	-
0.1406	-	512	419
0.1579	492	-	-

Table 12. Steel DP : Effect of TD Uniaxial Prestrain on the Proof Stress Determined in Subsequent Uniaxial Tensile Tests at Various Angles to the Prestrain. The Flow Stress is the True 0.2% Proof Stress in the Tensile Test.

Nominal Prestrain (%)	Uniform Elongation (Nominal %)		
	Angle Relative to Prestrain in Degrees		
	0	45	90
0	21.4	20.2	20.3
	22.0	19.4	19.3
2.9	-	20.5	19.8
	-	20.2	19.6
3.0	18.5	-	-
	19.1	-	-
4.5	17.4	-	-
	16.9	-	-
5.0	-	17.6	17.6
	-	18.1	17.5
7.4	-	13.7	14.3
	-	14.3	13.8
7.5	13.8	-	-
	13.4	-	-
9.8	-	8.1	9.0
	-	2.4	4.1
10.0	12.4	-	-
	11.4	-	-
12.4	-	0.9	2.2
	-	1.3	2.4
14.5	8.0	-	-
	6.3	-	-
15.1	-	1.2	1.4
	-	0.7	1.7
17.1	6.3	-	-
	4.6	-	-

Table 13. Steel DP : Effect of TD Uniaxial Prestrain on the Uniform Elongation Determined in Subsequent Uniaxial Tensile Tests at Various Angles to the Prestrain.

Nominal Prestrain (%)	Total Elongation (Nominal %)		
	Angle Relative to Prestrain in Degrees		
	0	45	90
0	36.5	33.9	34.3
	36.0	32.9	33.6
2.9	-	32.3	33.7
	-	32.3	33.4
3.0	33.4	-	-
	34.5	-	-
4.5	31.8	-	-
	31.5	-	-
5.0	-	30.2	31.4
	-	30.7	31.6
7.4	-	26.3	28.0
	-	26.7	28.5
7.5	28.5	-	-
	28.6	-	-
9.8	-	20.3	23.0
	-	20.8	22.7
10.0	27.4	-	-
	26.8	-	-
12.4	-	10.0	17.5
	-	10.6	17.3
14.5	22.6	-	-
	20.6	-	-
15.1	-	4.6	13.8
	-	4.2	14.2
17.1	18.1	-	-
	19.1	-	-

Table 14. Steel DP : Effect of TD Uniaxial Prestrain on the Total Elongation Determined in Subsequent Uniaxial Tensile Tests at Various Angles to the Prestrain.

Nominal Prestrain (%)	r-Values Measured at the Following Nominal Strains:-								
	2.0	3.0	4.0	5.0	6.0	8.0	10.0	12.0	15.0
0	2.71	-	-	2.30	-	-	2.18	2.14	2.10
3.0	7.55	4.10	3.30	2.95	2.79	2.51	2.42	-	2.28
4.2	2.59	2.47	2.39	2.28	2.20	2.16	2.11	-	2.06
7.3	3.00	2.70	2.62	2.54	2.41	2.30	2.24	-	2.14
10.1	2.71	2.56	2.37	2.24	2.18	2.15	2.10	-	2.00
15.0	3.37	2.79	2.53	2.42	2.35	2.21	2.15	-	1.99
18.9	2.26	2.15	2.06	1.99	1.97	1.92	1.88	-	1.73

Table 15. Steel AK: Effect of TD Uniaxial Prestrain on the r-Values Obtained in Subsequent Uniaxial Tensile Tests at 0 Degrees to the Prestrain (IE: Interrupted Tensile Test).

Nominal Prestrain (%)	r-Values Measured at the Following Nominal Strains:-								
	2.0	3.0	4.0	5.0	6.0	8.0	10.0	12.0	15.0
0	1.45	-	-	1.39	-	-	1.40	1.39	1.38
2.6	1.25	1.27	1.37	1.36	1.39	1.40	1.38	-	1.34
4.5	2.24	1.88	1.74	1.59	1.50	1.47	1.49	-	1.42
7.4	3.17	2.45	2.10	1.89	1.74	1.63	1.58	-	1.49
9.5	3.03	2.86	2.70	2.49	2.27	1.92	1.77	-	1.70

Table 16. Steel AK: Effect of TD Uniaxial Prestrain on the r-Values Obtained in Subsequent Uniaxial Tensile Tests at 45 Degrees to the Prestrain.

Nominal Prestrain (%)	r-Values Measured at the Following Nominal Strains:-								
	2.0	3.0	4.0	5.0	6.0	8.0	10.0	12.0	15.0
0	1.71	-	-	1.76	-	-	1.78	1.76	1.72
2.6	5.91	3.66	3.00	2.77	2.61	2.39	2.27	-	2.02
4.5	6.57	4.07	3.43	3.08	2.84	2.58	2.44	-	2.25
7.4	5.78	4.30	3.75	3.32	3.02	2.75	2.54	-	2.33
9.5	6.63	4.86	4.11	3.62	3.32	2.97	2.81	-	2.55

Table 17. Steel AK: Effect of TD Uniaxial Prestrain on the r-Values Obtained in Subsequent Uniaxial Tensile Tests at 90 Degrees to the Prestrain (RD).

Nominal Prestrain (%)	r-Values Measured at the Following Nominal Strains:-								
	2.0	3.0	4.0	5.0	6.0	8.0	10.0	12.0	15.0
0	2.75	2.51	-	2.36	-	-	2.20	2.19	2.18
3.0	4.26	2.79	2.56	2.45	2.43	2.33	2.34	2.18	2.09
5.0	2.05	2.16	2.08	2.08	2.07	2.06	2.01	1.94	1.95
7.4	2.35	2.19	2.09	2.06	2.03	2.01	1.99	1.94	-
8.1	3.45	2.37	2.20	2.14	2.03	1.99	1.98	1.95	-
9.7	3.10	2.59	2.42	2.30	2.21	2.13	2.10	2.05	-

Table 18. Steel RP: Effect of TD Uniaxial Prestrain on the r-Values Obtained in Subsequent Uniaxial Tensile Tests at 0 Degrees to the Prestrain (IE: Interrupted Tensile Test).

Nominal Prestrain (%)	r-Values Measured at the Following Nominal Strains:-								
	2.0	3.0	4.0	5.0	6.0	8.0	10.0	12.0	15.0
0	1.71	1.60	-	1.59	-	-	1.49	1.45	1.42
2.6	2.02	1.80	1.69	1.65	1.60	1.54	1.48	-	1.42
5.0	1.62	1.54	1.54	1.63	1.58	1.54	1.47	-	1.47
7.5	1.95	1.93	1.84	1.75	1.68	1.65	1.58	1.50	1.46
8.8	-	1.77	1.65	1.60	1.54	1.43	1.38	1.35	1.24
10.0	-	2.33	2.64	3.03	3.49	5.97	-	-	-

Table 19. Steel RP: Effect of TD Uniaxial Prestrain on the r-Values Obtained in Subsequent Uniaxial Tensile Tests at 45 Degrees to the Prestrain.

Nominal Prestrain (%)	r-Values Measured at the Following Nominal Strains:-								
	2.0	3.0	4.0	5.0	6.0	8.0	10.0	12.0	15.0
0	2.31	2.18	-	2.07	-	-	1.95	1.94	1.94
2.6	5.59	3.98	3.41	3.07	2.85	2.57	2.40	2.30	-
5.0	5.22	3.83	3.24	2.95	2.79	2.52	2.39	2.31	-
7.5	4.95	4.09	3.70	3.47	3.22	2.86	2.72	2.64	-
8.1	-	5.85	5.39	5.07	4.68	4.01	3.49	3.27	3.02
8.8	4.32	3.88	3.75	3.42	3.18	2.91	2.72	-	2.75
10.0	4.09	4.10	3.88	3.59	3.35	2.96	2.69	-	2.33

Table 20. Steel RP: Effect of TD Uniaxial Prestrain on the r-Values Obtained in Subsequent Uniaxial Tensile Tests at 90 Degrees to the Prestrain (RD).

Nominal Prestrain (%)	r-Values Measured at the Following Nominal Strains:-								
	2.0	3.0	4.0	5.0	6.0	8.0	10.0	12.0	15.0
0	1.73	-	-	1.51	-	-	1.46	1.44	1.43
3.0	4.15	3.00	2.56	2.26	2.10	1.89	1.80	1.71	1.57
4.5	1.62	1.58	1.52	1.52	1.50	1.50	1.50	1.50	1.49
7.5	2.00	1.84	1.68	1.65	1.62	1.58	1.58	1.56	1.54
10.0	2.34	1.95	1.78	1.61	1.50	1.37	1.29	1.25	-

Table 21. Steel DP: Effect of TD Uniaxial Prestrain on the r-Values Obtained in Subsequent Uniaxial Tensile Tests at 0 Degrees to the Prestrain (IE: Interrupted Tensile Test).

Nominal Prestrain (%)	r-Values Measured at the Following Nominal Strains:-								
	2.0	3.0	4.0	5.0	6.0	8.0	10.0	12.0	15.0
0	1.41	-	-	1.14	-	-	1.06	1.05	1.03
2.9	1.60	1.46	1.37	1.31	1.29	1.25	1.21	-	1.18
5.0	1.71	1.57	1.46	1.39	1.32	1.25	1.21	-	1.20
7.4	1.42	1.40	1.37	1.39	1.38	1.33	1.32	-	1.26
9.8	1.91	1.79	1.67	1.59	1.52	1.41	1.32	-	1.27
12.4	2.47	2.20	1.91	1.75	1.63	1.54	1.43	-	-

Table 22. Steel DP: Effect of TD Uniaxial Prestrain on the r-Values Obtained in Subsequent Uniaxial Tensile Tests at 45 Degrees to the Prestrain.

Nominal Prestrain (%)	r-Values Measured at the Following Nominal Strains:-								
	2.0	3.0	4.0	5.0	6.0	8.0	10.0	12.0	15.0
0	1.73	-	-	1.34	-	-	1.26	1.25	1.23
2.9	4.91	2.90	2.35	2.08	2.08	1.79	1.68	-	1.54
5.0	5.12	3.17	2.58	2.27	2.17	2.03	1.91	-	1.66
7.4	3.85	3.44	2.92	2.67	2.50	2.27	2.11	-	1.80
9.8	5.24	3.28	2.79	2.48	2.29	2.12	2.01	-	1.75
12.4	4.26	3.67	3.20	3.00	2.80	2.61	2.44	-	2.15

Table 23. Steel DP: Effect of TD Uniaxial Prestrain on the r-Values Obtained in Subsequent Uniaxial Tensile Tests at 90 Degrees to the Prestrain (RD).

True Effective Prestrain	True Flow Stress Measured in the Rolling Direction (MPa)	
	After Biaxial Prestrain	No Prestrain
0	177	177
0.0237	230	223
0.0491	282	268
0.0650	299	287
0.0723	330	294
0.0956	351	315
0.1390	374	344

Table 24. Steel AK : Effect of Equi-Biaxial Prestrain on the True Flow Stress determined in Subsequent Uniaxial Tensile Tests in the Rolling Direction of the Sheet. The Flow Stress after Biaxial Straining is the True 0.2% Proof Stress of the Tensile Test.

Nominal Effective Prestrain (%)	Elongation (Nominal %)	
	Uniform	Total
0	24.6	42.2
	25.2	42.9
	-	-
2.4	21.1	39.6
	23.0	38.5
	23.7	39.0
5.0	17.4	36.9
	18.0	35.7
	18.3	35.4
6.7	13.2	31.1
	13.8	30.6
	14.4	30.7
7.5	0.6	26.8
	0.8	27.4
	4.5	26.4
10.0	0.6	18.4
	0.6	15.0
	1.1	16.2
14.9	0.7	5.3
	1.0	4.7
	1.5	6.0

Table 25. Steel AK : Effect of Equi-Biaxial Prestrain on the Uniform and Total Elongation Determined in Subsequent Uniaxial Tensile Tests in the Rolling Direction of the Sheet.

True Effective Prestrain	True Flow Stress Measured in the Rolling Direction (MPa)	
	After Biaxial Prestrain	No Prestrain
0	256	256
0.0494	397	381
0.1052	464	445
0.1484	495	476

Table 26. Steel RP : Effect of Equi-Biaxial Prestrain on the True Flow Stress determined in Subsequent Uniaxial Tensile Tests in the Rolling Direction of the Sheet. The Flow Stress after Biaxial Straining is the True 0.2% Proof Stress of the Tensile Test.

Nominal Effective Prestrain (%)	Elongation (Nominal %)	
	Uniform	Total
0	19.4	32.7
	20.4	32.5
	-	-
5.1	12.7	26.8
	10.7	27.4
	11.0	26.6
11.3	0.6	10.9
	0.7	11.9
	0.6	10.5
16.0	0.6	5.8
	0.6	1.1
	0.5	3.2

Table 27. Steel RP : Effect of Equi-Biaxial Prestrain on the Uniform and Total Elongation Determined in Subsequent Uniaxial Tensile Tests in the Rolling Direction of the Sheet.

True Effective Prestrain	True Flow Stress Measured in the Rolling Direction (MPa)	
	After Biaxial Prestrain	No Prestrain
0	235	235
0.0260	328	321
0.0497	398	391
0.0730	438	434
0.0870	478	455
0.1180	507	489
0.1410	516	509

Table 28. Steel DP : Effect of Equi-Biaxial Prestrain on the True Flow Stress determined in Subsequent Uniaxial Tensile Tests in the Rolling Direction of the Sheet. The Flow Stress after Biaxial Straining is the True 0.2% Proof Stress of the Tensile Test.

Nominal Effective Prestrain (%)	Elongation (Nominal %)	
	Uniform	Total
0	20.3	34.3
	19.3	33.6
	-	-
2.6	17.0	31.1
	17.4	31.9
	16.7	30.6
5.1	15.8	29.0
	14.2	27.8
	13.5	28.5
7.6	11.7	24.3
	11.0	23.8
	11.2	23.3
9.1	0.5	15.0
	0.9	15.6
	3.7	16.0
12.5	0.9	10.8
	0.9	10.7
	0.6	10.3
15.1	1.2	6.3
	0.7	6.0
	0.5	5.2

Table 29. Steel DP : Effect of Equi-Biaxial Prestrain on the Uniform and Total Elongation Determined in Subsequent Uniaxial Tensile Tests in the Rolling Direction of the Sheet.

Nominal Effective Prestrain (%)	r-Values Measured at the Following Nominal Strains:-								
	2.0	3.0	4.0	5.0	6.0	8.0	10.0	12.0	15.0
0	1.71	-	-	1.76	-	-	1.78	1.76	1.72
2.4	1.61	1.54	1.53	1.52	1.55	1.54	1.51	-	1.52
5.0	1.50	1.37	1.30	1.27	1.27	1.26	1.25	-	1.30
6.7	1.82	1.26	1.20	1.18	1.17	1.12	1.12	-	1.17
	0.5	0.6	0.7	0.8	1.0				
10.0	4.00	1.88	1.54	1.27	1.15				
14.9	3.66	1.13	1.00	0.97	0.95				

Table 30. Steel AK : Effect of Equi-Biaxial Prestrain on the r-Values Obtained in Subsequent Uniaxial Tensile Tests in the Rolling Direction of the Sheet. Note the Change in the Strains at which the r-Values are Taken after 6.7% Prestrain.

Nominal Effective Prestrain (%)	r-Values Measured at the Following Nominal Strains:-								
	2.0	3.0	4.0	5.0	6.0	8.0	10.0	12.0	15.0
0	2.31	2.18	-	2.07	-	-	1.95	1.94	1.94
5.1	1.95	1.94	1.93	1.90	1.91	1.90	1.88	1.86	-
	0.5	0.6	0.7	0.8	1.0				
11.1	4.18	2.32	1.69	1.35	1.05				
16.0	3.28	1.93	1.39	1.10	0.85				

Table 31. Steel RP : Effect of Equi-Biaxial Prestrain on the r-Values Obtained in Subsequent Uniaxial Tensile Tests in the Rolling Direction of the Sheet. Note the Change in the Strains at which the r-Values are Taken after 5.1% Prestrain.

Nominal Effective Prestrain (%)	r-Values Measured at the Following Nominal Strains:-								
	2.0	3.0	4.0	5.0	6.0	8.0	10.0	12.0	15.0
0	1.73	-	-	1.34	-	-	1.26	1.25	1.23
2.6	1.28	1.31	1.26	1.25	1.20	1.19	1.15	-	1.07
5.1	0.88	1.01	1.00	0.98	0.99	0.95	0.92	-	0.87
7.6	1.44	1.10	0.91	0.88	0.84	0.79	0.77	-	0.75
	0.5	0.6	0.7	0.8	1.0				
9.1	3.08	1.25	1.06	0.92	0.80				
12.5	3.20	1.14	0.96	0.78	0.63				

Table 32. Steel DP : Effect of Equi-Biaxial Prestrain on the r-Values Obtained in Subsequent Uniaxial Tensile Tests in the Rolling Direction of the Sheet. Note the Change in the Strains at which the r-Values are Taken after 7.6% Prestrain.

True Effective Prestrain (%)	True Flow Stress in MPa		
	Angle Relative to Prestrain in Degrees		
	0	45	90
0	170	178	177
0.0240	238	-	-
0.0250	-	236	190
0.0490	281	-	-
0.0510	-	279	252
0.0710	310	307	291
0.0782	-	314	303
0.0915	329	-	-
0.0955	-	323	323
0.1040	338	-	-

Table 33. Steel AK : Effect of TD Plane-Strain Prestrain on the True Flow Stress Determined in Subsequent Uniaxial Tensile Tests at Various Angles to the Prestrain. The Flow Stress After the Prestrain is the True 0.2% Proof Stress of the Tensile Test.

Nominal Effective Prestrain (%)	Uniform Elongation (Nominal %)		
	Angle Relative to Prestrain in Degrees		
	0	45	90
0	22.7	22.4	24.6
	23.3	22.8	25.2
2.4	21.3	-	-
	21.7	-	-
2.5	-	19.3	24.0
	-	19.8	24.4
5.0	12.5	-	-
	12.0	-	-
5.2	-	8.6	7.5
	-	9.0	6.4
7.4	10.1	0.4	0.8
	8.8	0.7	2.4
8.1	-	0.8	0.8
	-	1.2	1.2
9.6	5.0	-	-
	4.2	-	-
10.0	-	0.5	0.7
	-	0.7	1.2
11.0	1.2	-	-
	2.5	-	-

Table 34. Steel AK : Effect of TD Plane-Strain Prestrain on the Uniform Elongation Determined in Subsequent Uniaxial Tensile Tests at Various Angles to the Prestrain.

Nominal Effective Prestrain (%)	Total Elongation (Nominal %)		
	Angle Relative to Prestrain in Degrees		
	0	45	90
0	41.3	40.5	42.2
	41.5	39.1	42.9
2.4	40.0	-	-
	39.5	-	-
2.5	-	37.4	41.7
	-	37.8	41.2
5.0	34.7	-	-
	35.1	-	-
5.2	-	30.6	34.7
	-	30.3	35.1
7.4	28.8	19.9	24.1
	29.4	19.2	24.5
8.1	-	12.8	19.7
	-	10.6	19.3
9.6	24.3	-	-
	24.7	-	-
10.0	-	5.0	16.2
	-	4.5	15.5
11.0	23.4	-	-
	23.7	-	-

Table 35. Steel AK : Effect of TD Plane-Strain Prestrain on the Total Elongation Determined in Subsequent Uniaxial Tensile Tests at Various Angles to the Prestrain.

True Effective Prestrain (%)	True Flow Stress in MPa		
	Angle Relative to Prestrain in Degrees		
	0	45	90
0	254	276	254
0.0260	-	350	260
0.0300	355	-	-
0.0400	-	386	313
0.0490	391	400	332
0.0710	428	-	-
0.0725	-	435	394
0.0790	440	-	-
0.0840	-	445	412
0.0930	450	-	-
0.0955	-	465	431

Table 36. Steel RP : Effect of TD Plane-Strain Prestrain on the True Flow Stress Determined in Subsequent Uniaxial Tensile Tests at Various Angles to the Prestrain. The Flow Stress After the Prestrain is the True 0.2% Proof Stress of the Tensile Test.

Nominal Effective Prestrain (%)	Uniform Elongation (Nominal %)		
	Angle Relative to Prestrain in Degrees		
	0	45	90
0	19.0	17.0	19.4
	17.8	17.6	20.4
2.6	-	15.3	18.4
	-	15.5	18.6
3.0	15.6	-	-
	16.2	-	-
4.1	-	12.6	10.3
	-	12.2	7.0
5.0	9.2	5.0	4.5
	8.9	5.4	4.0
7.4	5.4	-	-
	5.8	-	-
7.5	-	0.5	0.5
	-	2.4	0.6
8.2	4.0	-	-
	4.4	-	-
8.8	-	0.7	0.5
	-	0.7	0.5
9.7	1.8	-	-
	1.5	-	-
10.0	-	0.7	0.6
	-	0.7	0.6

Table 37. Steel RP : Effect of TD Plane-Strain Prestrain on the Uniform Elongation Determined in Subsequent Uniaxial Tensile Tests at Various Angles to the Prestrain.

Nominal Effective Prestrain (%)	Total Elongation (Nominal %)		
	Angle Relative to Prestrain in Degrees		
	0	45	90
0	32.5	25.8	32.7
	33.9	28.0	32.5
2.6	-	28.2	34.4
	-	28.5	34.6
3.0	30.2	-	-
	29.8	-	-
4.1	-	24.1	32.6
	-	23.7	32.9
5.0	25.0	19.6	27.8
	25.3	19.2	28.0
7.4	21.2	-	-
	21.5	-	-
7.5	-	11.2	14.2
	-	11.4	13.9
8.2	20.0	-	-
	19.7	-	-
8.8	-	7.9	12.0
	-	7.5	11.8
9.7	17.7	-	-
	17.9	-	-
10.0	-	5.6	10.6
	-	5.9	10.7

Table 38. Steel RP : Effect of TD Plane-Strain Prestrain on the Total Elongation Determined in Subsequent Uniaxial Tensile Tests at Various Angles to the Prestrain.

True Effective Prestrain (%)	True Flow Stress in MPa		
	Angle Relative to Prestrain in Degrees		
	0	45	90
0	235	239	235
0.0280	-	305	237
0.0300	339	-	-
0.0490	-	389	282
0.0497	401	-	-
0.0595	430	-	-
0.0610	-	416	347
0.0725	451	443	420
0.0915	-	479	462
0.0935	477	-	-

Table 39. Steel DP : Effect of TD Plane-Strain Prestrain on the True Flow Stress Determined in Subsequent Uniaxial Tensile Tests at Various Angles to the Prestrain. The Flow Stress After the Prestrain is the True 0.2% Proof Stress of the Tensile Test.

Nominal Effective Prestrain (%)	Uniform Elongation (Nominal %)		
	Angle Relative to Prestrain in Degrees		
	0	45	90
0	21.4	20.2	20.3
	22.0	19.4	19.3
2.8	-	20.6	20.5
	-	20.8	20.6
3.0	19.5	-	-
	19.9	-	-
5.0	-	14.5	15.9
	-	14.7	16.0
5.1	12.5	-	-
	12.7	-	-
6.1	10.3	-	-
	10.4	-	-
6.3	-	1.6	3.5
	-	0.9	3.6
7.5	9.1	0.6	2.3
	8.6	0.7	2.3
9.6	-	0.8	0.8
	-	0.7	0.8
9.8	5.1	-	-
	4.5	-	-

Table 40. Steel DP : Effect of TD Plane-Strain Prestrain on the Uniform Elongation Determined in Subsequent Uniaxial Tensile Tests at Various Angles to the Prestrain.

Nominal Effective Prestrain (%)	Total Elongation (Nominal %)		
	Angle Relative to Prestrain in Degrees		
	0	45	90
0	36.5	33.9	34.3
	36.0	32.9	33.6
2.8	-	32.5	34.0
	-	32.4	33.8
3.0	33.3	-	-
	33.6	-	-
5.0	-	29.5	30.0
	-	29.7	30.0
5.1	29.9	-	-
	29.6	-	-
6.1	26.5	-	-
	26.4	-	-
6.3	-	25.5	26.4
	-	25.1	26.3
7.5	23.1	19.4	23.5
	23.6	19.6	23.6
9.6	-	10.4	15.5
	-	10.3	15.6
9.8	20.5	-	-
	20.6	-	-

Table 41. Steel DP : Effect of TD Plane-Strain Prestrain on the Total Elongation Determined in Subsequent Uniaxial Tensile Tests at Various Angles to the Prestrain.

Nominal Effective Prestrain (%)	r-Values Measured at the Following Nominal Strains:-								
	2.0	3.0	4.0	5.0	6.0	8.0	10.0	12.0	15.0
0	2.71	-	-	2.30	-	-	2.18	2.14	2.10
2.4	2.85	2.68	2.58	2.51	2.47	2.41	2.38	-	2.27
5.0	3.46	2.90	2.74	2.64	2.61	2.51	2.53	-	2.41
7.4	4.91	3.66	3.22	3.00	2.84	2.73	2.67	-	2.58
9.6	6.88	5.16	4.02	3.53	3.32	3.17	3.01	-	2.80
11.0	6.71	4.02	3.45	3.26	3.08	2.97	2.88	-	2.73

Table 42. Steel AK: Effect of TD Plane-Strain Prestrain on the r-Values Obtained in Subsequent Uniaxial Tensile Tests at 0 Degrees to the Prestrain .

Nominal Effective Prestrain (%)	r-Values Measured at the Following Nominal Strains:-								
	2.0	3.0	4.0	5.0	6.0	8.0	10.0	12.0	15.0
0	1.45	-	-	1.39	-	-	1.40	1.39	1.38
2.5	2.06	1.80	1.66	1.61	1.58	1.57	1.54	-	1.54
5.2	2.26	2.01	1.89	1.82	1.78	1.78	1.77	-	1.76
7.4	3.38	2.71	2.39	2.18	2.02	1.94	1.92	-	1.92
8.1	5.90	3.49	2.93	2.74	2.58	2.44	2.35	-	-

Table 43. Steel AK: Effect of TD Plane-Strain Prestrain on the r-Values Obtained in Subsequent Uniaxial Tensile Tests at 45 Degrees to the Prestrain.

Nominal Effective Prestrain (%)	r-Values Measured at the Following Nominal Strains:-								
	2.0	3.0	4.0	5.0	6.0	8.0	10.0	12.0	15.0
0	1.71	-	-	1.76	-	-	1.78	1.76	1.72
2.5	6.21	4.00	3.36	3.09	2.91	2.70	2.58	-	2.34
5.2	6.87	4.39	3.74	3.39	3.15	2.91	2.75	-	2.57
7.4	7.01	4.62	4.06	3.63	3.34	3.07	2.85	-	2.67
8.1	7.12	5.19	4.25	3.85	3.64	3.23	3.04	-	2.78
10.0	7.02	5.00	4.47	4.18	3.93	3.62	3.51	-	3.24

Table 44. Steel AK: Effect of TD Plane-Strain Prestrain on the r-Values Obtained in Subsequent Uniaxial Tensile Tests at 90 Degrees to the Prestrain (RD).

Nominal Effective Prestrain (%)	r-Values Measured at the Following Nominal Strains:-								
	2.0	3.0	4.0	5.0	6.0	8.0	10.0	12.0	15.0
0	2.75	2.51	-	2.36	-	-	2.20	2.19	2.18
3.1	3.62	3.00	2.68	2.59	2.53	2.49	2.48	-	2.45
5.0	4.16	3.47	3.11	2.93	2.85	2.74	2.66	-	2.57
7.4	6.17	3.77	3.32	3.06	2.95	2.81	2.73	-	2.60
8.2	5.34	3.84	3.39	3.12	3.02	2.87	2.80	-	2.67
9.8	6.31	4.01	3.53	3.25	3.13	2.96	2.88	-	2.72

Table 45. Steel RP: Effect of TD Plane-Strain Prestrain on the r-Values Obtained in Subsequent Uniaxial Tensile Tests at 0 Degrees to the Prestrain.

Nominal Effective Prestrain (%)	r-Values Measured at the Following Nominal Strains:-								
	2.0	3.0	4.0	5.0	6.0	8.0	10.0	12.0	15.0
0	1.71	1.60	-	1.59	-	-	1.49	1.45	1.42
2.6	2.12	1.82	1.74	1.73	1.70	1.68	1.65	-	1.57
4.1	2.76	2.15	1.99	1.92	1.85	1.80	1.77	-	1.70
5.0	3.55	3.28	2.52	2.17	2.07	2.03	1.99	-	1.94
7.5	4.99	3.76	3.06	2.67	2.43	2.25	2.28	-	-
	0.5	0.6	0.7	0.8	1.0				
8.8	6.45	5.54	5.28	5.18	5.11				

Table 46. Steel RP: Effect of TD Plane-Strain Prestrain on the r-Values Obtained in Subsequent Uniaxial Tensile Tests at 45 Degrees to the Prestrain. Note the Change in the Strains at which the r-Values are Taken after 7.5% Prestrain.

Nominal Effective Prestrain (%)	r-Values Measured at the Following Nominal Strains:-								
	2.0	3.0	4.0	5.0	6.0	8.0	10.0	12.0	15.0
0	2.31	2.18	-	2.07	-	-	1.95	1.94	1.94
2.6	5.40	4.05	3.38	2.85	2.59	2.26	2.13	-	1.82
4.1	5.99	3.93	3.50	3.08	2.90	2.74	2.64	-	2.55
5.0	6.16	4.28	3.81	3.37	3.19	2.97	2.87	-	2.74
7.5	6.91	4.71	4.12	3.73	3.52	3.30	3.25	-	-
8.8	6.54	4.98	4.40	4.00	3.77	3.56	-	-	2.75
10.0	6.80	6.50	6.11	5.74	-	-	-	-	2.33

Table 47. Steel RP: Effect of TD Plane-Strain Prestrain on the r-Values Obtained in Subsequent Uniaxial Tensile Tests at 90 Degrees to the Prestrain (RD).

Nominal Effective Prestrain (%)	r-Values Measured at the Following Nominal Strains:-								
	2.0	3.0	4.0	5.0	6.0	8.0	10.0	12.0	15.0
0	1.73	-	-	1.51	-	-	1.46	1.44	1.43
3.1	2.08	1.77	1.65	1.60	1.56	1.54	1.53	-	1.49
5.1	2.97	2.37	1.91	1.81	1.74	1.73	1.70	-	1.68
6.1	3.64	2.57	2.05	1.91	1.86	1.82	1.79	-	1.77
7.5	3.77	2.74	2.17	2.03	1.97	1.94	1.90	-	1.86
9.8	4.25	3.18	2.78	2.46	2.22	2.10	2.04	-	1.97

Table 48. Steel DP: Effect of TD Plane-Strain Prestrain on the r-Values Obtained in Subsequent Uniaxial Tensile Tests at 0 Degrees to the Prestrain .

Nominal Effective Prestrain (%)	r-Values Measured at the Following Nominal Strains:-								
	2.0	3.0	4.0	5.0	6.0	8.0	10.0	12.0	15.0
0	1.41	-	-	1.14	-	-	1.06	1.05	1.03
2.8	1.25	1.26	1.25	1.24	1.25	1.22	1.24	-	1.21
5.0	2.64	1.94	1.60	1.43	1.35	1.23	1.16	-	1.12
6.3	3.97	2.26	1.92	1.76	1.64	1.51	1.50	-	1.44
7.5	4.03	2.73	2.30	2.07	1.98	1.89	1.85	-	-

Table 49. Steel DP: Effect of TD Plane-Strain Prestrain on the r-Values Obtained in Subsequent Uniaxial Tensile Tests at 45 Degrees to the Prestrain.

Nominal Effective Prestrain (%)	r-Values Measured at the Following Nominal Strains:-								
	2.0	3.0	4.0	5.0	6.0	8.0	10.0	12.0	15.0
0	1.73	-	-	1.34	-	-	1.26	1.25	1.23
2.9	5.54	3.46	2.52	2.10	1.87	1.85	1.82	-	1.76
5.0	4.15	3.27	2.80	2.42	2.18	2.04	2.01	-	1.94
7.4	4.00	3.54	3.17	2.93	2.73	2.52	2.46	-	2.33
9.8	4.27	3.71	3.38	3.17	2.94	2.72	2.60	-	2.49
12.4	5.18	3.97	3.54	3.28	3.02	2.80	2.67	-	-

Table 50. Steel DP: Effect of TD Plane-Strain Prestrain on the r-Values Obtained in Subsequent Uniaxial Tensile Tests at 90 Degrees to the Prestrain (RD).

REFERENCES

1. W.T. Lankford, S.C. Snyder and J.A. Bauscher: Trans.ASM, 1950, Vol 42, p1197-
2. M. Atkinson and I.M. Maclean: Sheet Metal Ind., 1965, Vol 42, p290-
3. P. Ludwik: 'Elemente der Technologischen Mechanik', 1909, Springer Verlag, Berlin, Germany
4. J.H. Holloman: Trans.AIME, 1945, Vol 162, p268-
5. H.W. Swift: J.Mech.Phys. Solids, 1952, Vol 1, p1-
6. E. Voce: J.I.M, 1947, Vol 74, p537-
7. A.K. Ghosh: Met.Trans., 1974, Vol 5A, p1607-
8. R. Hill: 'The Mathematical Theory of Plasticity', 1950, Oxford University Press, London, England
9. W.A. Backofen: 'Deformation Processing', 1972, Addison-Wesley, Reading, Mass., USA
10. S.F. Keeler and W.A. Backofen: Trans.Asm.Soc.Met., 1963, Vol 56, p25-
11. G.E. Dieter: 'Mechanical Metallurgy', 1976, International Student Edition, 2nd Edition, McGraw-Hill Kogakusha, Tokyo, Japan

12. Z. Marciniak and K.Kuczynski: Int.J.Mech.Sci., 1967, Vol 9, p609-
13. R. Hill: J.Mech.Phys. Solids, 1952, Vol 1, p19-
14. W.A. Backofen: Met.Trans., 1973, Vol 4A, p2682-
15. Y. Tozawa, M. Nakamura and I. Shinkai: Trans.ISIJ, 1971, Vol 11, p936-
16. A.K. Ghosh and W.A. Backofen: Met.Trans., 1973, Vol 4A, P1113-
17. G. Romano, D. Rault and M. Entringer: Working Group III, 8th Biennial Congr. IDDRG, 1974, Gothenburg, Sweden
18. H.J. Kleemola and M.T. Pelkkikangas: Sheet Metal Ind., 1977, Vol 54, (6), p591-
19. J.V. Laukonis and A.K. Ghosh: Met.Trans., 1978, Vol 9A, p1849-
20. A.J. Ranta-Eskola: Mem.Sci.Rev.Met., 1980, (4), p543-
21. W.B. Hutchinson, R. Arthey and P. Malmstroem: Scripta Met., 1976, Vol 10, p673-
22. D.J. Lloyd and H. Sang: ALCAN Report No.KR77/011, 1977
23. J.V. Laukonis: Met.Trans., 1981, Vol 12A, p467-
24. F. Ronde-Oustau and B. Baudelet: Acta Met., 1977, Vol 25, p1523-
25. M. Deugen, P. Parniere and G. Sanz: IRSID Report No.488(U.291), 1977

26. B. Baudelet, M. Deugen, L. Falgeres, P. Parniere, F. Ronde-Oustau and G. Sanz: Mem.Sci.Rev.Met., 1978, (7), p409-

27. D. Grzesik and C.M. Vlad: Proc.Conf. on 'Textures of Materials', Vol 11, 1978, Aachen, W. Germany

28. F. Garofalo and J.R. Low, Jnr: J.Mech.Phys. Solids, 1955, Vol 3, p275-

29. T. Kikuma and K. Nakazima: Trans.ISIJ, 1971, Vol 11, Supll.II, p827-

30. M. Hatherley and W.B. Hutchinson: Monograph No.5, 'An Introduction to Textures in Metals', 1979, The Institution of Metallurgists, London, England

31. L.G. Schultz: J.Appl.Phys., 1949, Vol 20, p1030-

32. J.P. Hirth and J. Lothe: 'Theory of Dislocations', 1968, McGraw-Hill, New York, USA

33. R. von Mises: Z.Angew.Math.Mech., 1928, Vol 8, p161-

34. D. Hull: 'Introduction to Dislocations', 1975, 2nd Edition, Pergamon Press, Oxford, England

35. W.C. Leslie: 'The Physical Metallurgy of Steels', 1982, International Student Edition, 1st Edition, McGraw-Hill Kogakusha, Tokyo, Japan

36. E. Orowan: 'Causes and Effects of Internal Stresses' in 'Internal Stresses and Fatigue in Metals', 1959, Elsevier, New York, USA

37. J.H. Schmitt and J.M. Jalinier: Acta Met., 1982, Vol 30, p1789-

38. F. Barlat, A. Barata Da Rocha and J.M. Jalinier: J.Mat.Sci., 1984, Vol 19, p4133-

39. M.S. Rashid: Proc.Symp. on 'Formable HSLA and Dual-Phase Steels' held in Chicago, Oct. 1977, 1979, (ed: A.T. Davenport), TMS-AIME, Warrendale, Pasadena, USA

40. D.K. Matlock, G. Krauss, L.F. Ramos and G.S. Huppi: Proc.Symp. on 'Structure and Properties of Dual-Phase Steels' held in New Orleans, Feb. 1979, 1979, (ed: R.A. Kot and J.W. Morris), TMS-AIME, Warrendale, Pasadena, USA

41. W.F. Hosford and C. Kim: Met.Trans., 1976, Vol 7A, p468-

42. W.B. Hutchinson and T. Davis: Proc.Conf. on 'Mechanical Behaviour of Materials-IV' held in Stockholm, Sept.1984, 1984, Vol 2, (ed: J. Carlsson and N.G. Ohlson), Pergamon Press, Oxford, England

43. G. Davies and R.A. Easterlow: Metals and Materials, 1985, Vol 1, (1), p20-

Acknowledgements

The author would like to thank SERC and BL Cars for financial support and G. Davies, P. Bate and D.V. Wilson for many helpful discussions. Special thanks is due to W.B. Hutchinson, who started the whole project off, and L.W. Crane, who saw it through to its conclusion.

Final thanks goes to my trusty old Apple computer and home-grown word-processor, without the use of which this thesis would not have been completed in time.